SEDIMENTOLOGY OF THERMOKARST LAKES FORMING WITHIN YEDOMA ON THE NORTHERN SEWARD PENINSULA

By

Louise M. Farquharson

RECOMMENDED:

Advisory committee co-chair

Advisory committee co-chair

Advisory committee co-chair

APPROVED:

Chair, Department of Geology and Geophysics

Dean, College of Natural Science and Mathematics

Dean of the Graduate School

April 19, 2012

Date

SEDIMENTOLOGY OF THERMOKARST LAKES FORMING WITHIN YEDOMA ON THE NORTHERN SEWARD PENINSULA

A

THESIS

Presented to the faculty

of the University of Alaska Fairbanks

in Partial Fulfillment of the Requirements

for the degree of

MASTER OF SCIENCE

By

Louise M. Farquharson, BSc.

Fairbanks, Alaska

May 2012

Abstract

Thermokarst lakes forming in yedoma (organic-rich permafrost containing massive syngenetic Pleistocene ice wedges) play an important role in periglacial landscape evolution. These lakes alter landscape elevation and topography, as well as redistribute upland sediment into lower basins. However, sediment deposition within yedoma thermokarst lakes is not well understood. Sedimentological, biogeochemical and macrofossil analyses enabled identification of five prominent facies in yedoma thermokarst lakes in my study region on the northern Seward Peninsula, Alaska. These include a Yedoma Taberal Silt facies situated below a sub-lacustrine unconformity, three types of basal facies and a Lacustrine Silt facies. A preliminary geomorphological model based on sediment cores from mature yedoma thermokarst lakes illustrates how facies distribution changes through the different stages of lake development. First-generation lakes (those forming in undisturbed upland) and later-generation lakes (those forming in thermokarst-affected lowland) were present on the northern Seward Peninsula. A comparison between these two lake types indicates that the depositional environments of later-generation lakes are much more variable than first-generation lakes. Understanding the depositional history and development of yedoma thermokarst lakes is critical to understanding their role in landscape evolution and the carbon cycle.

Table of Contents

List of Figures

Page

List of Tables

Page

List of Appendices

Acknowledgments

Firstly I would like to thank my co-advisers, Nancy Bigelow, Katey Walter Anthony and Jim Beget: Nancy Bigelow for her support, down to earth attitude, attention to detail and generosity with her time, Katey Walter Anthony for her consistently high expectations which pushed me to reach my full potential as a researcher, and Jim Beget for his guidance and advice. I would like to thank both my committee members, Mary Edwards and Guido Grosse, with whom I have enjoyed many thought-provoking and memorable discussions. I have had the pleasure of experiencing time in the field with Nancy Bigelow, Katey Walter Anthony, Mary Edwards and Guido Grosse. I am hugely grateful to my committee for valuable comments that sculpted the manuscript herein.

Many thanks to my fellow graduate students in Geology and Geophysics for putting a smile on my face each day. Thanks to Amy Myrbo at the National Lacustrine Core Facility, Department of Geology and Geophysics, University of Minnesota-Twin Cities (LacCore) for her indispensable advice in the field on the Seward Peninsula and at the LacCore. Thanks to Laura Brosius, Laurel McFadden, Marie Geai, Mike LaDouceur, Benjamin Jones, Nancy Bigelow, Mary Edwards, Guido Grosse and Katey Walter Anthony for helping to core lakes on the Seward Peninsula and making it an unforgettable experience. Also, I am grateful to Katey Walter Anthony, Mary Edwards and Emily Sousa for help with lake core analysis at the LacCore, and to Nancy Bigelow and Miriam Jones for help with macrofossil identification. I would like to give thanks to my mother, father and sister in the UK for their long distance love, understanding, encouragement and interest in my research. Finally I would like to thank Laura Oxtoby for help in the field and lab, but most importantly for her love and support.

Thanks to the Institute of Northern Engineering for a two-year research assistantship funded by the National Science Foundation International Permafrost Year grant #0732735, the Department of Geology for two semesters of funding as a teaching assistant, and the Alaska Quaternary Center for providing two semesters of funding as a research assistant.

Preface

This thesis is in manuscript format and has been divided into three chapters. Chapter One provides an overview of thermokarst lakes, their importance within arctic systems, and major gaps in knowledge that currently exist. This is also where my main hypotheses are presented. Chapter Two has been formatted and prepared for submission to *Quaternary Science Reviews*. Chapter Three provides a summary of how Chapter Two improves our understanding of thermokarst lake research.

Appendix One provides data on bulk density measurements and smear slide data for all sediment cores obtained during this study. Appendix Two provides metadata on sediment cores from the Seward Peninsula. Appendix Three contains details on using the National Lacustrine Facility nomenclature as applied to sediment cores. Appendix Three also contains additional data from two thermokarst lakes on the Seward Peninsula (Tea Lake and Prickly Pond) and laboratory description sheets of all sediment cores included within this study.

Chapter 1: Overall Introduction

1.1 Introduction

Thermokarst lakes dominate large areas of the Arctic and form from ground collapse when permafrost containing excess ice thaws. Thermokarst lakes modify arctic landscapes significantly through changes in geomorphology (Czudek and Demek 1970; Soloviev 1973a; Veremeeva and Gubin 2009), hydrology (Woo 1992), and vegetation cover (Jorgenson and Osterkamp 2005). Lakes forming in yedoma (silty, perennially frozen sediment containing massive syngenetic Pleistocene ice wedges) play a critical role in the global carbon cycle via the emission of CH_4 (methane) produced from the thaw of organic-rich Pleistocene sediment (Zimov et al. 1997; Walter et al. 2006; Zimov et al. 2006b; Walter et al. 2007c).

Given the importance of thermokarst lakes to landscape evolution (Tomirdiaro 1982), current trends in permafrost warming (Smith et al. 2010), and reported increases in the rate of thermokarst development (Jorgenson et al. 2006), it is necessary to better understand the factors that govern thermokarst lake formation and development.

Dating of thermokarst lake initiation (Shilo 2007 et al.; Walter et al. 2007a), analysis of alas (drained lake basin) elevations relative to fluvial landscape features (Veremeeva and Gubin 2009), and modeling of glacial-interglacial permafrost dynamics (Romanovskii et al. 2004) indicate that a peak in thermokarst activity occurred in the early Holocene. This was due to warming as a result of the transition from a glacial to interglacial period (Kaufman et al. 2004). Dating the exact timing of lake initiation is problematic because permafrost facilitates the storage of old carbon for long periods (Nelson et al. 1988; Oswald et al. 2005). This old carbon is released upon the thaw of permafrost, then transported and redeposited into the lake system. Therefore, radiocarbon ages of organic material within lake sediment may not be contemporaneous with deposition. Thermokarst lake margins are prone to erosion and shoreline change. Consequently, the most recently deposited lake sediment is situated towards the lake edge. This results in

basal lake sediments which greatly vary in age. Even if basal sediment age is synchronous with deposition into the lake, the age of basal sediment can still range from the time of lake initiation to present. Therefore dating true lake initiation partially depends on identifying where in the lake the first and oldest lacustrine sediment is located.

Numerous papers investigate morphological aspects of thermokarst lake behaviour, such as lake orientation (Livingstone 1954; Mackay 1956; Sellmann et al. 1975; Harry and French 1983; Cote and Burn 2002), lake cycling (Black and Barksdale 1949; Britton 1966; Billings and Peterson 1980; Rawlinson 1990; Jorgenson and Shur 2007), lake expansion and drainage (Jones et al. 2011), and influence on arctic landscape evolution (Czudek and Demek 1970; Soloviev 1973a, Soloviev 1973b; Astakov 1987). Other areas studied include the role of thermokarst lakes within the arctic carbon cycle (Hinkel et al. 2003; Walter et al. 2006; Walter et al. 2007b; Walter et al. 2007c), lake impacts on vegetation dynamics (Ovenden 1986; Katamura et al. 2006), lake biogeochemistry (Mesquita 2008; Breton et al. 2009; Bouchard et al. 2011), and modelling of lake and talik development (Tomirdiaro and Ryabchun 1973; Plug and West 2009; van Huissteden et al. 2011). However, geomorphological investigations of thermokarst lakes that address sedimentology and stratigraphy in detail (Murton 1996b; Wetterich et al. 2009) are less prevalent. These studies include observations that are often based on limited datasets (Carter 1988; Hopkins and Kidd 1988). To fully understand thermokarst lake processes, it is necessary to study lake sediment at more locations and at a higher sampling resolution (Murton 1996b).

The following sections present an overview of thermokarst lake research as it pertains to 1) regional contrasts in lake geomorphology, 2) arctic sedimentology and landscape evolution, 3) the carbon budget in permafrost regions, and 4) the role of lake generation in the thermokarst lake cycle. Important knowledge gaps are also identified.

1.2 Regional differences in thermokarst lake geomorphology and sediment characteristics

Thermokarst lake morphology is predominantly controlled by permafrost properties such as volume and depth of excess ice (Grosse et al. In press). Excess ice volume and depth is controlled by paleoenvironmental conditions, including glacial history, substrate formation, and past hydrological and permafrost conditions (French 1987, 1996; French and Shur 2010). As a result, thermokarst regions can display contrasting morphological characteristics such as variation in elevation differences and abundance of thermokarst lakes and drained lake basins. In this section, I compare morphological characteristics of various thermokarst lake types from different regions: shallow oriented lakes found on the Arctic Coastal Plain, Liverpool Bay and Banks Island in the North West Territories (NWT); small palsa ponds in the Hudson Bay Lowlands; large deep lakes on the Tuktoyuktuk Peninsula; and yedoma thermokarst lakes forming in northeast Siberia, the Brooks Range Foothills, the northern Seward Peninsula and Interior Alaska.

1.2.1 Shallow oriented lakes

Shallow oriented lakes dominating the Arctic Coastal Plain have been the topic of many thermokarst lake studies (Black and Barksdale 1949; Sellmann et al. 1975; Hinkel et al. 2005). These lakes are typically oriented and elliptical (Hinkel et al. 2005) and are characterized by relatively uniform depths (Livingstone 1954) of between 1.5 and 3 m (Britton 1966). Shallow (less than three meters) epigenetic ice wedge polygon networks are the dominant ground ice structure. These ice wedges formed within the Pleistocene marine silts and gravels of the Gubik formation (Black and Barksdale 1949; Black 1964). These lakes expand mainly through wave cut erosion (Hinkel et al. 2003). Sediments are often described as a basal layer of coarse peat that that becomes increasingly fine towards the sediment-water interface, which is then overlain by organic detritus and silt (Britton 1966).

Oriented thermokarst lakes have been reported in the Liverpool Bay area, NWT, Canada (Mackay 1954) and southwest Banks Island, Canada (Harry and French 1983). Lakes on

southwest Banks Island formed within glacial outwash deposits that contain up to 60% excess ice, mainly in the form of epigenetic ice wedges. Thaw settlement is between five to six meters (Harry and French 1983). Thaw depths are greater than seen on the Arctic Coastal Plain due to excess ice bodies penetrating to greater depths in the Liverpool Bay area. The sedimentology of these lakes has not been described in detail. It is noteworthy that lakes of a similar morphology (shallow and oriented) can form within contrasting substrates (marine and glaciofluvial).

1.2.2 Palsa thermokarst ponds

In the Hudson Bay Lowlands, small (less than 30 m in diameter), shallow (up to three meters in depth), thermokarst ponds form from the thaw of low, mostly oval frost heave features, also known as palsas (Breton et al. 2009; Bouchard et al. 2011). These thermokarst ponds formed within organic-poor marine silts which were deposited during the Tyrell Sea transgression approximately 7,600 years BP (Bouchard et al. 2011), after the retreat of the Laurentide ice sheet (Dyke 2004). An organic-rich layer provides a transition from marine silt to organic-rich and humic muds (Bouchard et al. 2011). Lake sedimentology was found to be consistent between lakes, despite a wide range of limnological characteristics.

1.2.3 Deep non-yedoma thermokarst lakes

On Richards Island, on the Tuktoyaktuk Peninsula, deep lakes form from the thaw of buried glacial and intrasedimental ice in an area that was within the limits of a late Wisconsin glaciation (Murton et al. 2007). Lakes on Richards Island reach three kilometres in diameter and 15 m in depth. Lake expansion is largely via retrogressive thaw slumping which occurs when massive ground ice bodies thaw (Murton 1996a, 2001; Kokelj et al. 2009). Sediments are characterized by a thick basal detrital layer (up to four meters thick) consisting of blocks of fibrous woody peat and diamicton and overlain by a muddy lacustrine fill.

1.2.4 Yedoma thermokarst lakes

Deep (typically >10 m) thermokarst lakes forming from the thaw of late Pleistocene syngenetic ice wedges up to 50 m in depth occur within yedoma and yedoma-like sediment (Czudek and Demek 1970; Grosse et al. 2007). Most research pertaining to yedoma and yedoma-type thermokarst lake formation focuses on Siberia (Czudek and Demek 1970; Soloviev 1973a; Tomirdiaro and Ryabchun 1973; Zimov et al. 1997; Schirrmeister et al. 2008; Schirrmeister et al. 2011b; van Huissteden et al. 2011), yet extensive areas of the Seward Peninsula (Hopkins 1949; Hopkins and Kidd 1988), sections of the Brooks Range Foothills (Carter 1988; Rawlinson 1990), various regions of Alaska (Kanevskiy et al. 2011), and the Yukon Territory in Northwest Canada (Reyes et al. 2010) are overlain by yedoma-like sediment that have been reworked by thermokarst lakes. Thaw of massive syngenetic ice wedges results in settlement depths of up to 40 m (Czudek and Demek 1970) and the formation of high, steep sub-aerial and sub-aqueous bluffs. Yedoma thermokarst lake sediments are characterized by a sandy, organic-rich basal detrital unit containing a mineral fraction which ranges from sand to silt, overlain by fine grained, silt dominated, thin-bedded central basin deposits (Hopkins and Kidd 1988).

1.2.5 Other yedoma-type thermokarst lakes

Yedoma type thermokarst lakes also form in Interior Alaska. Near Fairbanks, Alaska, loess was deposited intermittently from 3 Ma to 10 ka BP (thousand years before present), although retransportation continued after air-fall loess accumulation halted (Pewe et al. 2009). Periods of disturbance and re-sedimentation are evident from erosional unconformities within loess deposits in the U.S. Army CRREL (Cold Regions Research and Engineering Laboratory) permafrost tunnel. With the youngest disturbance dating from 8.5 - 4 ka BP (Sellmann 1967; Hamilton et al. 1988). Loess deposits within valleys are composed of silt directly deposited by wind and colluvium redeposited from slopes by solifluction and slope wash (Sellmann 1967; Muhs et al. 2003). These deposits can reach up to 100 m in thickness (Pewe et al. 2009).

The cryostructure of upper sediment in Interior Alaska valley bottoms is characterized by a combination of pore ice, segregated ice, and small (up to one meter wide and one to two m deep) foliated ice wedges of epigenetic origin (Hamilton et al. 1988; Pewe et al. 2009). Thermokarst lakes forming from the thaw of this type of ice tend not to exhibit the same morphological characteristics as yedoma thermokarst lakes forming on the northern Seward Peninsula and in northeast Siberia. This is likely due to the loess redeposition events disturbing the development and structure of massive Pleistocene ice wedges. Reported lake depths for two interior Alaska thermokarst lakes are shallow, averaging ~ 2 m (Brosius 2010).

1.2.6 Regional variation in lake morphology

Local geomorphological diversity also occurs within regions. For example, in contrast to the shallow oriented lakes on the Arctic Coastal Plain that form from the thaw of shallow epigenetic ice wedges in marine sands, thermokarst lakes in the northern Brooks Range Foothills form within yedoma-type loess deposits that are 30 m thick and contain syngenetic ice wedges up to 25 m deep (Carter 1988). Local geomorphological diversity is also present in the Northwest Territories exemplified by the occurrence of both oriented and non-oriented lakes (Murton 1996b; Burn 2002; Cote and Burn 2002). Orientation can be due to either preferential erosion perpendicular to the long axis of the lake as a result of wind direction or to glacial fluting (Cote and Burn 2002). A complex glacial history results in a combination of both shallow and deep lakes up to 2 and 15 m deep, respectively (Murton 1996b; Burn 2002).

In the case of yedoma thermokarst lakes, regional variation is evident between lakes forming in upland yedoma compared to those forming in drained lake basins. Drained lake basins are more depleted of excess ice compared to upland virgin yedoma. This restricts the maximum depth of thaw (Morgenstern et al. 2011). As a result, the lakes are typically much shallower (Jones et al. 2011).

Further research is needed to identify whether regional variation in sediment composition and cryostructure results in different morphological characteristics within thermokarst

lakes and to what degree morphology varies within a region. As yet, no systematic comparison of the sediments between thermokarst lake regions has been conducted.

1.3 Thermokarst lake sedimentology and arctic landscape evolution

Within thermokarst lake regions, sediment is continuously reworked by repeated lake formation, drainage, and ice aggradation within the topographic lows of drained thermokarst lake basins (Billings and Peterson 1980; Jorgenson and Shur 2007). This results in the repeated formation of later-generation thermokarst lakes. In contrast, first-generation thermokarst lakes form within virgin permafrost that has not been thermokarst-affected. Later-generation lakes form, at least partially, within drained thermokarst lake basins, also termed alases (Jones et al. In press).

Continued lake formation, drainage, and re-initiation greatly modify landscape topography and elevation. During the Holocene, generations of thermokarst lakes reworked extensive areas of ice-rich permafrost in the Arctic. Approximately 91% of yedoma between the Alazeya and Chukochya Rivers, in the Kolyma River Lowlands (Veremeeva and Gubin, 2009), ~35% of yedoma surrounding Yakutsk in the central Yakutian lowlands (Czudek and Demek, 1970) and 72% of the Late Pleistocene Gubik Formation on Alaska's Barrow Peninsula (Hinkel et al. 2003) have been affected by thermokarst lake processes. The mapping of yedoma topography in Middle Chukochya, Kolyma River Lowlands, Siberia, reveals an elevation difference of up to 35 m between drained thermokarst lake basins and upland virgin yedoma (Veremeeva and Gubin 2009). In contrast the formation of thermokarst lakes on the Arctic Coastal Plain causes elevation differences of approximately two meters (Hinkel et al. 2003). These settlement values are conservative as they do not take into account lacustrine sediment accumulation within thermokarst lake basin depressions. A contrast in hydrology has been observed between better-drained upland yedoma and alases which were found to be poorly drained and water logged (Veremeeva and Gubin 2009).

Further investigation is needed to identify how sediment distribution changes as the

landscape evolves, with emphasis on similarities and differences between yedoma uplands, first-generation thermokarst lakes, and later-generation thermokarst lakes.

1.4 The role of yedoma thermokarst lakes within the permafrost-related carbon budget

Permafrost-affected soils contain ca. 1672 Pg (petagrams) of soil organic carbon (Tarnocai et al. 2009), approximately 304.51 Pg of which is between 30 – 100 cm depth and susceptible to thawing. Yedoma deposits are among these permafrost-affected soils but exist at depths greater than 100 cm. Yedoma deposits have average carbon contents of 2.38 ± 0.38% in northeast Siberia (Zimov et al. 2006a). Within Interior Alaska, yedoma-type loess deposits have total organic carbon contents ranging from 0.5 - 3.5% (Muhs et al. 2003). Organic carbon values have been reported to range from 1 - 6.2% by weight in the case of the northeast Siberian Shelf region (Schirrmeister et al. 2008; Schirrmeister et al. 2011a) and 0.38 – 2.39% in Interior Alaska yedoma-type loess deposits (Péwé 1952). Yedoma deposits have a gravimetric ice content of 40 - 120% (Zimov et al. 1997; Schirrmeister et al. 2008), and an average thickness of ~25 m in northeast Siberia (Zimov et al. 2006b) and ~30 m in Alaska (Carter 1988; Kanevskiy et al. 2011).

Thermokarst lakes play an important role in the carbon budget by eroding and redepositing upland sediment and releasing methane (CH_4). Within yedoma thermokarst lakes, methane production is mainly fueled by the anaerobic decomposition of Pleistocene labile organic carbon in yedoma sediment (Zimov et al. 1997). As thermokarst lakes develop and deepen, a thaw bulb or talik (zone of perennially thawed permafrost) forms beneath the lake and persists year-round (Plug and West 2008), which facilitates continuous CH_4 and CO_2 production (Zimov et al. 1997; Walter et al. 2006). Once lake drainage occurs, basins can act as a source or a sink for carbon (Jones et al. In press). In the case of well drained areas, aerobic decomposition can take place, releasing CO_2 (Camill et al. 2001). Alternatively, water-logged soils may retard decomposition and

facilitate the sequestration of carbon in the form of peat (Hinkel et al. 2003; Bockheim et al. 2004).

The role thermokarst lakes play in the permafrost-related carbon budget also greatly depends on whether they are located on yedoma uplands or within previously thawed substrates. Based on observations (Walter et al. 2006) and modeling (Kessler et al. 2012) it has been found that CH_4 ebullition is greater where margins are eroding into virgin yedoma. This suggests that later-generation lakes are thawing sediment that is more depleted in labile carbon than upland yedoma, and therefore these lakes are expected to emit less CH_4. Differentiating between first- and later-generation lakes in the sediment record is therefore important in reconstructing CH_4 emissions from yedoma thermokarst lakes during the Late Pleistocene and Holocene.

Given the geomorphological controls over carbon cycling in permafrost-rich arctic environments, an improved understanding of land surface processes, such as the thermokarst lake cycle, provides a powerful tool with which to predict changes in carbon cycling in a warming climate.

1.5 Conclusion

Different thermokarst lake regions can display contrasting morphological characteristics due to variations in excess ice volume and depth. Distinguishing between thermokarst lake morphotypes is important when reconstructing periglacial landscape evolution. Sediment composition and distribution may be one way to differentiate between thermokarst lake morphotypes. Modern sedimentology and stratigraphy can be directly linked to active thermokarst processes. Specific margin types, such as previously thawed substrates or virgin yedoma upland margins, can be correlated with adjacent subaqueously-deposited lacustrine facies. Lakes at different stages of lake development can be sampled and applied to a geomorphological model of yedoma thermokarst lake formation. By applying modern observations to a process-based model, such as that of Kessler et al. (2012), it is possible to reconstruct the magnitude and extent of past thermokarst activity and develop informed projections of ecosystem shifts and future

carbon cycling.

1.6 Thesis goals and hypotheses:

This study focuses on yedoma thermokarst lakes forming on the northern Seward Peninsula, Alaska. I will discuss the facies present, their distribution, and factors affecting facies formation. In my thesis research I address the following hypotheses:

1) Yedoma thermokarst lake sediment consists of a suite of facies, each representing a different depositional environment.
2) First-generation yedoma thermokarst lakes exhibit changing facies distribution through time both horizontally and vertically.
3) Differences in dominant margin geomorphology result in dissimilar facies distribution between first- and later-generation yedoma thermokarst lakes.
4) Yedoma lakes in regions other than the Seward Peninsula exhibit similar facies and facies distribution.
5) Differences in parent material, excess ice volume and cryostructure result in differences between yedoma and non-yedoma thermokarst lakes.

1.7 References

Astakov, V., 1987. Origin of west Siberian lakes. Paleohydrology of the temperate zone. Valgus, pp. 144-155.

Billings, W. D., Peterson, K. M., 1980. Vegetational change and ice-wedge polygons through the thaw-lake cycle in Arctic Alaska. Arctic and Alpine Research, 12: 413-432.

Black, R. F., 1964. Gubik formation of Quaternary age in northern Alaska U.S. Geological Survey Professional Paper, 302-C,

Black, R. F., Barksdale, W. L., 1949. Oriented lakes of northern Alaska. Journal of Geology, 57: 105-188.

Bockheim, J. G., Hinkel, K. M., Eisner, W. R., Dai, X. Y., 2004. Carbon pools and accumulation rates in an age-series of soils in drained thaw-lake basins, Arctic Alaska. Soil Science Society of America Journal, 68: 697-704.

Bouchard, F., Francus, P., Pienitz, R., Laurion, I., 2011. Sedimentology and geochemistry of thermokarst ponds in discontinuous permafrost, subarctic Quebec, Canada. Journal of Geophysical Research-Biogeosciences, 116: G00M04.

Breton, J., Vallieres, C., Laurion, I., 2009. Limnological properties of permafrost thaw ponds in northeastern Canada. Canadian Journal of Fisheries and Aquatic Sciences, 66: 1635–1648.

Britton, M. E., 1966. Vegetation of the Arctic tundra, 2nd edition ed. Oregon State University Press, Corvallis, 2nd edition

Brosius, L. S., 2010. Investigating Controls Over Methane Production and Bubbling from Interior Alaskan Lakes Useing Stable Isotopes and Radiocarbon Ages. M.Sc. thesis, University of Alaska Fairbanks.

Burn, C. R., 2002. Tundra lakes and permafrost, Richards Island, western Arctic coast, Canada. Canadian Journal of Earth Sciences, 39: 1281-1298.

Camill, P., Lynch, J. A., Clark, J. S., Adams, J. B., Jordan, B., 2001. Changes in biomass, above ground net primary production, and peat accumulation following permafrost thaw in the boreal peatlands of Manitoba, Canada. Ecosystems, 4: 461-478.

Carter, L. D., 1988. Loess and deep thermokarst basins in arctic Alaska, In: Permafrost, Fifth International Conference, Proceedings. Tapir Publishers, Trondheim, Norway, pp. 706–711.

Cote, M. M., Burn, C. R., 2002. The oriented lakes of Tuktoyaktuk Peninsula, western Arctic coast, Canada: A GIS-based analysis. Permafrost and Periglacial Processes, 13: 61-70.

Czudek, T., Demek, J., 1970. Thermokarst in Siberia and its influence on the development of lowland relief. Quaternary Research, 1: 103-120.

Dyke, A. S., 2004. An outline of North American Deglaciation with emphasis on central and northern Canada. In: Ehlers, J. and Gibbard, P. L. (Eds.), Quaternary Glaciations-Extent and Chronology. pp. 373-424.

French, H., 1987. Periglacial geomorphology in North America: current research and future trends. Ecological Bulletins, 38: 5-16.

French, H., 1996. The Periglacial Environment, 2nd ed. Longman, London, pp 478.

French, H., Shur, Y., 2010. The principles of cryostratigraphy. Earth-Science Reviews, 101: 190-206.

Grosse, G., Jones, B., Arp, C., In press. Thermokarst Lakes, Drainage, and Drained Basins. Treatise on Geomorphology. Elsevier.

Grosse, G., Schirrmeister, L., Siegert, C., Kunitsky, V., Slagoda, E. A., Andreev, A., Dereviagin, A., 2007. Geological and geomorphological evolution of a sedimentary periglacial landscape in northeast Siberia during the Late Quaternary. Geomorphology, 86: 25-51.

Hamilton, T., Craig, J. L., Sellmann, P. V., 1988. The Fox permafrost tunnel: A late Quaternary geologic record in Central Alaska. Geological Society of America Bulletin, 100: 948-969.

Harry, D. G., French, H. M., 1983. The orientation and evolution of thaw lakes, southwest Banks Island, Canadian Arctic. , In: Permafrost, Forth International Conference, Proceedings. National Academy of Sciences, Fairbanks, Alaska, pp. 456-461.

Hinkel, K., Eisner, W. R., Bockheim, J. G., Nelson, F. E., Peterson, K. M., Dai, X. Y., 2003. Spatial extent, age, and carbon stocks in drained thaw lake basins on the Barrow Peninsula, Alaska. Arctic Antarctic and Alpine Research, 35: 291-300.

Hinkel, K., Frohn, R. C., Nelson, F. E., Eisner, W. R., Beck, R. A., 2005. Morphometric and spatial analysis of thaw lakes and drained thaw lake basins in the western Arctic Coastal Plain, Alaska. Permafrost and Periglacial Processes, 16: 327-341.

Hopkins, D. M., 1949. Thaw lakes and thaw sinks in the Imuruk Lake area, Seward Peninsula, Alaska. The Journal of Geology, 57: 1949.

Hopkins, D. M., Kidd, J., 1988. Thaw lake sediments and sedimentary environments, In: Permafrost, Fifth International Conference, Proceedings. Tapir Publishers, Trondheim, Norway, Trondheim, Norway, pp. 790-795.

Jones, B. M., Grosse, G., Arp, C. D., Jones, M. C., Walter Anthony, K. M., Romanovsky, V. E., 2011. Modern thermokarst lake dynamics in the continuous permafrost zone, northern Seward Peninsula, Alaska. Journal of Geophysical Research – Biogeosciences: G00M03.

Jones, M., Grosse, G., Jones, B. M., Walter Anthony, K. M., In press. Peat accumulation in a thermokarst-affected landscape in continuous ice-rich permafrost, Seward Peninsula, Alaska. Journal of Geophysical Research – Biogeosciences.

Jorgenson, M. T., Osterkamp, T. E., 2005. Response of boreal ecosystems to varying modes of permafrost degradation. Canadian Journal of Forest Research, 35: 2100-2111.

Jorgenson, M. T., Shur, Y., 2007. Evolution of lakes and basins in northern Alaska and discussion of the thaw lake cycle. Journal of Geophysical Research-Earth Surface, 112.

Jorgenson, M. T., Shur, Y., Pullman, E. R., 2006. Abrupt increase in permafrost degradation in Arctic Alaska. Journal of Geophysical Research – Biogeosciences, 33.

Kanevskiy, M., Shur, Y., Fortier, D., Jorgenson, M. T., Stephani, E., 2011. Cryostratigraphy of late Pleistocene syngenetic permafrost (yedoma) in northern Alaska, Itkillik River exposure. Quaternary Research, 75: 584-596.

Katamura, F., Fukuda, M., Bosikov, N. P., Desyatkin, R. V., Nakamura, T., Moriizumi, J., 2006. Thermokarst formation and vegetation dynamics inferred from a palynological study in Central Yakutia, Eastern Siberia, Russia. Arctic Antarctic and Alpine Research, 38: 561-570.

Kaufman, D. S., Ager, T. A., Anderson, N. J., Anderson, P. M., Andrews, J. T., Bartlein, P. T., Brubaker, L. B., Coats, L. L., Cwynar, L. C., Duvall, M. L., Dyke, A. S., Edwards, M. E., Eisner, W. R., Gajewski, K., Geirsdottir, A., Hu, F. S., Jennings, A. E., Kaplan, M. R., Kerwin, M. W., Lozhkin, A. V., MacDonald, G. M., Miller, G. H., Mock, C. J., Oswald, W. W., Otto-Bliesner, B. L., Porinchu, D. F., Ruhland, K., Smol, J. P., Steig, E. J., Wolfe, B. B., 2004. Holocene thermal maximum in the western Arctic (0-180 degrees W) (vol 23, pg 529, 2003). Quaternary Science Reviews, 23: 2059-2060.

Kessler, M. A., Plug, L. J., Walter Anthony, K. M., 2012. Simulating the decadal- to millennial-scale dynamics of morphology and sequestered carbon mobilization of two thermokarst lakes in NW Alaska. Journal of Geophysical Research – Biogeosciences, 117: G00M06.

Kokelj, S. V., Lantz, T. C., Kanigan, J., Smith, S. L., Coutts, R., 2009. Origin and polycyclic behaviour of tundra thaw slumps, Mackenzie Delta Region, Northwest Territories, Canada. Permafrost and Periglacial Processes, 20: 173-184.

Livingstone, D. A., 1954. On the orientation of lake basins. American Journal of Science, 252: 547-554.

Mackay, J. R., 1954. Notes on oriented lakes of the Liverpool Bay area, Northwest Territories. Revue Canadienne de Géographie, 10: 169-173.

Mesquita, P. S., 2008. Effects of Retrogressive Permafrost Thaw Slumping on Benthic Macrophyte and Invertebrate Communities of Upland Tundra Lakes. M.Sc. thesis, University of Victoria.

Morgenstern, A., Grosse, G., Gunther, G., Fedorova, I., and Schirrmeister, L., 2011. Spatial analyses of thermokarst lakes and basins in Yedoma landscapes of the Lena Delta. The Cryosphere, 5: 849–867.

Muhs, D. A., Ager, T., Bettis, A., McGeehin, J., Been, J. M., Beget, J. E., Pavich, M. J., Stafford, T. W., Stevens, D. S. P., 2003. Stratigraphy and palaeoclimatic significance of Late Quaternary loess–palaeosol sequences of the Last Interglacial–Glacial cycle in centralAlaska. Quaternary Science Reviews, 22.

Murton, J. B., 1996a. Morphology and paleoenvironmental significance of Quaternary sand veins, sand wedges, and composite wedges, Tuktoyaktuk Coastlands, Western Arctic Canada. Journal of Sedimentary Research, 66: 17-25.

Murton, J. B., 1996b. Thermokarst-lake-basin sediments, Tuktoyaktuk Coastlands, western Arctic Canada. Sedimentology, 43: 737-760.

Murton, J. B., 2001. Thermokarst sediments and sedimentary structures, Tuktoyaktuk Coastlands, western Arctic Canada. Global and Planetary Change, 28: 175-192.

Murton, J. B., Frechen, M., Maddy, D., 2007. Luminessence dating of mid- to late Wisconsin aeolian sand as a constraint on the last advance of the Laurentide Ice Sheet accross the Tuktoyaktuk Coastlands, western Arctic Canada. Canadian Journal of Earth Sciences, 44: 857-869.

Nelson, R. E., Carter, D. L., Robinson, S. W., 1988. Anomalous radiocarbon ages form a Holocene detrital organic lens in Alaska and their implications for radiocarbon dating and paleoenvironmental reconstructions in the arctic. Quaternary Research, 29: 66-71.

Oswald, W. W., Anderson, P. M., Brown, T. A., Brubaker, L. B., Hu, F. S., Lozhkin, A. V., Tinner, W., Kaltenrieder, P., 2005. Effects of sample mass and macrofossil type on radiocarbon dating of arctic and boreal lake sediments. Holocene, 15: 758-767.

Ovenden, L., 1986. Vegetation colonizing the bed of a recently drained thermokarst lake (illisarvik), Northwest Territories. Canadian Journal of Botany, 64: 2688-2692.

Péwé, T. L., 1952. Geomorphology of the Fairbanks area, Alaska. Ph.D. thesis, Stanford University.

Pewe, T. L., Westgate, J. A., Preece, S. J., brown, P. M., Leavitt, S. W., 2009. Late Pliocene Dawson Cut Forest Bed and new tephrochronological findings in the Gold Hill Loess, east-central Alaska. Geological Society of America Bulletin, 121: 294-320.

Plug, L. J., West, J. J., 2008. Time-dependent morphology of thaw lakes and taliks in deep and shallow ground ice. Journal of Geophysical Research-Biogeosciences, 113: F01009.

Plug, L. J., West, J. J., 2009. Thaw lake expansion in a two-dimensional coupled model of heat transfer, thaw subsidence, and mass movement. Journal of Geophysical Research-Earth Surface, 114: F01002.

Rawlinson, S. E., 1990. Surficial Geology and Morphology of the Alaskan central Arctic Coastal Plain. . University of Alaska Fairbanks.

Reyes, A. V., Froese, D. G., Jensen, B. J. L., 2010. Permafrost response to last interglacial warming: field evidence from non-glaciated Yukon and Alaska. Quaternary Science Reviews, 29: 3256-3274.

Romanovskii, N. N., Hubberten, H. W., Gavrilov, A., Tumskoy, V. E., Kholodov, A. L., 2004. Permafrost of the east Siberian Arctic shelf and coastal lowlands. Quaternary Science Reviews, 23: 1359-1369.

Schirrmeister, L., Grosse, G., Wetterich, S., Overduin, P. P., Strauss, J., Schuur, E. A. G., Hubberten, H. W., 2011a. Fossil organic matter characteristics in permafrost deposits of the northeast Siberian Arctic. Journal of Geophysical Research – Biogeosciences, 116: G00M02.

Schirrmeister, L., Kunitsky, V., Grosse, G., Wetterich, S., Meyer, H., Schwamborn, G., Babiy, O., Derevyagin, A., Siegert, C., 2011b. Sedimentary characteristics and origin of the Late Pleistocene Ice Complex on north-east Siberian Arctic coastal lowlands and islands - A review. Quaternary International, 241: 3-25.

Schirrmeister, L., Meyer, H., Wetterich, S., Siegert, C., Kunitsky, V. V., Grosse, G., Kuznetsova, T. V., Derevyagin, A. Y., 2008. The Yedoma Suite of the northeastern Siberian Shelf Region: Characteristics and Concept of Formation. Ninth international Conference on Permafrost, University of Alaska Fairbanks: 1595-1600.

Sellmann, P. V., 1967. Geology of the USA. CRREL permafrost tunnel, Fairbanks, Alaska. Technical Report 199, US Army CRREL.

Sellmann, P. V., Brown, J., Lewellen, R. I., McKim, H., Merry, C., 1975. The classification and geomorphic implications of thaw lakes on the Arctic coastal plain, Alaska. . CRREL Research Report 344, Institute of Electrical and Electronics Engineers.

Shilo, N., A. Lozhkin, and P. Anderson, 2007. Radiocarbon dates of evolution cycles of thermokarst lakes on the Kolyma Lowland. Doklady Earth Sciences, 413: 259-261.

Smith, S. L., Romanovsky, V. E., Lewkowicz, A. G., Burn, C. R., Allard, M., Clow, G. D., Yoshikawa, K., Throop, J., 2010. Thermal State of Permafrost in North America: A Contribution to the International Polar Year. Permafrost and Periglacial Processes, 21: 117–135.

Soloviev, P. A., 1973a. Alas thermokarst relief of Central Yakutia. Guidebook, Permafrost: 2nd International Conference on Permafrost., USSR Academy of Sciences, Section of Earth's Sciences, Siberian Division.

Soloviev, P. A., 1973b. Thermokarst phenomena and landforms due to frostheaving in central Yakutia. Biuletyn Peryglacjalny, 23: 135–155.

Tarnocai, C., Canadell, J. G., Schuur, E. A. G., Kuhry, P., Mazhitova, G., Zimov, S., 2009. Soil organic carbon pools in the northern circumpolar permafrost region. Global Biogeochemical Cycles, 23: GB2023.

Tomirdiaro, S. V., 1982. Evolution of lowland landscapes in northeastern Asia during late Quaternary time. In: Hopkins, D. M., Jr., J. V. M., Schweger, C. E. and Young, S. B. (Eds.), Paleoecology of Beringia Academic Press, New York, pp. 29–37.

Tomirdiaro, S. V., Ryabchun, V. K., 1973. Lake thermokarst on the lower Anadyr lowland, In: Permafrost, 2nd International Conference, Proceedings. National Academy of Sciences, Yakutsk, pp. 94-100.

van Huissteden, J., Berrittella, C., Parmentier, F. J. W., Mi, Y., Maximov, T. C., Dolman, A. J., 2011. Methane emissions from permafrost thaw lakes limited by lake drainage. Nature Climate Change, 1: 119-123.

Veremeeva, A., Gubin, S., 2009. Modern tundra landscapes of the Kolyma Lowland and their evolution in the Holocene. Permafrost and Periglacial Processes, 20: 399-406.

Walter, K. M., Edwards, M. E., Grosse, G., Zimov, S. A., Chapin, F. S., 2007a. Thermokarst lakes as a source of atmospheric CH_4 during the last deglaciation. Science, 318: 633-636.

Walter, K. M., Edwards, M. E., Grosse, G., Zimov, S. A., Chapin, F. S., III, 2007b. Thermokarst lakes as a source of atmospheric CH(4) during the last deglaciation. Science, 318: 633-636.

Walter, K. M., Smith, L. C., Chapin, F. S., 2007c. Methane bubbling from northern lakes: present and future contributions to the global methane budget. Philosophical Transactions of the Royal Society a-Mathematical Physical and Engineering Sciences, 365: 1657-1676.

Walter, K. M., Zimov, S. A., Chanton, J. P., Verbyla, D., Chapin, F. S., III, 2006. Methane bubbling from Siberian thaw lakes as a positive feedback to climate warming. Nature, 443: 71-75.

Wetterich, S., Schirrmeister, L., Andreev, A., Pudenz, M., Plessen, B., Meyer, H., Kunitsky, V., 2009. Eemian and Late Glacial/Holocene palaeoenvironmental records from permafrost sequences at the Dmitry Laptev Strait (NE Siberia, Russia). Palaeogeography Palaeoclimatology Palaeoecology, 279: 73-95.

Woo, M., 1992. Consequences of climatic change for hydrology in permafrost zones. Journal of Cold Regions Engineering, 4: 15-20.

Zimov, S. A., Davydov, S. P., Zimova, G. M., Davydova, A. I., Schuur, E. A. G., Dutta, K., III, F. S. C., 2006a. Permafrost carbon: Stock and decomposability of a globally significant carbon pool. Geophysical Research Letters, 33: L20502.

Zimov, S. A., Schuur, E. A. G., Chapin, F. S., 2006b. Permafrost and the global carbon budget. Science, 312: 1612-1613.

Zimov, S. A., Voropaev, Y. V., Semiletov, I. P., Davidov, S. P., Prosiannikov, S. F., Chapin, F. S., Chapin, M. C., Trumbore, S., Tyler, S., 1997. North Siberian lakes: A methane source fueled by Pleistocene carbon. Science, 277: 800-802.

Chapter 2 : Sedimentology of yedoma thermokarst lakes on the northern Seward Peninsula, Alaska[1]

2.1 Abstract

Thermokarst lakes form from the thaw and collapse of ice-rich permafrost. Understanding the sediment composition and distribution of thermokarst lakes has practical applications for reconstructing temporal and spatial patterns of periglacial landscape development. Of particular importance are yedoma-type lakes, which dramatically alter the land surface, lowering elevation and redistributing upland sediment into lower basins. However, the sediment of yedoma thermokarst lake basins has yet to be systematically described. Using sedimentological, biogeochemical and macrofossil analysis, five prominent facies associated with yedoma thermokarst lakes on the northern Seward Peninsula were identified. These include a Yedoma Taberal Silt facies situated below a sub-lacustrine unconformity, three types of basal deposits and a Lacustrine Silt facies.

Interpretation of sediment cores from first-generation lakes reveals that facies distribution changes through the different stages of development. A comparison of sedimentology of first- and later-generation yedoma thermokarst lakes reveals that sediment of later-generation lakes is much more variable than first-generation lakes. Sediment facies distribution in both first- and later-generation lakes is largely controlled by the local factors of margin type and proximity. In some cases later-generation lake sediment composition and distribution is influenced by a mix of virgin yedoma upland margins and drained lake basin lowland margins. In other later-generation lakes, sedimentology is influenced by drained lake basin lowland margins only.

---

[1] Farquharson, L.M., Walter Anthony, K. M., Bigelow, N.H.B., Grosse, G., Edwards, M.E. and Beget, J.E., 2012. Sedimentology of thermokarst lakes forming in yedoma on the northern Seward Peninsula, Alaska. Prepared for submission to Quaternary Science Reviews.

Based on an extensive literature review, strong similarities between sediment sequences on the northern Seward Peninsula and those described in other yedoma lakes in Alaska and Siberia were found. My findings improve our ability to differentiate between first- and later-generation yedoma thermokarst lakes and between yedoma and non-yedoma thermokarst lakes within the periglacial sediment record.

2.2 Introduction

An understanding of thermokarst lake sediment composition and distribution in yedoma regions is valuable when interpreting the periglacial sediment record. Yedoma consists of silty to sandy permafrost deposits with excess ice contents of 60-120% (Schirrmeister et al. 2008a), comprised mainly of segregated ice lenses, ice bands, and large syngenetic Pleistocene ice wedges. Organic carbon content of yedoma deposits averages 2.2-3.7% (Schirrmeister et al. 2011). Thermokarst lakes form when excess ice in permafrost melts, causing water to collect in a closed depression (van Everdingen 1988; French 1996). Thermokarst lakes forming in yedoma uniquely develop from the thaw and collapse of large syngenetic Pleistocene ice wedges up to 50 m in depth (Czudek and Demek 1970; Grosse et al. 2007). The thaw of these large ice wedges drastically impacts landscape topography. Settlement depths of up to 40 m have been reported for yedoma deposits in central Yakutia (Czudek and Demek 1970). Upon thaw and collapse, some sediment remains *in situ*, while others are redistributed both sub-aerially and sub-aqueously within the depression. Relatively few investigations of yedoma thermokarst lakes address sedimentology and stratigraphy (Murton 1996; Wetterich et al. 2009)

Changes in margin proximity through lateral lake expansion (Murton 1996) and the extent of vertical subsidence control thermokarst lake facies distribution (Kidd 1988). Lateral expansion of lake margins facilitates the sorting of sediment between the lake margin and center (Britton 1966; Murton 1996). Water depth controls the extent of transportation and redeposition through wave action. Deeper, central waters also enable finer material to settle out of suspension (Hopkins and Kidd 1988; Kidd 1988). Two facies that reflect the effect of sorting between the lake margin and lake center are repeatedly identified in yedoma and non-yedoma thermokarst lake studies: a detrital basal facies that consists of coarse material deposited in close proximity to the margin (Hopkins and Kidd 1988; Burn and Smith 1990; Rawlinson 1990; Murton 1996); and a fine-grained fill facies (Britton 1966; Tomirdiaro and Ryabchun 1973; Hopkins and Kidd

1988; Murton 1996) which forms from settling of fine material deposited away from the lake margin (Murton 1996; Kessler et al. 2012).

Thermokarst lakes go through distinct stages of development that likely cause shifts in sediment composition as well as both vertical and lateral sediment distribution (Czudek and Demek 1970; Plug and West 2009). Initial thaw and collapse of large Pleistocene ice wedges lead to the formation of a pond. Lake diameter and depth continue to increase through thermoerosion and thaw settlement, respectively. Once the layer with excess ice has thawed, the lake reaches a maximum depth, but lateral erosion may continue until lake drainage occurs. This will affect the degree of sorting that occurs between the margin and the location of redeposition. Fine, well-sorted lacustrine fills overlying poorly sorted basal sediment has been reported within lakes on Richards Island, Tuktoyuktuk Peninsula (Murton 1996, 2001), and in the Brooks Range Foothills (Tedrow 1969).

Lake development may ultimately lead to lake drainage (Mackay 1988; Jones et al. 2011) and the formation of alases (drained lake basins) that support growth of epigenetic ice wedges. Initiation of new 'later-generation' lakes is facilitated by the growth and eventual thaw of shallow epigenetic ice wedges within alases. High steep bluffs and water depths of up to 25 m characterize first-generation lakes forming within the Pleistocene yedoma uplands. Because later-generation lakes form from the thaw of shallower epigenetic ice which restricts lake depth, shallower lakes with lower bluffs result (Hopkins and Kidd 1988). On the Seward Peninsula, bluff heights were found to vary by up to 16.5 m between first- and later-generation lakes (Jones et al. 2011). The shape of later-generation lakes frequently deviates from round or elongate (shapes which often characterize first-generation basins) as these lakes do not necessarily remain contained within a single alas basin. Many later-generation lakes erode into a combination of upland yedoma and adjacent alases of varying generation. Studies of yedoma thermokarst lakes on the Seward Peninsula describe up to six partially overlapping lake generations (Jones et al. In press). Due to contrasting lake morphology,

a variation in facies distribution is expected between first- and later-generation lakes.

Differences in excess ice depth, volume, and subsequently lake morphology occur between yedoma and non-yedoma thermokarst lakes. For example, in contrast to the relatively deep thermokarst lakes formed in Pleistocene yedoma, non-yedoma thermokarst lakes have been reported to form from the thaw of pore ice, ice lenses, ice veins, and shallow (less than three meters) ice wedges (Hinkel et al. 2007) within marine silts and gravels on the Arctic Coastal plain (Black 1964). Other non-yedoma thermokarst lakes include those that form as a result of melting of large ice bodies which extend up to seven meters or more into the ground; these form in diamicton on the Tuktoyaktuk Peninsula (Murton 1996). Deep (greater than three meters) non-yedoma thermokarst lakes are also found to form from the thaw of dead ice within sandy deposits in the Arga complex of the Lena River Delta (Schwamborn 2000 et al.). Still other non-yedoma thermokarst lakes form due to the degradation of palsas and lithalsas that formed within marine silts in the Hudson Bay Lowlands (Breton et al. 2009; Bouchard et al. 2011). I hypothesize that a variation in cryostructure and surficial geology between yedoma and non-yedoma thermokarst lakes is likely to result in different sediment composition and distribution within the lakes.

To develop a better understanding of yedoma thermokarst lake sediment composition and both vertical and horizontal distribution I analyzed sediment cores extracted from a suite of seven lakes on the northern Seward Peninsula, Alaska. Sediment cores were taken from a variety of first-, mixed-, and later-generation lakes. I characterize lake facies using visual interpretation and sedimentological and biogeochemical measurements.

2.3 Field study area

My study area is located on the coastal lowlands of the northern Seward Peninsula, Alaska, on the eastern side of the Bering Strait, within one of the major lake districts of Alaska (Arp and Jones 2009). During the Late Pleistocene, extensive areas of unglaciated Beringia accumulated ice-rich silt deposits (Schirrmeister et al. 2008a).

Roughly one million km^2 of northeast Siberia (Zimov et al. 2006) and about 260,000 km^2 of Alaska and northwest Canada (Grosse et al. 2011; Kanevskiy et al. 2011) are overlain by yedoma deposits. The genesis of yedoma is widely disputed, but the main mechanisms are thought to be eolian (Tomirdiaro 1982; Carter 1988; Hopkins and Kidd 1988) and alluvial or polygenetic (Popov 2008; Schirrmeister et al. 2008a; Kanevskiy et al. 2011). Sedimentation buried a range of organic material derived from in-situ vegetation and soil organic matter, plus animal-derived materials, including, on rare occasions, carcasses of megaherbivores such as the woolly mammoth (*Mammuthus primigenius*), caribou (*Rangifer* spp.) and horses (*Equus ferus*). Organic carbon is sequestered in soils that average 2.2 ± 0.9% (Late Weichselian ice complex) to 3.7 ± 4.2% (Middle Weichselian ice complex) TOC in Siberia. This quantity of organic carbon, combined with the extensive distribution and thickness (sometimes greater than 50 m) of yedoma, make up a significant carbon reservoir (Schirrmeister et al. In press).

Networks of ice wedge polygons are widely distributed across upland yedoma areas on the northern Seward Peninsula. Existing and drained thermokarst lake basins cover >70% of my study area in the Cape Espenberg Lowland (Jones et al. In press), leaving little yedoma upland remaining. Extensive basaltic tephra deposits from the eruption of Devil Mountain Maar Lake 17,500 years B.P. (Beget et al. 1996) can be greater than one meter thick at the study sites and lie 6 - 300 cm below the surface in upland virgin yedoma deposits. Upland vegetation cover consists of shrub tundra commonly populated by *Empetrum nigrum, Vaccinium uliginosum, Betula nana* and *Betula glandulosa* (nomenclature from Hulten, 1968). Upland yedoma bluff slopes adjacent to lake margins are populated largely by *Salix* spp., *Betula nana, Spiraea stevenii, Ledum palustre* and Poaceae. Lower elevation drained lake basins are wetter and populated by *Eriophorum* spp., *Carex aquatilis, Sphagnum riparium* and *Calamagrostis* spp. The mean annual air temperature is 6°C, with a mean summer temperature of 12.6°C and a mean winter temperature of -19.7°C. The mean annual precipitation is 255 mm for the period 1971 - 2000 (Western Regional Climate Center, Western U.S. Climate Historical Summaries,

http://www.wrcc.dri.edu).

I studied in detail the composition and distribution of sediment from two lakes, Lake Claudi and Lake Rhonda (all lake names are informal) and sampled five other lakes at a lower resolution: Three Loon Lake; Tea Lake; Cocker Gap Lake; Prickly Pond; and Lake Jaeger (Figures 2.1 and 2.2, Table 2.1). Lake Claudi is a first-generation lake that formed in yedoma upland. A paleo drainage channel has eroded the north bank of the lake and appears close to reactivation. The southern margin of Lake Claudi is eroding into a first-generation drained lake basin, the basin of former Pear Lake (Plug and West 2009). Modeling of Lake Claudi's formation suggests that it formed from the coalescence of two smaller lakes (Kessler et al. 2012). Lake Rhonda is a later-generation lake, forming within a series of overlapping alases. Lake Rhonda has <25% upland yedoma margin to the south, and >75% low bluff alas margin. The main margin types within Lake Rhonda are high-centered polygon, low-centered polygon, floating vegetation mat and thermokarst-affected upland yedoma. High- and low-centered polygon margins are characterized by low bluffs, 0.2 to 1.0 m high, while floating vegetation mat margins lack bluffs and sit at lake level; both form where Lake Rhonda is eroding into a drained lake basin. Thermokarst-affected upland yedoma margins are characterized by steep bluffs that are up to 20 m high. Three Loon and Cocker Gap Lakes are both of mixed generation, eroding into both upland yedoma and drained lake basins. Lake Jaeger is a first-generation lake similar to Lake Claudi, forming primarily in upland yedoma. The hourglass-shaped outline of Lake Jaeger suggests that it may also have formed from coalescence of two lakes. Tea Lake is a smaller, first-generation lake, <100 m in diameter along the short axis, forming within yedoma upland. Vertical and lateral sediment distribution of both Tea Lake and Pear Pond is available in Appendix Three.

2.4 Methods

2.4.1 Fieldwork

I conducted high-resolution sedimentological analysis on lake cores and established facies distributions from cross-lake transects of sediment cores. With the help of other members of our field crew, I retrieved sediment cores during two field campaigns on the northern Seward Peninsula. In spring 2009, we retrieved 51 cores, totaling 46 m from 31 coring locations across seven lakes (Figure 2.1 and 2.2, Appendix 2). In summer 2010, we obtained 38 cores, totaling 20 m of core from 15 coring locations in two lakes (Figure 2.1 and 2.2). At my intensively studied lakes, Lake Claudi and Lake Rhonda, at each coring location, bathymetry data were recorded at one meter intervals along a N-S and an E-W ten meter transect. Within Lake Claudi, this enabled me to determine the location of baydjarakh highs and lows. Baydjarakhs are the conical mounds of sediment remaining after ice wedge polygons thaw (Kanevskiy et al. 2011). I obtained sediment using a combination of coring systems. Upper sediment was obtained using a square rod Livingstone corer (Wright et al. 1984) modified with a 7.0 cm polycarbonate barrel (Bolivia corer). We obtained deeper, stiffer sediment using a standard square rod Livingston corer (Wright et al. 1984) with a 5.0 cm metal barrel. Continuous cores containing upper and lower sediment were also obtained with a Percussion corer (Reasoner 1993). I obtained two long deep central cores from Lake Claudi using a UWITEC© piston corer (8 kg weight and transparent PVC core liners of 6.35 cm diameter). Coring took place until core refusal occurred due to the presence of stiff silt, coarse tephra or peat.

2.4.2 Lab work

With help from a subset of the project team, I cut polycarbonate core tubes using a medical cast saw and split cores using either a knife or fishing line, depending on the sediment texture. One half of each core was archived at the National Lacustrine Core Facility, Department of Geology and Geophysics, University of Minnesota-Twin Cities (LacCore). I pre-processed and subsampled working core halves at the LacCore lab

facilities. We measured split core point magnetic susceptibility using a GEOTEK multi-sensor core logger-XYZ. I removed anomalously low magnetic susceptibility measurements at core breaks from the data set. I described split cores according to Schnurrenberger et al. (2003) and visually identified key facies according to color, composition, texture, boundary type and sedimentary structure. I identified sediment color using a Munsell color chart, working with wet sediment.

I analyzed a subset of key cores for $\delta^{13}C$, percent total organic carbon (TOC), percent nitrogen (TON), grain size, and macrofossils (Appendix 3). I pretreated 167 bulk sediment samples to remove inorganic carbon by overnight acidification using 2N HCl. Samples were then rinsed with high purity water until neutral (Wolfe et al. 2001), freeze dried, homogenized, weighed, and submitted to the Alaska Stable Isotope Facility at the University of Alaska Fairbanks's Water & Environmental Research Center for determination of $\delta^{13}C$, TOC and % TON on a Delta V isotope ratio mass spectrometer interfaced with a Costech ESC 4010 elemental analyzer. Stable isotope ratios are reported for 167 samples in δ notation as parts per thousand (‰) deviation from the international standard for carbon (PDB). Typically, analytical precision is <0.2 ‰.

I submitted 42 samples for grain size analysis to LacCore. Grain size samples were pretreated with hydrogen peroxide (H_2O_2) to remove organics, sodium hydroxide (NaOH) to remove biogenic silica (BSi) and hydrochloric acid (HCl) to neutralize the sodium and remove carbonates. Pretreated samples were then run on a Horiba particle size analyzer LA-920 according to the LacCore standard operating procedure and based on Jiilavenkatesa et al. (2001) and Horiba particle size analyzer LA-920 manuals.

I processed 92 macrofossil samples according to Birks (2002). Wet sample volume was measured using water displacement, and then samples were then sieved through a 250 μm mesh. Macrofossils were identified using the Alaska Quaternary Center macrofossil collection at the University of Alaska Fairbanks and reference texts (Katz et al. 1965; Ireland 1982). Macrofossil counts were standardized to a volume of seven

cubic centimeters of wet sediment. For all samples, macrofossil counts included chironomid head capsules, seeds identified to genus, *Daphnia* spp. ephippia, *Cenococcum* sclerotia and oribatid mites.

2.4.3 Preliminary geomorphological model

To create the model of facies distribution through time I took into consideration cores taken from first-generation lakes. Some first-generation thermokarst lakes are thought to form from a geographically central point (Hopkins and Kidd 1988). Taking into account local topography and any evidence of coalescence, I used sediment cores from different areas of the lake as analogues for stages of development. Within lakes Claudi and Jaeger, sediment located further from the margin and immediately above the taberal facies is interpreted as the oldest in the lake. As sediments gain distance from the geographic lake center, they are considered to decrease in age. The temporal and spatial scale for lake development is based on 3-D numerical modeling (Kessler et al. 2012) and observed lake expansion rates on the Seward Peninsula (Jones et al. 2011).

2.4.4 Sample statistics

Data sets were tested for normality using the Kolmogorov-Smirnov test. As they were not normally or log normally distributed, I used the non-parametric, rank order, Kruskal Wallis one-way analysis of variance test. When significant differences in variance were found, the Games-Howell test was used to conduct pairwise comparisons, assuming unequal variance. Due to the non-normal distribution of the data, median values are given, as they are based on rank order statistics. All statistical tests were conducted at a confidence limit of $\alpha = 0.05$.

2.5 Results

Section 2.5.1 summarizes results of visual analyses of color, macrofossils, banding and inclusions, and sediment structure. Section 2.5.2 presents results of TOC, C/N, $\delta^{13}C$, grain size, magnetic susceptibility and identification of discrete macrofossils. Section 2.5.3. describes the facies recovered from four individual core sites by facies type for the two intensively studied lakes, Lake Claudi and Lake Rhonda. Sections 2.5.4. and 2.5.5

present results of facies distributions across lakes as functions of distance from thermokarst margins and lake generation. Section 2.5.6 presents a geomorphological model of yedoma thermokarst lake development and changes in facies distribution.

2.5.1 Visual characteristics of facies in sediment cores of northern Seward Peninsula thermokarst lakes

Facies one [F1]: Yedoma Taberal Silt facies. Taberal sediment refers to permafrost which has thawed beneath a water body (Romanovskii et al. 2004). The term is not unique to yedoma lakes (Romanovskii 1993), though yedoma thermokarst lakes are the systems in which taberal sediment has most commonly been recognized (Romanovskii et al. 2004; Grosse et al. 2007; Wetterich et al. 2009). In the northern Seward Peninsula cores, the Yedoma Taberal Silt facies units consist of massive bluish-grey (ca. 5Y 4/1) silt, often containing rootlets and small pieces of terrestrial organic detritus. Black inclusions of unknown composition frequently occur within this facies and range in size from 1 - > 5 cm in diameter. The sediment cores do not penetrate the base of the Yedoma Taberal Silt facies, but the thickness of the taberal unit is expected to be a function of lake depth and lake age (Plug and West 2008). Taberal sediment is expected to be thickest below the oldest section of the lake basin, as vertical thaw will be most advanced there.

Facies two [F2]: Trash Basal facies. Although basal sediment has been described within thermokarst lakes systems previously (Hopkins and Kidd 1988; Murton 1996; Katamura et al. 2006) a Trash Basal facies has not yet been identified. Within this study the Trash Basal facies is interpreted as the terrestrial sediment that existed prior to lake initiation, which then underwent in-situ settlement. In my sediment cores, the Trash Basal facies contains abundant organic detrital material mainly of terrestrial origin (ie. *Carex* spp., *Alnus* spp., and *Empetrum* spp. seeds). Aquatic indicators, including ostracods and *Daphnia* spp. ephippia are also present. The Trash Basal facies was only identified with confidence within Lake Claudi and Lake Jaeger. Within these lakes the Trash Basal facies ranges from eight to ten cm in thickness and the upper and lower

boundaries of the Trash Basal facies are diffuse to distinct. The Trash Basal facies may also be present within Tea Lake, where a trash facies was found to be 35 cm in thick.

Facies three [F3], Layered Basal facies: The Layered Basal facies is found directly above taberal sediment. When present together with a Chaotic Basal facies (discussed below), the Layered Basal facies is found underneath it. The Layered Basal facies is not found with the Trash Basal facies. The Layered Basal facies is characterized by the presence of coarse bands and few fine laminations. Bands and laminations are composed mainly of detrital organic material, silt and retransported tephra. The organic fraction of the Layered Basal facies contains a combination of well-preserved *Drepanocladus capillifolius* leaves and *Carex* spp. seeds, suggesting that terrestrial input mainly comes from a shallow water environment with emergent sedges (Janssens 1983). Bands and laminations vary in width from 1-10 cm and 0.3-1.0 cm respectively and have diffuse boundaries. As a unit, the Layered Basal facies reaches a maximum thickness of 1.25 meters in my sediment cores.

Facies four [F4], Chaotic Basal facies: The predominant characteristic of this facies is a massive silt matrix containing occasional peat balls, lenses or distorted bands of Pleistocene and/or Holocene peat, thawed Pleistocene yedoma and redeposited Devil Mountain tephra. The tephra was originally deposited by the Devil Mountain Maar eruption ca. 17, 500 years B.P. (Hofle et al. 2000; Goetcheus and Birks 2001). Inclusions, bands and lenses of peat, silt and tephra vary greatly in dimension from less than one cm to approximately ten cm, or in the case of silt and tephra, appear as massive facies. Boundaries range from abrupt to diffuse. Tephra inclusions tend to be poorly sorted (based on visual observations) with high magnetic susceptibilities (>50 SI 10^{-6}). The Chaotic Basal facies reaches a thicknesses of approximately two meters.

Facies five [F5], Lacustrine Silt facies: The Lacustrine Silt facies consists of brown silt, generally 2.5Y 3/1, 2.5Y 3/2, 5Y 3/1 or 5Y 3/2. Upper sections of this facies, within 10 cm of the sediment-water interface, are often less firm. Upper sediment frequently contains shell fragment horizons of varying thickness. Horizontal to sub-horizontal

laminations frequently characterize this facies and range in color from 2.5Y 3/1 (light laminations) to 10YR 2/1 to 10YR 3/2 (dark laminations). Lamination width is generally less than 2.0 cm and frequently between 0.3-1.0 cm, although the diffuse boundaries make exact width measurements difficult. Smear slide analysis (Table A.1.4.) shows that dark laminations have a larger fraction of detrital organic matter and a smaller mineral fraction than light laminations. The Lacustrine Silt facies reaches a maximum thickness of approximately 2.0 m in my cores.

2.5.2 Biogeochemical characteristics of facies

Cores from first-generation lakes Claudi and Jaeger and later-generation lakes Three Loon, Cocker Gap and Rhonda were all analyzed for TOC, $\delta^{13}C$, C/N and magnetic susceptibility. Only cores from Lake Claudi were analyzed for grain size.

TOC values are significantly different between facies ($p<0.001$) ($p<0.05$ is considered significant) (Table 2.2). Pairwise comparisons show a significant difference between the TOC of the Lacustrine Silt and Chaotic Basal facies ($p=0.018$), and the Lacustrine Silt and Yedoma Taberal Silt facies ($p=<0.001$) (Table 2.3). The median value of 11.85 TOC for the Trash Basal facies ($n=2$) is highest, followed by the Lacustrine Silt facies, which has a median TOC value of 3.91%. The Chaotic Basal and Yedoma Taberal Silt facies exhibit the lowest median values of 1.32 ($n=22$) and 1.58 ($n=27$) respectively (Figure 2.3, Table 2.4). The Lacustrine Silt facies TOC is not significantly different between any lakes (Table 2.2).

$\delta^{13}C$ values are found to be significantly different between facies ($p<0.001$) (Table 2.2). Pair-wise comparisons show a significant difference between the Lacustrine Silt and Chaotic Basal facies ($p<0.001$), and the Lacustrine Silt and Yedoma Taberal Silt facies ($p<0.001$) (Table 2.5). The bulk organic matter of the Yedoma Taberal Silt facies and the Chaotic Basal facies have higher median $\delta^{13}C$ values (-25.25‰ and -25.63‰, respectively) than that of the Lacustrine Silt, Layered Basal or Trash Basal facies (median values -27.07 ‰, -26.5 ‰ and -27.76 ‰ respectively) (Figure 2.4, Table 2.4). There is a significant difference in $\delta^{13}C$ values of bulk organic matter for the Lacustrine Silt facies

between first-generation Lake Claudi and Lake Jaeger (Table 2.2), because the Lacustrine Silt facies within Lake Jaeger had more depleted $\delta^{13}C$ values. No significant difference in $\delta^{13}C$ values of organic matter in the Lacustrine Silt facies is found between later-generation lakes Three Loon, Cocker Gap and Rhonda. There is a statistically significant difference in the $\delta^{13}C$ values of organic matter in the Lacustrine Silt facies between first- and later-generation lakes (Table 2.2). The organic matter in the Lacustrine Silt facies in later-generation lakes exhibits a lower $\delta^{13}C$ values than that of first-generation lakes (Figure 2.5).

Carbon: nitrogen (C/N) ratios are significantly different between facies ($p<0.001$, Table 2.2). Pairwise comparisons show a significant difference in C/N between the Lacustrine Silt and Yedoma Taberal Silt facies ($p<0.001$) and between the Layered Basal and Yedoma Taberal Silt facies ($p<0.001$), (Table 2.6). The Trash Basal facies exhibits the highest median C/N value of 18, followed by the Lacustrine Silt and Layered Basal facies with C/N values of 13.75 and 13.35 respectively (Table 2.4). The C/N values are not significantly different between the Lacustrine Silt facies in first-generation Lake Claudi and those in Lake Jaeger. Lacustrine Silt facies C/N values are significantly different between later-generation lakes Three Loon, Cocker Gap and Rhonda. The lowest median values are for Cocker Gap Lake.

Mean grain size is significantly different between facies ($p<0.001$, Table 2.2). Pairwise comparisons show a significant difference between the Lacustrine Silt and the Yedoma Taberal Silt facies ($p=0.023$) (Table 2.7). The Lacustrine Silt facies exhibits the lowest mean grain size, with a median value of 22.1 μm, but the greatest inter-quartile range, (Figure 2.6). The Yedoma Taberal Silt facies and Chaotic Basal facies show similar grain sizes, with median values of 26.40 μm and 28.60 μm respectively, both with a positive skew. Grain size distribution curves reflect these characteristics (Figure 2.7).

Magnetic susceptibility is significantly different between facies ($p<0.001$, Table 2.2. Figure 2.8). Pairwise comparison shows a significant difference between all facies, except for the Layered Basal and Lacustrine Silt facies. Magnetic susceptibility of the

Lacustrine Silt facies is significantly different between first-generation lakes and is higher in Lake Claudi than Lake Jaeger (Table 2.2). Magnetic susceptibility of the Lacustrine Silt facies is significantly different between later-generation lakes Three Loon, Cocker Gap and Rhonda (Table 2.2). Rhonda exhibits the lowest magnetic susceptibility and Three Loon, the highest. Finally, magnetic susceptibility for the Lacustrine Silt facies is found to be significantly different between first-generation and second-generation lakes (Table 2.2). The Lacustrine Silt facies of first-generation lakes has a higher median magnetic susceptibility than second-generation lakes.

Qualitative observations of the >250 μm fraction from each facies (see Figure 2.9 for key for subsequent figures)(Figure 2.10.), show that the Lacustrine Silt facies is comprised mainly of fine herbaceous detrital material with a smaller fraction of coarse detrital herbaceous material and lignified detritus. Shell fragments and amorphous detrital material are most abundant in the Lacustrine Silt facies compared to other facies. Shell fragments are also found in the Layered Basal facies. The Chaotic Basal facies is mainly composed of coarse herbaceous and lignified detritus. Wood and insect fragments are present in higher abundance in basal and Yedoma Taberal Silt facies than the Lacustrine Silt facies. The Layered Basal facies has a similar macrofossil composition to the Chaotic Basal facies but contains abundant well-preserved *Drepanocladus capillifolius* (M. Jones pers. comm.). The Yedoma Taberal Silt facies 250 μm fraction is composed mainly of coarse and fine herbaceous material and lignified detritus, possibly of graminoid origin.

2.5.3 Discrete macrofossils

Yedoma Taberal Silt facies (n=3) were found to lack discrete macrofossils with the exception of one *Empetrum* seed. These observations may not be representative of the facies, as only three samples were analyzed. The Trash Basal facies (n=5) is very similar in composition to the Layered Basal facies. It is dominated by *Cenococcum* sclerotia (50%), oribatid mites (16%), ostracods (10%), terrestrial seeds (*Carex* spp., *Alnus* spp., and *Empetrum* spp. combined, 10%) and aquatic seeds (*Potomageton* spp. and *Hippurus*

spp. combined, 6%). Small quantities of *Daphnia* spp. ephippia (6%) and chironomid head capsules (3%) are also observed (Figure 2.11). The Layered Basal facies (n=14) is composed of *Cenococcum* sclerotia (54%), oribatid mites (20%), aquatic seeds (5% *Hippurus* spp. and *Potentilla palustris*), and terrestrial seeds (9%) *Carex* spp. trigonal, *Carex* spp. lenticular and *Empetrum* spp.). Small quantities of *Daphnia* spp. ephippia (3%), chironomid head capsules (3%) and ostracods (7%) are also present (Figure 2.12). The Chaotic Basal facies (n=25) is composed of ostracods (71%), oribatid mites (13%) and terrestrial seeds (12% *Carex* spp. and *Betula* spp.) (Figure 2.13). Discrete macrofossil composition in the Lacustrine Silt facies (n=41) consists of ostracods (81%), with small quantities of chironomid head capsules (6%), *Cenococcum* sclerotia (8%) *Daphnia* spp. ephippia (4%), oribatid mites (1%) and terrestrial seeds (*Carex* spp., *Betula* spp. and *Ericaceae* spp. combined, <1%) (Figure 2.14). No aquatic seeds are present within the Lacustrine Silt facies, suggesting that they are deposited close to the lake margin.

2.5.4 Lake sediment cores

Within the core diagrams, five facies are numbered as follows: F1, Yedoma Taberal Silt facies (oldest deposits); F2, Trash Basal facies; F3, Layered Basal facies; F4, Chaotic Basal facies; F5, Lacustrine Silt facies (youngest deposits). The numbering system reflects the order in which facies were typically deposited, but exceptions occur. Additionally, not every facies is present at each coring site.

SPA-CLAU09 SITE 1 (Figures 2.15 and 2.16) is located in the geographic center of Lake Claudi at a combined ice and water depth of 7.66 m (Figure 2.2). The core was retrieved from a baydjarakh top.

F1, Yedoma Taberal Silt facies: 225 – 250 cm. F1 is comprised of homogenous grey (5Y 4/1) silt with some small (0.5 cm^2) black inclusions with distinct boundaries. Magnetic susceptibility is low, varying from 6.2 to 46.4 SI 10^{-6} with a mean value of 34.44 ± 9.89 SI 10^{-6}. TOC varies from 0.9 to 3.28%, with a mean value of 2.10 ± 1.67% (n=2). The mean C/N value is 9.52 (n=2). The $\delta^{13}C$ of organic matter varies by 1.35 ‰,

with an average value of -26.22 ‰. No macrofossils were found in the sieved 7 cc subsamples (n=2). The >250 μm fraction consists of herbaceous fragments and lignified detritus.

F4, Chaotic Basal facies: 180 – 225 cm. F4 is comprised of brown (5Y 3/1) silty mud mixed with gritty tephra and lacks clear structure. Contacts between tephra and silt are diffuse. Magnetic susceptibility values are high, especially in tephra-dominated sections, with values varying from 60.2 to 8.7 SI 10^{-6} with a mean value of 39.56 SI 10^{-6}. Tephra-dominated sections tend to have a magnetic susceptibility of >50 SI 10^{-6}, peaking at 150 SI 10^{-6}. The TOC values are low, varying from 0.34 to 1.78%, with a mean value of 1.14 ± 0.52% (n=6). C/N values vary from 10.86 to 16.89, with a mean value of 13.82 ± 2.67 (n=6). High C/N values correspond to low nitrogen values of 0.14% or less. The $\delta^{13}C$ values of organic matter vary from -26.65‰ to – 24.38‰, with a mean value of -25.82‰ ± 0.94 (n=6). No macrofossils were identified within this section of the core. The >250 μm fraction is mainly composed of herbaceous fragments and lignified detrital material.

F2, Trash Basal facies: 150 – 180 cm. This facies is composed of dark brown (5Y 3/1) poorly decomposed terrestrial organic material. Large pieces of graminoid stem, leaves, and rootlets protrude from the sediment. The upper and lower boundaries of the facies are diffuse. Magnetic susceptibility makes a sharp negative excursion at the base of the Trash Basal facies, varying from 0.3 to 48.2 SI 10^{-6}, with a mean value of 19.75 ± 12.59 SI 10^{-6}. A sharp positive excursion of TOC occurs throughout this facies. Values vary from 3.84 to 12.81%, with a mean value of 9.20 ± 4.73% (n=3). C/N values record an initial drop to 10.86 followed by an increase to 16.89. $\delta^{13}C$ values of organic matter show little variation. Values ranged from -27.81‰ to -27.37‰, with a mean value of -27.56 ± 0.23 ‰ (n=3).

Standardized numbers of macrofossils show some aquatic indicators in the Trash Basal facies: ostracods and *Daphnia* spp. ephippia. Terrestrial indicators, such as seeds from *Carex, Empetrum* spp. and *Betula* spp. that are characteristic of water-logged alases

(Jones et al. 2011) are present within this facies. *Cenococcum* sclerotia and oribatid mites are also common (ca. 20 per 7cc). The >250 μm fraction is mainly composed of both fine and coarse herbaceous detritus and lignified detritus.

F5, Lacustrine Silt facies: 0-150 cm. This facies is composed of brown (2.5 Y 3/1) silt with darker brown (5Y 3/1) horizontal laminations with diffuse boundaries. Lamination width ranges from 1-3 mm. Lamination spacing is not consistent and ranges from <1 mm to >5 cm. Laminations vary from distinct to indistinct. Magnetic susceptibility ranges from 6.80–69.30 SI 10^{-6} with a mean value of 51.72 ± 12.05 SI 10^{-6}. No trend is apparent and there are no significant excursions. TOC ranges from 2.13 to 4.34%, with a mean value of 3.51 ± 0.68% (n=10). There is a slight decrease in TOC of ca. 1% between 102 and 117 cm depth. The C/N values range from 11.8 to 17, with an average value of 14.25 ± 1.5 (n=10). Values also decrease between 102 - 117 cm depth, as seen in TOC. $\delta^{13}C$ values for organic matter vary only slightly from -27.2 to – 26.7‰, with a mean value of -26.97 ± 0.17‰ (n=10). High numbers of ostracods (maximum of 308 valves per 7 cc) and *Daphnia* spp. ephippia egg cases (maximum of 35 per 7 cc) are present at the top of the core and decrease downcore. The >250 μm fraction is mainly composed of coarse herbaceous fragments with a smaller quantity of fine herbaceous fragments and detrital amorphous material. The lignified detrital material is present at most depths sampled from 55 cm downwards. Shell fragments are also present consistently throughout the facies.

SPA-CLAU09-SITE 2 (Figures 2.17 and 2.18) was taken 30 m from the west margin of Lake Claudi, where water depth was 3.66 m (Figure 2.2). The core was retrieved from a baydjarakh top.

F4 Chaotic Basal facies: 35 – 120 cm. This facies is composed of grey (5Y 4/1) silt with dark brown (5Y 3/1) and black, chaotic, spherical inclusions and bands with diffuse to indistinct boundaries. Inclusions and bands are composed of either tephra of peat. A redeposited black tephra inclusion occurs at 40 – 60 cm depth, coinciding with a magnetic susceptibility peak of 150 SI 10^{-6}. A brown (5Y 4/1) organic detrital band

occurs at 85 and 105 cm depth. Aside from the tephra at 40-60 cm, magnetic susceptibility of this facies ranges from 2.6 to 46.6 SI 10^{-6} with a mean value of 28.77 ± 8.51 SI 10^{-6}. Peaks in magnetic susceptibility coincide with sections dominated by tephra. A drop in magnetic susceptibility occurs between 85 and 105 cm depth, likely due to the organic detrital inclusion and a lack of tephra. TOC values range from 1.43% to 2.83%, with a mean value of 2.08% (n=8). A peak in TOC occurs at 85 – 105 cm depth, due to a peat inclusion. $\delta^{13}C$ values range only slightly downcore from -26.39‰ to -25.25‰, with a mean value of -25.8‰ (n= 8). C/N values also vary little, from 8.82 to 12.36 with a mean value of 11.04 (n=8).

F5, Lacustrine Silt facies: 0-35 cm. This facies is composed of brown (5Y 3/1) silty mud with abundant shell fragments visible at 0-15 cm depth. A faint horizontal black band with diffuse boundaries is present at 5-12.2 cm depth. Well preserved *Drepanocladus capillifolius* fragments are found protruding from this section of the core. Magnetic susceptibility values vary from 20.3 to 74.10 SI 10^{-6} with a mean value of 52.15 ± 14.45 SI 10^{-6}. No tephra is observed within facies five and there are no magnetic susceptibility peaks that exceeded 75 SI 10^{-6}. TOC values range from 2.01 to 4.66%, with a mean value of 3.18 ± 1.24% (n=5). $\delta^{13}C$ values range from -28.56‰ to 26.19‰. Standardized macrofossil counts show an abundance of chironomid head capsules (peaking at 15 per 7cc) and ostracods (peaking at 135 per 7cc). *Carex* spp. seeds are present throughout the core, likely because of high terrestrial input due to close margin proximity. The >250 μm fraction is mainly composed of fine and coarse herbaceous fragments, moss leaflets and shell fragments. Small quantities of lignified detritus and rootlets are also present.

SPA-CLAU10 SITE 2 (Figures 2.2 and 2.19) was retrieved 25 m from SPA-CLAU09 SITE 1, during a summer coring effort in 2010. Water depth was 8.20 m. The core was retrieved from a baydjarakh low (note that SPA-CLAU09-Site 1 was retrieved from a baydjarakh top).

F1, Yedoma Taberal Silt facies: 200 – 225 cm. This facies consists of massive grey (5Y 4/1) silt. Magnetic susceptibility varies from 56.3 to 22.7 SI 10^{-6} with a mean value of 34.98 ± 7.51 SI 10^{-6}. Mean grain size varies from 18.54 to 27.3 μm (n=6)

F4, Chaotic Basal facies: 120 – 200 cm. This facies consists of gritty tephra inclusions or bands in a matrix of grey silt. Boundaries between tephra inclusions are diffuse to distinct. Tephra inclusions vary in diameter from 1 – 7 cm. Magnetic susceptibility varies from 2.2 to 56.3 SI 10^{-6} with a mean value of 29.59 SI 10^{-6}. Peaks of up to 120 SI 10^{-6} coincide with the presence of tephra. Mean grain size ranges from 18.54 to 29.30 μm (n=5).

F5, Lacustrine Silt facies: 0 – 120 cm. This facies has the same visual characteristics and magnetic susceptibility as the lacustrine silt from SPA-CLAU09 SITE 1. Magnetic susceptibility values range from 10.6 to 58.9 SI 10^{-6} and have a mean value of 41.95 SI 10^{-6}, similar to SPA-CLAU09 SITE 1 Lacustrine Silt facies. No extreme peaks in magnetic susceptibility, as seen in facies four, are observed here. Mean grain size varies from 21.7 to 28.7 μm (n=27).

SPA-RHO09 SITE 2 (Figure 2.20 and 2.21) was retrieved 40 m from the north shore of Lake Rhonda (Figure 2.1). The shoreline is currently eroding into the drained lake basin of "Mama" Rhonda, an earlier-generation of thermokarst lake. Water depth was ca.1 meter.

F4, Chaotic Basal facies: 110 – 250 cm. This facies consists of grey (5Y 3/2) silt with inclusions of organic detrital material at varying stages of decomposition, wood fragments and gritty tephra. Inclusions vary in width from 0.5 to 4 cm. Magnetic susceptibility ranges from 0.6 to 151.8 SI 10^{-6}, with a mean value of 49.88 ± 8.91 SI 10^{-6} (n=84). Magnetic susceptibility peaks are caused by the presence of tephra. Their cyclical nature may be caused by inwash events at the lake margin. TOC varies from 0.43 to 12.32%, with a mean value of 9.88 ± 3.56% (n=19). TOC alternates between high and low values downcore with no overall trend. $\delta^{13}C$ values range from -28.13 to

-23.62 ‰, with a mean value of -26.45 ± 1.35 ‰ (n=19). C/N values range from 8.98 to 17.3 and have a mean value of 12.93 ± 2.19 (n=19). No identifiable macrofossils are present within this facies. The >250 μm fraction is mainly composed of fine herbaceous fragments and lignified detritus.

F3, Layered Basal facies: 60-110 cm. This facies consists of a tan (2.5 Y 4/2) silt matrix with bands of both tephra and peat. Bands range in thickness from 1-3 cm. The mean value for magnetic susceptibility is 8.144 ± 5.96 SI 10^{-6} (n=16). The mean value for TOC is 6.16 ± 4.98 % (n=16). TOC increases downcore, with clear peaks at 79 and 105 cm depth. Clear peaks in TOC are frequent through the facies and occur where peat inclusions are present. The mean value for $\delta^{13}C$ is -27.33 ± 0.47 ‰ (n=16). The mean value for C/N is 7.68 ± 6.06 (n=16). A distinct peak in C/N values also occurs at 62 cm depth. Standardized macrofossil counts show abundant seeds towards the top of the facies, both terrestrial (*Carex* both lenticular and trigonal, and *Empetrum*) and aquatic (*Potomageton*, *Hippurus*, *Potentilla palustrus*). Fine herbaceous detritus is abundant. A prominent decrease in MS occurs at 95 – 100 cm depth. TOC has average values of 9.97 ± 1.51% (n=13).

F2, Trash Basal facies: 49 – 60 cm: This facies is composed of dark brown (5Y 3/1), poorly decomposed terrestrial organic material. The upper and lower boundaries of the facies are diffuse. Magnetic susceptibility values have a mean value of 4.40 ± 3.49 SI 10^{-6}. Standardized numbers of macrofossils show the presence of only *Carex* seeds, *Cenococcum* sclerotia and oribatid mites. The >250 μm fraction is composed of herbaceous detritus, lignified detritus and wood fragments.

F5, Lacustrine Silt facies: 0 - 49 cm: This facies consists of brown 2.5Y 3/1 fine silty mud. Darker horizontal laminations with diffuse boundaries occur throughout the facies. Lamination width ranges from 1mm - 0.5 cm. Magnetic susceptibility values have a mean value of 14.11 ± 4.36 SI 10^{-6} (n=112). $\delta^{13}C$ values range from -28.4 ‰ to -27.19 ‰ and have a mean value of -27.79 ± 0.31 ‰ (n=13). The mean value of C/N is 16.83 ± 1.7 (n=13). No identifiable macrofossils are present in this facies. The >250 μm

fraction is mainly composed of fine detrital herbaceous fragments and lignified detritus. Lignified detritus increases down through the facies.

2.5.5 Facies distribution

Lake Claudi, first-generation (Figure 2.22): Yedoma Taberal Silt facies deposits are consistently identified beneath both the Chaotic Basal and Layered Basal facies. Either Chaotic Basal or Layered Basal facies are present at all sites sampled. The combined thickness of the Chaotic Basal and Layered Basal facies increases with distance from the lake margin (see section 2.4.5 below). Chaotic Basal facies thickness ranges from 1 to 2 m. The Layered Basal facies ranges in thickness from 0.2 to 1 m. The Lacustrine Silt facies is not present <20 m from the lake margin but increases in thickness between 20 and 150 m from the lake margin. The Lacustrine Silt facies thickness ranges from 0.3 to 2 m.

Lake Jaeger, first-generation (Figure 2.23): Yedoma Taberal Silt facies deposits are only identified at the lake center and are found to be below all other facies. Chaotic Basal facies thickness ranges from 0.6 - 1.5 m. The Layered Basal facies is only present close to the margin (<20 m), where the Chaotic Basal facies is present also. At this location, the Layered Basal facies thickness is 0.45 m. The Lacustrine Silt facies is present at every location sampled and exhibits a general increase in thickness between the lake margin and lake center. The Lacustrine Silt facies thickness ranges from 0.2 to 0.7 m.

Lake Rhonda, later-generation (Figure 2.24): The two sampling locations within 50 m of Lake Rhonda's northern alas margin exhibit similar sediment composition and structure. The Chaotic Basal facies, ranging in thickness from 0.39-0.59 m, is present at Lake Rhonda's northern alas margin. Above the Chaotic Basal facies is the Lacustrine Silt facies, ranging in thickness from 0.48 - 0.57 m. At Lake Rhonda's center, ca. 700 m from the northern alas margin, the Trash Basal facies and Chaotic Basal facies are absent. A 1.19 m thick unit of the Layered Basal facies was identified, above which is a 1.05 m thick unit of the Lacustrine Silt facies.

Cocker Gap, later-generation (Figure 2.25): Yedoma Taberal Silt facies sediment is present within sediment cores adjacent to both the upland yedoma margin and the alas margin, but not at the lake center. The Chaotic Basal facies is present at all locations sampled and ranges in thickness from 0.5 to 0.91 m. The Lacustrine Silt facies, lacking laminations, is present above the Chaotic Basal facies at the alas margin and lake center. The Lacustrine Silt facies ranges in thickness from 0.26 - 0.35 m.

Three Loon, later-generation (Figure 2.26): Yedoma Taberal Silt facies sediment is not present at Three Loon Lake. Closer to the margin, the Layered Basal facies is overlain by the Chaotic Basal facies. Toward the lake center, the Layered Basal facies is overlain by the Lacustrine Silt facies. The Chaotic Basal facies is 0.4 m thick, the Layered Basal facies is 0.8 m thick and the Lacustrine Silt facies is 0.1 m thick.

2.5.6 Relationship between facies thickness and lake margin

To explore the relationship between facies thickness and distance from the margin within first-generation lakes Claudi and Jaeger, I calculated the *r* coefficient for distance from the margin and both Lacustrine Silt facies and basal facies combined (F4 and F3) thickness. I only used data from sediment accumulating on baydjarakhs highs, not baydjarakh lows. I found a statistically positive correlation between Lacustrine Silt facies thickness and distance from the margin (r^2=0.73, n=7, p<0.03) as well as a statistically negative correlation between thickness of basal facies and distance from the margin (r^2= -0.75, n=7, p<0.02), (Figure 2.27). Basal facies thickness ranges from as little as 0 cm at the lake center, to ca. 150 cm at the lake margin. The Lacustrine Silt facies thickness ranges from ca. 20 cm at the lake margin to over 200 cm at the lake center. The Trash Basal facies, which is found primarily in the center of the lake, is not identified at enough locations across the lakes to be included in this analysis.

2.6 Discussion

2.6.1 Characteristics of northern Seward Peninsula thermokarst lake facies identified

Five key facies occur within yedoma thermokarst lakes on the Seward Peninsula: Yedoma Taberal Silt facies, Trash Basal facies, Chaotic Basal facies, Layered Basal facies and Lacustrine Silt facies. Visual analysis (Table 2.4, Figures 2.16, 2.18 and 2.21), and downcore trends (Figure 2.15, 2.17, 2.19 and 2.20) indicate key differences between facies. Trends in downcore data complement visual facies identification well, especially in the case of magnetic susceptibility (Figures 2.15, 2.17, 2.19, and 2.20).

Kruskal Wallis tests comparing median values of $\delta^{13}C$, TOC, grain size and magnetic susceptibility show significant differences among all facies. Despite this, pairwise comparisons show that differences between some facies are not significant. For example, the Kruskal Wallis test shows that median TOC values are significantly different between facies, but pairwise comparisons show that there are no significant differences between the Lacustrine Silt facies, the Layered Basal facies and the Trash Basal facies (Table 2.3). Similarly, pairwise comparisons of $\delta^{13}C$ values show no significant difference between the Lacustrine Silt facies and either the Layered Basal facies or the Trash Basal facies (Table 2.5). In light of this, median biogeochemical values alone are not a satisfactory method for differentiating between facies and must be combined with other parameters including visual analysis, macrofossil identification, and downcore trends.

Macrofossil analysis reveals differences between facies, although composition varies more between some facies than others (Figures 2.10). The Chaotic Basal facies and Yedoma Taberal Silt facies display similar compositions, as do the Trash Basal facies, the Layered Basal facies and to a lesser degree the Lacustrine Silt facies.

Both the Chaotic Basal facies and Yedoma Taberal Silt facies are dominated by similar fractions of lignified detritus, wood fragments, fine (<300 μm) herbaceous detritus and coarse (300 >μm) herbaceous detritus. Similarity of macrofossil composition indicates

that sections of the Chaotic Basal facies directly originated from deformed Yedoma Taberal Silt facies. The main difference between the Chaotic Basal facies and Yedoma Taberal Silt facies is the presence of rootlets and moss fragments in the Yedoma Taberal Silt facies.

The Layered Basal and Trash Basal facies, and to a lesser degree the Lacustrine Silt facies, also display similar compositions (Figure 2.10). The shallow margin depositional environment of both the Layered Basal and Trash Basal facies is reflected by a higher percentage of lignified detritus. The Lacustrine Silt, Layered Basal and Trash Basal facies display the most diverse macrofossil compositions, reflecting different levels of input from yedoma, peat and aquatic sources (Figure 2.10). In contrast, both the Chaotic Basal facies and Yedoma Taberal Silt facies macrofossils illustrate a more similar, less diverse macrofossil composition.

Discrete macrofossil assemblages within each facies also vary. The Yedoma Taberal Silt facies lacks discrete macrofossils with the exception of a single *Empetrum* spp. seed. This lack of discrete macrofossils could either be due to the small number of samples analyzed or generally low concentrations of discrete macrofossils within the Yedoma Taberal Silt facies. Yedoma sediment from the Lena Delta region is also found to be macrofossil-poor (Wetterich et al. 2008).

The discrete macrofossils present in both the Trash and Layered Basal facies indicate that there are similarities in the depositional environments in which they form (Figures 2.11 and 2.12). Both are dominated by the terrestrial indicators *Cenococcum* sclerotia and oribatid mites. Within the Trash Basal facies, seeds from shallow margin areas (*Hippurus* spp., *Potomageton* spp.) are present alongside seeds typical of slopes and uplands (*Carex* spp., *Alnus* spp., and *Empetrum* spp.). Similarly, within the Layered Basal facies, seeds from plants that inhabit lake shore environments (*Pontentilla palustris*), shallow margin areas (*Hippurus* spp.), terrestrial slopes and yedoma uplands (*Carex* trigonal, *Carex* lenticular, *Empitrum* spp.) are all present, indicating a margin depositional environment.

Although the Chaotic Basal facies lacks aquatic seeds, it does contain high numbers of both ostracods and chironomid head capsules (Figure 2.13). The absence of aquatic seeds may be due to high sedimentation rates in areas of Chaotic Basal facies formation. High sedimentation rates may prevent the establishment of aquatic plants such as *Hippurus* spp. and *Potomageton* spp. Interestingly, *Cenococcum* sclerotia are also absent from the Chaotic Basal facies. One possible explanation is that they may have been broken down.

Ostracods and chironomid head capsules, the aquatic indicators, dominate the Lacustrine Silt facies (Figure 2.14). Terrestrial indicators are less abundant within the Lacustrine Silt facies than the Trash Basal and Layered Basal facies. This is likely due to most discrete terrestrial macrofossils being deposited close to the margin.

Interpretation of discrete macrosfossil abundances of *Daphnia* spp. ephippia, seeds and chironomid head capsules are complicated by changes in sedimentation rates at different stages of lake development. Aquatic macrofossils are also likely to be affected by changes in nutrient availability and trophic shifts as the lake develops (Wetzel 2001). Macrofossil abundance is also affected by variation in sedimentation due to productivity shifts and changes in terrestrial inputs. At a constant level of productivity, the concentration of macrofossils would be lower at times of high sediment accumulation as opposed to low sediment accumulation (Wetzel 2001).

The Yedoma Taberal Silt facies occurs beneath all other facies in some of the longer cores. The thaw of permafrost and subsequent melting of excess ice results in the deformation of any sedimentary structures present. The presence of this subaerially deposited taberal facies is a consistent feature in both yedoma and non-yedoma thermokarst lakes (Hinkel et al. 2003; Romanovskii et al. 2004; Wetterich et al. 2009). Within this study, taberal sediment forms from the in-situ thaw of permafrost below yedoma thermokarst lakes.

Above the Yedoma Taberal Silt facies, Basal deposits are consistently identified. Because of a range in characteristics, I divided them into three different facies: F2) a visually distinct band consisting of poorly decomposed organics (the Trash Basal facies); F3) coarsely layered, redeposited mineral and organic sediment (the Layered Basal facies); and F4) chaotic redeposited mineral and organic sediment (the Chaotic Basal facies). Basal sediments provide a transition between (F5) the Lacustrine Silt facies and (F1) the Yedoma Taberal Silt facies (Figures 2.15 and 2.19).

The Trash Basal facies in first-generation lakes appears to be a transition from the terrestrial to aquatic environment that occurs upon initial thaw and collapse. High TOC, low magnetic susceptibility values and the appearance of aquatic indicators such as *Daphnia* spp. ephippia characterize the Trash Basal facies (Figures 2.11, 2.15 and 2.20).

The Trash Basal facies is the least prevalent facies identified along the margin to center transects in first-generation lakes on the northern Seward Peninsula. In the majority of first-generation lake cores, especially those taken closer to the margin, the Trash Basal facies is not apparent (Figure 2.17 and 2.19). One possibility is that the Trash Basal facies may become increasingly disturbed as high, steep bluffs develop (Figure 2.28), slumps occur, and sediment washes in. However, during fieldwork in summer 2009 in Siberia, I observed that an intact Trash Basal facies extended across the entire basin of numerous yedoma thermokarst lakes in northeast Siberia. This may be due to lower angle, more gently sloping bluffs at the lake margin as a result of differences in sediment composition, vegetation cover, and the extent to which roots bind together the terrestrial organic layer. Further investigation into controls on Trash Basal facies formation and distribution within yedoma thermokarst lakes is needed. Within a lake that forms and expands equally in all directions from a central point, the Trash Basal facies will represent lake initiation. Therefore the Trash Basal facies is the most important facies for lake chronology, as dating this facies will provide the approximate time of lake initiation.

Unfortunately, yedoma thermokarst lakes do not consistently expand from a point of initiation at the geographic center as suggested previously (Hopkins and Kidd 1988).

Expansion rates are understood to be largely dependent on topography (Kessler et al. 2012) and excess ice content (Plug and West 2008; West and Plug 2008). Variations in both factors will lead to different lake expansion rates along different margins. Margin slope aspect also may affect rate of expansion, as south facing slopes probably receive more sunlight. Coalescence may also occur during lake formation (Grosse et al. In press), further complicating the relationship between age and location within the lake basin. Interpretation of the Trash Basal facies should take into account these variables.

The Layered Basal facies represents a low energy margin environment where sorting of course detrital material occurs. Alternating beds of silt, tephra and detrital organics suggest that material entering the lake is retransported, sorted and redeposited in layers by wave action at the lake margin. I propose that the development of the Layered Basal facies relies on the presence of a shallow margin shelf, facilitating reworking of material by wave winnowing. This is supported by the presence of the Layered Basal facies within lakes with larger surface areas (Table 2.1): Claudi; Jaeger; Three Loon; and Rhonda. The Layered Basal facies is absent in smaller lakes, Prickly Pond and Tea Lake (Figures A-3-2 and A-3-3), where wave fetch may be insufficient to rework material into the Layered Basal facies. Deposition of detrital material, in the form of the Chaotic Basal facies from bluffs, must also occur close to the location of the Layered Basal facies deposition. Material must be deposited close by and not directly at the location of Layered Basal facies formation in order to preserve facies structure. Material is then retransported, sorted and deposited in the form of the Layered Basal facies. Prevailing winds largely control the direction of surface currents within lake systems (Wetzel 2001). Therefore, it would be expected that the prevailing wind direction would affect the spatial distribution of the Layered Basal facies around the lake margin. Margin sections of the lake receiving the highest energy and most frequent wave action are probably more susceptible to margin erosion and sorting of material.

I interpret the Chaotic Basal facies to represent both a margin depositional environment and a zone of disturbance beneath subaqueously deposited material. Within a mature

yedoma thermokarst lake, coarse material is deposited close to the margin and fine debris and sediment are transported towards the lake center. Lack of sorting within the Chaotic Basal facies is reflected in a chaotic structure. The Chaotic Basal facies exhibits similar grain size to Yedoma Taberal Silt facies sediment, suggesting that the Yedoma Taberal Silt facies makes up a large portion of the Chaotic Basal facies and that deposition occurs in close proximity to the sediment source. Another possible mechanism responsible for the development of the Chaotic Basal facies is the distortion of Yedoma Taberal Silt facies due to continuing subsidence and thaw of excess ice as the lake expands. Evidence of this process in the form of basal sediment faulting has been described for thermokarst lakes that formed on the Tuktoyaktuk Peninsula (Murton 1996). Basal faulting is a plane of weakness within the sediment that is visible as a linear fracture or unconformity.

Both the Layered Basal and Chaotic Basal facies contain tephra from the Devil Mountain Maar eruption (Beget et al. 1996). The thickness of the tephra from the Devil Mountain Maar eruption is not constant at the study sites (Hofle et al. 2000; Goetcheus and Birks 2001) but reaches a maximum of up to a few meters (Charron 1995; Beget et al. 1996). The closest study site to Devil Mountain Maar is Tea Lake, with a distance of approximately 11.5 km, while the farthest study site is Lake Rhonda, with a distance of approximately 16 km. In addition to the Devil Mountain Maar tephra, the Aniakchak (3,400 yrs BP) and White Fish (>100,000 yrs BP) tephras were also found in the region, but consist of much finer particles (Beget et al. 1991). Within Chaotic Basal and Layered Basal facies, tephra inclusions and layers directly correlate with high magnetic susceptibility. Large grain size is also evident within deposits containing tephra. Despite local variation in tephra thickness, the amount of tephra incorporated into Layered Basal and Chaotic Basal facies, and subsequently magnetic susceptibility values and grain sizes, is expected to decrease with increased distance from the Devil Mountain Maars.

The Lacustrine Silt facies is the most prevalent facies and forms within deeper, calmer waters where fine material is able to settle out of suspension. The presence of the Lacustrine Silt facies within less than 20 m of Lake Jaeger's margin (Figure 2.23)

suggests that this depositional environment develops relatively quickly following margin expansion.

Partial lake drainage events either within the lake or from adjacent lakes that can rapidly affect lake water levels and may also affect sedimentology, most likely causing a lithological unconformity. Drainage could take place into adjacent lakes, potentially introducing new sediment into a lake system. Partial drainage events within a lake system may result in the removal of surface material from the lake sediment package. During summer fieldwork in the Kolyma River Lowlands, I observed drained yedoma thermokarst lake basins where enough sediment had been removed to create drainage channels up to 15 m deep. Drainage of adjacent lakes may cause redeposition of sediment which would likely lack clear structure, potentially making them difficult to distinguish from the Chaotic Basal facies. Partial drainage events may be equally challenging to identify. Depending on the degree of water level change and the duration of the event, the drainage event may cause an increase in productivity and aquatic plant growth, potentially leading to an increase in total organic carbon levels and aquatic macrofossils. Full or partial drainage events have been found to occur catastrophically on time scales ranging from hours to a few days or as a gradual process continuing for years to decades (Grosse et al. In press). Identification of drainage events is important when reconstructing landscape dynamics and evolution.

Lake water level may also be affected on decadal scales by climate patterns, such as the warmer, drier temperatures experienced within the Arctic during the late 1970's that was induced by shifts in the Pacific Decadal Oscillation (Hartmann 2005; Labrecque et al. 2009). Warmer temperatures would have increased evaporation of lake water. Shifts in lake levels would likely have an effect on erosion and sediment accumulation within thermokarst lakes.

All facies identified within first-generation lakes are found in later-generation lakes. The distribution of facies in later-generation lakes is more challenging to explore due to high variability of margin type and extent. As a result of this variability, margin types appear

to affect facies development within later-generation lakes. Short cores were collected from Lake Rhonda at different margin types (high-centered polygon, low-centered polygon, floating vegetation mat and thermokarst-affected upland yedoma). Sediment accumulation at high- and low-centered polygon margins (those eroding into drained lake basins) is characterized by thin, frequent bands of fine organic detritus. This likely represents frequent reworking of terrestrial material from the eroding margin into the lake. In contrast, sediment accumulation at the thermokarst-affected upland yedoma margin is largely unlaminated silt with fewer, thicker bands of organic detritus, possibly an indication of large, infrequent erosion events.

The Yedoma Taberal Silt facies is present within later-generation thermokarst lakes where margins are eroding into upland virgin yedoma, but absent where margins are eroding into drained lake basins. The apparent absence of taberal deposits beneath other areas is likely due failure to penetrate deep enough to sample previous generation(s).

Differentiating between earlier and current generation basal facies within later-generation lakes proved to be challenging. If the lake does not drain fully in all areas and remnant lakes persist, there may not be any clear indication, such as a Trash Basal facies, of a transition between generations. It is often unclear whether the Chaotic Basal facies is from the previous generation, preserved and in-situ, or whether cryoturbation has transformed the previous generations facies into the Chaotic Basal facies. Cryoturbation may occur within drained lake basins (Hinkel et al. 2003) during periods of ice aggregation, or during winter months when shallower remnant lakes freeze to the bottom. However, terrestrial peat – lake sediment contacts in the study region were found to be largely unaffected by cryoturbation (Jones et al. In press; G. Grosse pers. comm.).

Unlike in first-generation lakes, the different basal facies are not consistently present between the Yedoma Taberal Silt facies and the Lacustrine Silt facies. They are only present at margins eroding into upland virgin yedoma.

In conclusion, yedoma thermokarst lake sediment on the Seward Peninsula consists of five different facies. Identification of facies is possible by combining visual, biogeochemical, downcore and macrofossil characteristics. Interpretation of thermokarst lake sediment must be done with caution, taking into account adjacent geomorphology, geology, permafrost characteristics, evidence of past lake dynamics such as coalescence and drainage events, and age of a lake.

2.6.2 Stages of first-generation thermokarst lake formation and their affect on facies distribution

Lateral and vertical facies distribution is found to vary in first-generation lakes Jaeger and Claudi. Changes in facies distribution appear to be at least partially a function of distance from the lake margin. Data from both lakes illustrate a negative relationship (R^2 =0.5692) between distance from lake margin and combined thickness of basal facies and a positive correlation between Lacustrine Silt facies thickness and distance from margin (R^2 = 0.53316) (Figure 2.27). A thinner Chaotic Basal facies at the lake center may be explained by the absence of steep high bluffs during the first 100 years of lake development, although the Chaotic Basal facies formed through the thawing of the Yedoma Taberal Silt facies under the lake should remain consistent across the lake. I used a mean expansion rate of 0.16 m/yr for lakes with an area of 0.1 - 1 ha (Jones et al. 2011) and assumed a constant expansion rate over time. I then applied these measurements to Lake Claudi and calculated that it would have expanded 16 m over 100 years at each margin, totaling 32 m of expansion. Therefore, Lake Claudi was approximately 32 m in diameter before lake subsidence progressed enough to produce steep, high bluffs.

Interestingly, within Lake Claudi both vertical and horizontal variation in the distribution of facies between baydjarakh highs and lows is observed. Overall, baydjarakh lows display thicker sediment packages, possibly due to redeposition of material down slope. Baydjarakh lows closer to the margin contain the Layered Basal facies and no Chaotic

Basal facies in contrast to baydjerakh highs that consist of the Chaotic Basal facies only, suggesting better preservation of layering produced through lacustrine processes within baydjarakh lows. During my summer field season in 2010 I observed similar characteristics in baydjarakh lows exposed at the southern margin of Lake Claudi, where the lake erodes into the margin of Pear Basin. Towards the center of Lake Claudi (>40 m from the lake margin), the Layered Basal facies was absent from both baydjarakh highs and lows. One possible explanation for this is that continued deformation due to lake settlement results in the eventual deformation of layers preserved within baydjarakh lows. Alternatively, the Layered Basal facies may never have existed due to insufficient wave fetch.

Distance from the margin and time since initial thaw and collapse may explain why Lacustrine Silt facies increases in thickness towards the lake center. Lake depth also tends to increase with distance from margin, producing deeper waters where waves may not propagate to the water-sediment interface. In calmer areas of the lake, finer material can settle out of suspension (Shaw 1988). Within a perfect system, the lake will expand from a geographic center (Hopkins and Kidd 1988), therefore sediment accumulation has been occurring for the longest period of time at the center of the lake (Figure 2.28).

2.6.3 Geomorphological model of lake development and exceptions to the model

My preliminary geomorphological model of yedoma thermokarst lake development illustrates the facies present and their changing distribution within a lake through time (Figure 2.28). The age ranges for each developmental stage are preliminary. They are based on observed Seward Peninsula yedoma thermokarst lake expansion rates (Jones et al. 2011), and numerical modeling of both yedoma thermokarst lake talik development (Kessler et al. 2012) and bluff development (M. Kessler., pers. comm.). In the first stage of development (0-50 years), initial thaw and collapse occurs, leading to the formation of

the Trash Basal facies. No other facies are present (Figure 2.28a). The time frame for this initial stage of lake development (0-50 years) takes into account the potential for a small pond to remain undeveloped until the right climatic or hydrological conditions facilitate further development. In the second stage of lake development (50-100 yrs [Figure 2.28b]), vertical subsidence and lateral erosion deepens the lake and the Yedoma Taberal Silt facies forms beneath the lake. The Lacustrine Silt facies begins to accumulate in central areas of the lake. In the third stage of development (100-500 years [Figure 2.28c]), baydjarakh topography emerges as ice wedge thaw progresses downward. Bluff height increases and the Chaotic Basal and Layered Basal facies appear as a result. Further deformation of sediment below a sub-lacustrine unconformity occurs. The Yedoma Taberal Silt facies thickens. Lacustrine Silt continues to accumulate in the center of the lake and also towards the lake margin. While the Lacustrine Silt facies exhibits thinning towards the lake margin, the Chaotic and Layered Basal facies exhibit thickening because of continued slumping and increasing bluff height at the lake margin. In the final stage of lake development (>1,000 years [Figure 2.28d]), excess ice becomes completely depleted beneath the lake center and downward thaw bulb growth continues. The lake bottom begins to flatten from the center outwards.

Although the sediment distribution and thickness are based on average values from lakes Claudi and Jaeger, some exceptions to the model are identified. Within Jaeger, the Lacustrine Silt facies shows a general increase in thickness away from the lake margin, but thickness was greater 70 m from the lake margin than 140 m from the margin. Although a positive correlation exists between distance from lake margin and thickness of the lacustrine facies (Figure 2.27), this suggests that the relationship is not necessarily linear. One possible explanation is that Jaeger did not expand from a central point but initiated somewhere closer to the margin. This would mean that the current lake center is not where sediment accumulation has been taking place for the longest, but instead this point lies closer to the lake margin. In addition, sediment distribution patterns and thickness may vary due to the specific baydjarakh and trough configuration, causing very local highs and lows in the bathymetry of these lakes.

Partial drainage may occur gradually or catastrophically (Jones et al. 2011; Grosse et al. In press). Partial drainage is evident at Lake Claudi in the form of an inactive drainage channel located at the north margin. This preliminary geomorphological model does not take into account the effect of drainage events on facies distribution. Sediment accumulation rates and distribution may also be affected by these aforementioned drainage events. Sediment loss may occur through partial drainage during lake development. Similarly, sediment influx from neighboring lakes experiencing gradual or catastrophic drainage may occur.

The model is based on a simple, linear expansion rate, yet in reality, expansion rates are complicated by bank retreat, which is regulated by how rapidly material is removed from thawing banks and transported into the lake and surrounding basins (Kessler et al. 2012). Until in-situ thawed bank material is removed, it protects underlying material from further thaw, thereby preventing margin retreat. The temporal scale of lake development could be improved by dating basal sediment between the lake center and lake margin. This would provide additional information regarding expansion and sediment accumulation rates and their variability through the life span of the lake.

This study does not incorporate radiocarbon dates because samples of discrete terrestrial macrofossils taken from the Trash Basal facies of Lake Claudi and Lake Three Loon, yielded dates that were unreasonably old (>20,000 and 4,615 years BP respectively, Table A.3.1). This is likely due to the storage of old soil carbon within permafrost for long periods (Nelson et al. 1988, Oswald et al. 2005). Old carbon is released upon thaw and incorporated into the lake system. In addition, modern, living, aquatic plants yielded radiocarbon ages of ~ 2,000 years BP (Table A.3.1). This suggests that old carbon released upon thaw in the form of methane (Walter et al. 2007) is being metabolized by modern aquatic plants.

In light of this, radiocarbon dates from yedoma thermokarst lakes should be interpreted with caution. One potential aide to interpretation would be to date sets of identifiable terrestrial macrofossils throughout the Lacustrine Silt facies. This would enable the

development of an age-depth model that would highlight anomalous ages. Another option would be to explore the application of optically stimulated luminescence (OSL) dating to yedoma thermokarst lake sediment (Long et al. 2011). OSL dating determines when specific minerals were last exposed to sunlight. The effectiveness of this method would depend on whether sufficient light penetrates through the lake water to reset the signal in mineral grains suitable for OSL.

Thaw bulb, or talik development and vertical subsidence also depend on a number of factors that are likely to vary within and between thermokarst lake regions. Thermal conductivity of material below the lake and subsequent heat transfer from the lake water into the thaw bulb depends on the average temperature of the lake bed, substrate density, and ice density (Kessler et al. 2012). Thaw bulb development is initially more rapid. Development slows as existing sections of the thaw bulb begin to insulate underlying permafrost and heat has to be transferred through more material.

This preliminary model of thermokarst lake development does not represent all first-generation yedoma thermokarst lakes, in particular those influenced by coalescence, sediment loss due to partial drainage (Kessler et al. 2012), or sediment redeposition due to adjacent lake drainage. Despite this, the model provides a platform from which to explore yedoma thermokarst facies composition and distribution through time in greater detail and an opportunity to identify scenarios that deviate from the model in future lake sediment investigations.

2.6.4 Comparison between first- and later lake generation

Visual characteristics, magnetic susceptibility, and TOC values of the Lacustrine Silt facies are the same between lake generations, whereas C/N and $\delta^{13}C$ values are found to be significantly different (Table 2.2). C/N is higher and $\delta^{13}C$ values are more depleted in later-generation lakes Rhonda, Cocker Gap and Three Loon than in first-generation lakes Claudi and Jaeger. High levels of C/N indicate either a higher rate of terrestrial input or more rapid decomposition of organic matter (Meyers 2003) within later-generation lakes. This is contradicted by the fact that decomposition generally results in enrichment of $\delta^{13}C$

because lighter isotopes are preferentially utilized (Meyers and Lallier-Vergès 1999). Depleted $\delta^{13}C$ values in later-generation lakes may be a result of different algal productivity rates, differences in the $\delta^{13}C$ signature of terrestrial material entering later-generation lakes compared to first-generation lakes (Meyers and Lallier-Vergès 1999), or methane oxidation within later-generation lake sediment (Barker and Fritz 1981). Lastly, the availability and uptake of HCO_3 may also vary between first- and later-generation lakes. For example, there may be more plants able to take up HCO_3 within later-generation lakes, leading to more depleted bulk sediment $\delta^{13}C$ values (Keeley and Sandquist 1992).

Facies distribution in later-generation lakes Rhonda, Cocker Gap and Three Loon, (Figures. 2.24, 2.25, and 2.26) exhibits more heterogeneity than facies distribution in first-generation Lake Claudi and Lake Jaeger (Figures 2.22 and 2.23). Interestingly, Cocker Gap exhibits similar sediment facies distribution to margin sections of first-generation lakes Jaeger and Claudi because part of the Cocker Gap shoreline is eroding into upland yedoma. Therefore, a lake's or drained lake's position relative to surrounding alases and upland yedoma should be taken into account when interpreting sediment. Unlike first-generation lakes, later-generation lakes do not appear to contain baydjarakhs and their lake bottoms are relatively flat. It is possible that baydjarakhs are present, left over from the first-generation lake's formation, but their expression at the surface is muted due to subsequent sediment infilling. It is plausible that baydjarakhs could be absent in some later-generation lakes due to erosion associated with lake drainage and succession.

2.6.5 Comparison to existing research on yedoma thermokarst lake sediment composition and distribution

My findings are supported by existing research on northern Seward Peninsula yedoma thermokarst lakes (Hopkins and Kidd 1988) (Table 2.9, see Figure 2.29 for all sites discussed within sections 2.6.5 and 2.6.6). Hopkins and Kidd (1988) identified both a sandy, organic-rich detrital basal unit and an overlying unit of fine-grained, bedded

sediment similar to my basal facies and lacustrine silt facies, respectively. I also identified two main differences between our findings and those of Hopkins and Kidd (1988). First, basal deposits vary enough visually to be divided into three sub-facies, instead of the single basal facies described by Hopkins and Kidd (1988). Second, Hopkins and Kidd (1988) described ice wedge pseudomorphs filled in by alternating layers of detrital organic material and mineral deposits, which is only sometimes similar to our observations of baydjarakhs filled by the Layered Basal facies. Through field observations based on up to 13 core sites per lake in two lakes (Claudi and Jaeger), I found that the presence of the Layered Basal facies is limited to within 40 m of the lake margin in first-generation lakes, while baydjarakh topography is more extensive and continued across the lake. As ice wedge pseudomorphs develop over time, they become filled with the Lacustrine Silt facies. Eventually, lake settlement may lead to the deformation of sedimentary structures and the creation of the Chaotic Basal facies within the ice wedge pseudomorph.

Analyses of yedoma thermokarst lake exposures within approximately 30 km of my study lakes by Charron (1995, Sections 3 and 4) indicate the presence of two facies with structures similar to the Chaotic Basal, Layered Basal, and Trash Basal facies (Table 2.9). Charron (1995) describes an inorganic matrix with organic silt inclusions (Section 3, Unit A), which I interpret as a Chaotic Basal facies. Charron (1995) describes a unit consisting of alternating bands of peat and organic silt (Section 3, Unit D) that I interpret as the Layered Basal facies. Charron's (1995) Chaotic and Layered Basal facies equivalents are separated by a 14 cm thick band of peat composed of flat lying twigs and moss (Section 3, Unit C), which appears to be a Trash Basal facies separating two generations of thermokarst lake. Within Charron's (1995) study, three forms of lacustrine fill are present. Charron (1995) describes Section 3, Unit B, as containing a facies consisting of massive organic-rich silt, with identifiable macrofossils and a high % loss on ignition (LOI) (20.0, 21.4, and 25.8%). This stands in contrast to a second Lacustrine Silt facies that contains no visible organics (Charron, 1995) (Section 3, Unit

D). Within section four, Charron (1995) describes a bedded Lacustrine Silt fill, with greater similarity to the Lacustrine Silt facies of this study.

Interestingly, organic carbon contents for the basal facies presented by Charron (1995), are higher (8.4-26.7% Wt. LOI for Section 3, Units B and D), than those calculated for my study lakes after loss on ignition values are converted to total organic carbon content. Variation in organic carbon contents between this study and Section 3 in Charron (1995) may be a result of analyzing different material. This may be because the Layered Basal and Chaotic Basal facies are inherently heterogeneous in composition, which results in highly variable TOC. Charron (1995) suggests that local variation in organic carbon values are due to differences in landscape productivity during lake formation. The bedded lacustrine sediment (Section 4, Unit B), exhibited similar organic carbon contents to the Lacustrine Silt facies (2 - 2.8% and 3.91% respectively).

Thermokarst lake deposits located within 10 km of the Devil Mountain maar (Section 2) formed within airfall tephra deposits and all facies within them are tephra-dominated, including the upper ~ 20 cm of silty material (Figure 2.5, Charron 1995). Instead of a Yedoma Taberal Silt facies, taberal units dominated by tephra (Charron, 1995, Section 2) and sand containing marine fossils (Section 4) underlie sub-aqueously deposited facies. This exemplifies how greatly thermokarst lake sediment composition can vary within a region, and how morphological differences may be caused by variation in parent material.

In another region of Alaska, the Brooks Range Foothills, Rawlinson (1990, Figure. 5.5) (Table 2.9) identified two generations of thermokarst lakes in exposures that formed within yedoma-like sediment. The facies described are similar to those I have identified in this study (Table 2.4). First-generation lake sediment is described as organic silt, which I interpreted as possibly similar to the Lacustrine Silt facies. Later-generation sediment is described as bedded organic silt, also similar to our Lacustrine Silt facies when exhibiting laminations. The two are separated by a basal organic facies, similar to our Trash Basal facies. Rawlinson (1990) also noted that ice wedge pseudomorphs influence sediment distribution.

In northeastern Siberia, yedoma thermokarst lake sequences containing the Yedoma Taberal Silt facies and facies similar to the Lacustrine Silt, Layered Basal and Chaotic Basal facies are identified within exposures of drained yedoma thermokarst lakes (Schirrmeister et al. 2008b; Wetterich et al. 2009; Schirrmeister et al. 2011) (Table 2.10). Schirrmeister et al. (2008b) and Wetterich et al. (2009) describe two sections similar to my Chaotic Basal facies. Firstly a silt matrix with peat inclusions, and secondly a disturbed, bedded dark grey, silty fine sand. A facies similar to my Layered Basal facies is also described (Schirrmeister et al. 2008b; Wetterich et al. 2009) as alternating layers of plant detritus, grey silt and grey sand. Similarly, thermokarst lakes forming within Central Yakutia are found to contain an organic-rich silt fill, overlying a sandy basal unit which contains woody fragments (Katamura et al. 2006).

The presence of the tephra from the Devil Mountain Maar eruption is a key difference between yedoma thermokarst lakes forming in the Cape Espenberg Lowland on the Seward Peninsula and yedoma thermokarst lakes forming in other areas of Alaska and Siberia. The relatively high magnetic susceptibility of the Lacustrine Silt facies fill in Seward Peninsula lakes (Table 2.4) compared to facies studies in Siberia may be explained by the presence of tephra (Table 2.10). Measurements of TOC, C/N, $\delta^{13}C$, grain size and magnetic susceptibility for the Yedoma Taberal Silt facies in northeast Siberia are similar to those seen within our Yedoma Taberal Silt facies on the Seward Peninsula (Table 2.4).

Two Interior Alaska thermokarst lakes (Goldstream and Killarney lakes), forming in redeposited yedoma-type loess, were studied by Brosius (2010) for their biogeochemical properties, including a brief analysis of the sediment present (Table 2.11). Brosius (2010) identified taberal sediment with a massive structure below a silty lacustrine fill in Goldstream Lake. Taberal sediment analyzed by Brosius (2012) contains 0.6 - 0.9% organic carbon, slightly lower than the 1.58% (Table 2.4) total organic carbon observed for lakes discussed in this study. Variation in taberal total organic carbon may be because of different total organic carbon contents of parent material, or to a longer period

of thaw. The interior Alaska thermokarst lakes are thought to be younger than Lakes Claudi and Jaeger (M. Edwards pers. comm.), therefore dissimilarity between TOC values is likely due to differences in the original TOC of parent material. Descriptions of the lacustrine fill refer to visible layering, as seen within the Lacustrine Silt facies identified within this study. Organic carbon contents of the lacustrine facies are 19.1% ± 1.4 and 1.0-9.3% for Goldstream Lake and Killarney Lake respectively. In my study, with the exception of TOC for the Trash Basal facies (11.85%), facies are characterized by lower organic carbon values with smaller ranges (Table 2.4). The large range in total organic carbon seen in Interior Alaskan lakes may be explained by the fact that organic detrital basal deposit TOC values were combined with those of the lacustrine fill, although no detrital basal units were described.

Overall, both similar sediment composition and distribution are seen between yedoma-type thermokarst lakes. A key difference between the Seward Peninsula and other regions is the presence of tephra. The organic content of facies is also found to vary between and within regions. This variation is likely due to regional variation in the organic carbon content of parent material and the heterogeneous composition of basal facies.

2.6.6 Comparison to non-yedoma lakes

Sediment of non-yedoma thermokarst lakes has been studied in the eastern Hudson Bay region (Bouchard et al. 2011) (Table 2.12). The lakes studied by Bouchard et al. (2011) formed within silty marine sediment that was deposited and uplifted via isostatic rebound as recently as 6,000 years BP. These non-yedoma thermokarst lakes develop from the degradation of permafrost mounds: palsas and lithalsas. Bouchard et al. (2011) analyzed short (<20 cm) lake cores and identified an upper facies, a lower facies, and a transitional zone. Approximate TOC values of the Hudson Bay thermokarst lakes' upper facies are less than one percent lower than that of my Lacustrine Silt facies. Conversely, approximate TOC values of the lower facies (composed of marine sediment) are higher than our median Yedoma Taberal Silt facies TOC values by two to three percent. The

transition zone between the upper and lower facies contains macroscopic plant and peat remains that are interpreted by Bouchard et al. (2011) as the ancient palsa or lithalsa summits. I interpret this facies to be similar to my Trash Basal facies. No other form of basal layer was described by Bouchard et al. (2011). Upper facies thickness is ca. four centimeters, significantly thinner than maximum thicknesses seen in our Lacustrine Silt facies (*ca.* three meters). Facies distribution within the lakes is not discussed.

Non-yedoma thermokarst lakes on the Tuktoyuktuk Peninsula initiate due to the thaw and collapse of massive ice of intrasedimental and buried glacial origin (Murton 2001) (Table 2.12). Settlement is up to 15 m. Investigations by Murton (1996) of drained thermokarst lake exposures identified thick (four to five meters) basal deposits composed of diamicton, pebbly sand, and sandy gravel with lenses of impure sand and inclusions of detrital peat. The disturbed and chaotic structure of the basal unit identified by Murton (1996) is similar in structure to that of the Chaotic Basal facies within my study lakes; however the mineral component is substantially coarser-grained. The main differences between the two types of Chaotic Basal facies are the composition and thickness of the unit. The Tuktoyuktuk lakes studied by Murton (1996) are found to contain a stratified mud fill with abundant terrestrial organics, up to three meters in thickness, forming from settling of suspended fine material. Due to the abundance of peat within the central fill (Murton 1996), this facies is not similar to any of those identified within my study. It is interesting to note that ice wedge pseudomorphs were not identified within the exposures studied by Murton (1996). This may be due to the absence of regularly spaced Pleistocene patterned ground in the immediate area of lake development (Mackay and Dallimore 1992). Another possible explanation is that any ice wedge pseudomorphs structures have been deformed due to settlement.

Non-yedoma thermokarst lakes also form within sandy deposits of the Arga complex of the Lena River Delta. Lakes develop from the thaw of remnant glacial ice, averaging two meters in thickness but reaching depths of 30 m (Schwamborn et al. 2000; Andreev et al. 2004). Andreev et al. (2004) identified two prominent facies within Lake Nikolay: an

organic-rich and an organic-poor fine sand unit. The lower unit appears to be deposited prior to lake formation and may therefore be a kind of taberal facies. Within a drained lake basin, 30 km from Lake Nikolay, sandy peat and poorly decomposed peat deposits are also identified at the base of organic-rich fine sand. I interpret these deposits to be similar to my Chaotic Basal facies. TOC values measured by Andreev et al. (2004) are similar to this study, ranging from 0.5-3.9% (Table 2.12). In contrast, grain size values measured by Andreev et al. (2004) (~ 64 μm, Table 2.12), are much greater than those identified within this study (~22 - 28 μm, Table 2.4), due to their thermokarst lakes forming within sandy deposits.

Although a similar set of facies are identified within non-yedoma thermokarst lakes (basal facies overlain by a fine-grained fill), the composition and thickness of facies varies greatly between regions.

2.7 Conclusions

This study illustrates how dynamic thermokarst lake sedimentology is both spatially and temporally. I identified five key facies that are present in both first- and later-generation yedoma thermokarst lakes. Facies distribution changes as first-generation yedoma thermokarst lakes develop. Although first- and later-generation lakes are found to contain the same facies, the distribution of facies is more consistent in first-generation lakes and more variable in later-generation lakes. Based on the literature review, I found strong similarities between the northern Seward Peninsula and sediment sequences described in other yedoma lakes. The presence of tephra in Seward Peninsula yedoma thermokarst lakes is found to be unique to the region. Differences in number, composition, and thickness of facies were found between yedoma thermokarst lakes forming in the Seward Peninsula and non-yedoma thermokarst lakes. Although some features, such as the presence of baydjarakhs, appear unique to yedoma thermokarst lakes, a better understanding of non-yedoma thermokarst lake sediment facies distribution and bathymetry is needed to verify this.

Results from this study provide some insight into the shifts in carbon cycling that occurs as a result of yedoma thermokarst lake development. Comparison of TOC of yedoma sediment and peat to the five lacustrine facies enables a preliminary look at shifts in carbon storage that occur through the thermokarst lake cycle.

Components of the preliminary model of yedoma thermokarst lake development can be applied to other thermokarst lake regions. Universal features include the initial thaw of excess ice and collapse of a terrestrial environment to create a trash layer. Other features include transgressive lake margins that result in the formation of detrital basal layers and the development of taberal sediment via thaw bulb growth. Variations may be seen due to the absence of baydjarakh topography and its subsequent influence on sedimentology. Rates of both vertical subsidence and lateral expansion may also vary between yedoma and non-yedoma thermokarst lakes.

2.8 Acknowledgements

This study is part of the National Science Foundation International Permafrost Year grant #0732735. Any opinions, findings, conclusions, or recommendations expressed in this material are those of the authors and do not necessarily represent the views of the National Science Foundation. I thank all those who helped me conduct fieldwork, including Amy Myrbo, Laura Oxtoby, Laurel McFadden, Benjamin Jones, Laura Brosius, Marie Gaei, Michael LaDoucer, Emily Sousa, Mary Edwards, Nancy Bigelow, Guido Grosse, and Katey Walter Anthony. I received lab help from Laura Oxtoby, Mary Edwards, Nancy Bigelow, and Katey Walter Anthony. I thank the US National Park Service for permission to do work within the Bering Land Bridge National Preserve. I thank researchers at LacCore for use of laboratory facilities.

2.9 References

Andreev, A., Tarasovb, P., Schwamborna, G., Ilyashukc, B., Ilyashukc, E., Bobrovd, A., Klimanove, V., Racholda, V., Hubbertena, H., 2004. Holocene paleoenvironmental records from Nikolay Lake, Lena River Delta, Arctic Russia. Palaeogeography, Palaeoclimatology, Palaeoecology, 209: 197-217.

Arp, C. D., B. M. Jones, 2009. Geography of Alaska lake districts: Identification, description, and analysis of lake-rich regions of a diverse and dynamic state. U.S. Geological Survey, Scientific Investigations Report, 2008-5215.

Barker, J. F., Fritz, P., 1981. Carbon isotope fractionation during microbial methane oxidation. Nature, 293: 289-291.

Beget, J. E., Hopkins, D. M., Charron, S. D., 1996. The largest known Maars on earth, Seward Peninsula, northwest Alaska. Arctic, 49: 62-69.

Beget, J. E., Mason, O., Anderson, P., 1991. Age and extent of the ca. 3400 BP Aniakchak tephra. The Holocene, 2: 117–123.

Birks, H., 2002. Plant Macrofossils In: Last, W. M. and Smol, J. P. (Eds.), Tracking Environmental Change Using Lake Sediments: Terrestrial, algal and silicious indicators. Kluwer Academic Publications, p. 400.

Black, R. F., 1964. Gubik formation of Quaternary age in northern Alaska U.S. Geological Survey Professional Paper, 302-C.

Bouchard, F., Francus, P., Pienitz, R., Laurion, I., 2011. Sedimentology and geochemistry of thermokarst ponds in discontinuous permafrost, subarctic Quebec, Canada. Journal of Geophysical Research-Biogeosciences, 116: G00M04.

Breton, J., Vallieres, C., Laurion, I., 2009. Limnological properties of permafrost thaw ponds in northeastern Canada. Canadian Journal of Fisheries and Aquatic Sciences, 66: 1635–1648.

Britton, M. E., 1966. Vegetation of the Arctic tundra, 2nd edition ed. Oregon State University Press, Corvallis, 2nd edition

Brosius, L. S., 2010. Investigating Controls Over Methane Production and Bubbling from Interior Alaskan Lakes Useing Stable Isotopes and Radiocarbon Ages. M.Sc. thesis, University of Alaska Fairbanks.

Brosius, L. S., Anthony, K. M. W., Grosse, G., Chanton, J. P., Farquarson, L. M., Overduin, P. P., Meyer, H., 2012. Using δD of permafrost melt water to constrain thermokarst lake contributions to atmospheric CH4 during the last deglaciation. Journal of Geophysical Research-Biogeosciences, 117: G01022.

Burn, C. R., Smith, M. W., 1990. Development of thermokarst lakes during the Holocene at sites near Mayo, Yukon Territory Permafrost and Periglacial Processes, 1: 161-175.

Carter, L. D., 1988. Loess and deep thermokarst basins in arctic Alaska, In: Permafrost, Fifth International Conference, Proceedings. Tapir Publishers, Trondheim, Norway, pp. 706–711.

Charron, S. D., 1995. Surficial mapping of the Cape Espenberg-Devil Mountain region and lakecore analyses from North Killeak Lake, Bering Land Bridge National Preserve, western Alaska. University of Massachusetts.

Czudek, T., Demek, J., 1970. Thermokarst in Siberia and its influence on the development of lowland relief. Quaternary Research, 1: 103-120.

French, H., 1996. The Periglacial Environment, 2nd ed. Longman, London, 478, 2nd.

Goetcheus, V. G., Birks, H., 2001. Full-glacial upland tundra vegetation preserved under tephra in the Beringia National Park, Seward Peninsula, Alaska. Quaternary Science Reviews, 20: 135-147.

Google (2011). "Google Earth (Version 6.1.0.5001) [Software]. Available from http://www.google.com/earth/index.html."

Grosse, G., Harden, J., Turetsky, M., McGuire, A. D., Camill, P., Tarnocai, C., Frolking, S., Schuur, E. A. G., Jorgenson, T., Marchenko, S., Romanovsky, V., Wickland, K. P., French, N., Waldrop, M., Bourgeau-Chavez, L., Striegl, R. G., 2011. Vulnerability of high-latitude soil organic carbon in North America to disturbance. Journal of Geophysical Research-Biogeosciences, 116.

Grosse, G., Jones, B., Arp, C., In press. Thermokarst Lakes, Drainage, and Drained Basins. Treatise on Geomorphology. Elsevier.

Grosse, G., Schirrmeister, L., Siegert, C., Kunitsky, V., Slagoda, E. A., Andreev, A., Dereviagin, A., 2007. Geological and geomorphological evolution of a sedimentary periglacial landscape in northeast Siberia during the Late Quaternary. Geomorphology, 86: 25-51.

Hartmann, B., and G. Wendler, 2005. The significance of the 1976 Pacific climate shift in the climatology of Alaska. Journal of Climate, 18: 4824-4839.

Hinkel, K., Eisner, W. R., Bockheim, J. G., Nelson, F. E., Peterson, K. M., Dai, X. Y., 2003. Spatial extent, age, and carbon stocks in drained thaw lake basins on the Barrow Peninsula, Alaska. Arctic Antarctic and Alpine Research, 35: 291-300.

Hinkel, K., Jones, B., Eisner, W. R., Cuomo, C. J., Beck, R. A., Frohn, R. C., 2007. Methods to assess natural and anthropogenic thaw lake drainage on the western Arctic coastal plain of northern Alaska. Journal of Geophysical Research-Biogeosciences, 112.

Hofle, C., Edwards, M. E., Hopkins, D. M., Mann, D. H., 2000. The Full-Glacial Environment of the Northern Seward Peninsula, Alaska, Reconstructed from the 21,500-Year-Old Kitluk Paleosol. Quaternary Research, 53: 143-153.

Hopkins, D. M., Kidd, J., 1988. Thaw lake sediments and sedimentary environments, In: Permafrost, Fifth International Conference, Proceedings. Tapir Publishers, Trondheim, Norway, Trondheim, Norway, pp. 790-795.

Ireland, R. R., 1982. Moss flora of the maritime provinces. National Museums of Canada, National Museum of the Natural Sciences, Ottawa,

Janssens, J. A., 1983. Past and extant distribution of *Drepanocladus* in North America, with notes on the differentiation of fossil fragments. The Journal of the Hattori Botanical Laboratory devoted to Bryology and Lichenology 54: 251-298.

Jiilavenkatesa, A., Dapkunas, S. J., Lum, L. H., 2001. Size characterization by laser light diffraction techniques. In: Commerce, U. S. D. o. (Ed.), Particle Size Characterization. pp. 960-961.

Jones, B. M., Grosse, G., Arp, C. D., Jones, M. C., Walter Anthony, K. M., Romanovsky, V. E., 2011. Modern thermokarst lake dynamics in the continuous permafrost zone, northern Seward Peninsula, Alaska. Journal of Geophysical Research – Biogeosciences: G00M03.

Jones, M., Grosse, G., Jones, B. M., Walter Anthony, K. M., In press. Peat accumulation in a thermokarst-affected landscape in continuous ice-rich permafrost, Seward Peninsula, Alaska. Journal of Geophysical Research – Biogeosciences.

Kanevskiy, M., Shur, Y., Fortier, D., Jorgenson, M. T., Stephani, E., 2011. Cryostratigraphy of late Pleistocene syngenetic permafrost (yedoma) in northern Alaska, Itkillik River exposure. Quaternary Research, 75: 584-596.

Katamura, F., Fukuda, M., Bosikov, N. P., Desyatkin, R. V., Nakamura, T., Moriizumi, J., 2006. Thermokarst formation and vegetation dynamics inferred from a palynological study in Central Yakutia, Eastern Siberia, Russia. Arctic Antarctic and Alpine Research, 38: 561-570.

Katz, N. J., Katz, S. V., Kipiani, M. G., 1965. Atlas and keys of fruits and seeds occuring in the Quaternary deposits of the USSR. Publishing House Nauka, Moscow,

Keeley, J. E., Sandquist, D. R., 1992. Carbon: freshwater plants. Plant, Cell and Environment 15: 1021-1035.

Kessler, M. A., Plug, L. J., Walter Anthony, K. M., 2012. Simulating the decadal- to millennial-scale dynamics of morphology and sequestered carbon mobilization of two thermokarst lakes in NW Alaska. Journal of Geophysical Research – Biogeosciences, 117: G00M06.

Kidd, J., 1988. Thaw lake development and its effect on plant macrofossil deposition. Current Research in the Pleistocene, 5: 50-52.

Labrecque, S., Lacelle, D., Duguay, C., Lauriol, B., Hawking, J., 2009. Contemporary (1951–2001) evolution of lakes in the Old Crow Basin, Northern Yukon, Canada: remote sensing, numerical modeling, and stable isotope analysis. Arctic, 62.

Long, H., Lai, Z., Wang, N., Zhang, J., 2011. A combined luminescence and radiocarbon dating study of Holocene lacustrine sediments from arid northern China. Quaternary Geochronology, 6: 1-9.

Mackay, J. R., 1988. Catastrophic lake drainage, Tuktoyaktuk Peninsula area, District of Mackenzie. Current Research, Current Research Part D, Geologic Survey Canada.

Mackay, J. R., Dallimore, S. R., 1992. Massive ice of the lhktoyaktuk area, western Arctic coast, Canada. Canadian Journal of Earth Sciences, 29: 1235-1249.

Meyers, P. A., 2003. Applications of organic geochemistry to paleolimnological reconstructions: a summary of examples from the Laurentian Great Lakes. Organic Geochemistry, 34: 261-289.

Meyers, P. A., Lallier-Vergès, E., 1999. Lacustrine sedimentary organic matter records of Late Quaternary paleoclimates. Journal of Paleolimnology, 21: 345–372.
Murton, J. B., 1996. Thermokarst-lake-basin sediments, Tuktoyaktuk Coastlands, western Arctic Canada. Sedimentology, 43: 737-760.

Murton, J. B., 2001. Thermokarst sediments and sedimentary structures, Tuktoyaktuk Coastlands, western Arctic Canada. Global and Planetary Change, 28: 175-192.

Nelson, R. E., Carter, D. L., Robinson, S. W., 1988. Anomalous radiocarbon ages form a Holocene detrital organic lens in Alaska and their implications for radiocarbon dating and paleoenvironmental reconstructions in the arctic. Quaternary Research, 29: 66-71.

Oswald, W. W., Anderson, P. M., Brown, T. A., Brubaker, L. B., Hu, F. S., Lozhkin, A. V., Tinner, W., Kaltenrieder, P., 2005. Effects of sample mass and macrofossil type on radiocarbon dating of arctic and boreal lake sediments. Holocene, 15: 758-767.

Plug, L. J., West, J. J., 2008. Time-dependent morphology of thaw lakes and taliks in deep and shallow ground ice. Journal of Geophysical Research-Biogeosciences, 113: F01009.

Plug, L. J., West, J. J., 2009. Thaw lake expansion in a two-dimensional coupled model of heat transfer, thaw subsidence, and mass movement. Journal of Geophysical Research-Earth Surface, 114: F01002.

Popov, A. I., 2008. Genesis and conditions of formation of the Yedoma cryogenic sedimentary complex on the coastal plains of the subarctic. Polar Geography, 7: 60-66.

Rawlinson, S. E., 1990. Surficial Geology and Morphology of the Alaskan central Arctic Coastal Plain. . University of Alaska Fairbanks.

Reasoner, M. A., 1993. Equipment and procedure improvements for a lightweight, inexpensive, percussion core sampling system. Journal of Paleolimnology, 8: 273-281.

Romanovskii, N. N., 1993. Fundamentals of cryogenesis of lithosphere. Moscow University Press, Moscow.

Romanovskii, N. N., Hubberten, H. W., Gavrilov, A., Tumskoy, V. E., Kholodov, A. L., 2004. Permafrost of the east Siberian Arctic shelf and coastal lowlands. Quaternary Science Reviews, 23: 1359-1369.

Schirrmeister, L., Froese, D. G., Tumskoy, V., Grosse, G., Wetterich, S., In press. Yedoma: Late Pleistocene ice-rich syngenetic permafrost of Beringia. Encyclopedia of Quaternary Science. 2nd edition. Elsevier.

Schirrmeister, L., Grosse, G., Wetterich, S., Overduin, P. P., Strauss, J., Schuur, E. A. G., Hubberten, H. W., 2011. Fossil organic matter characteristics in permafrost deposits of the northeast Siberian Arctic. Journal of Geophysical Research – Biogeosciences, 116: G00M02.

Schirrmeister, L., Meyer, H., Wetterich, S., Siegert, C., Kunitsky, V. V., Grosse, G., Kuznetsova, T. V., Derevyagin, A. Y., 2008a. The Yedoma Suite of the northeastern Siberian Shelf Region: Characteristics and Concept of Formation. Ninth international Conference on Permafrost, University of Alaska Fairbanks: 1595-1600.

Schirrmeister, L., Wetterich, S., Kholodov, A. L., 2008b. The joint Russian-German Expedition Beringia/Kolyma 2008 during the International Polar Year (IPY) 2007/2008, ISSP RAS - AWI.

Schnurrenberger, D., Russell, J., Kelts, K., 2003. Classification of lacustrine sediments based on sedimentary components. Journal of Paleolimnology, 29: 141-154.

Schwamborn, G., Andreev, A.A, Rachold, V., Hubberten, H.-W., Grigoriev, M.N., Tumskoy, V., Pavlova, E.Yu., Dorozkhina, M.V., 2000. Evolution of Lake Nikolay, Arga Island, Western Lena Delta, during Late Pleistocene and Holocene time. Polarforschung, 70: 69-82.

Shaw, J., 1988. Discussion: coarse-grained sediment flow facies in a large supraglacial lake. Sedimentology, 35: 527-529.

Tedrow, J. C. F., 1969. Thaw lakes, thaw sinks and soils in northern Alaska. Biuletyn Peryglacjalny, 20: 337-334.

Tomirdiaro, S. V., 1982. Evolution of lowland landscapes in northeastern Asia during late Quaternary time. In: Hopkins, D. M., Jr., J. V. M., Schweger, C. E. and Young, S. B. (Eds.), Paleoecology of Beringia Academic Press, New York, pp. 29–37.

Tomirdiaro, S. V., Ryabchun, V. K., 1973. Lake thermokarst on the lower Anadyr lowland, In: Permafrost, 2nd International Conference, Proceedings. National Academy of Sciences, Yakutsk, pp. 94-100.

van Everdingen, R. O., 1988. Multi-language glossary of permafrost and related ground-ice terms. National Snow and Ice Data Center/World Data Center for Glaciology, Boulder, CO.

Walter, K. M., Smith, L. C., Chapin, F. S., 2007. Methane bubbling from northern lakes: present and future contributions to the global methane budget. Philosophical Transactions of the Royal Society a-Mathematical Physical and Engineering Sciences, 365: 1657-1676.

West, J. J., Plug, L. J., 2008. Time-dependent morphology of thaw lakes and taliks in deep and shallow ground ice. Journal of Geophysical Research-Earth Surface, 113.

Wetterich, S., Kuzmina, S., Andreev, A., Kienast, F., Meyer, H., Schirrmeister, L., Kuznetsova, T., Sierralta, M., 2008. Palaeoenvironmental dynamics inferred from late Quaternary permafrost deposits on Kurungnakh Island, Lena Delta, northeast Siberia, Russia. Quaternary Science Reviews, 27: 1523– 1540.

Wetterich, S., Schirrmeister, L., Andreev, A., Pudenz, M., Plessen, B., Meyer, H., Kunitsky, V., 2009. Eemian and Late Glacial/Holocene palaeoenvironmental records from permafrost sequences at the Dmitry Laptev Strait (NE Siberia, Russia). Palaeogeography Palaeoclimatology Palaeoecology, 279: 73-95.

Wetzel, R. G., 2001. Limnology: Lake and River Ecosystems. Third Edition. Academic Press, p. 1006.

Wolfe, B. B., Edwards, T. W. D., Elgood, R. J., R.M., B., 2001. Carbon and Oxygen Isotope Analysis of Lake Sediment Cellulose: Methods and Applications In: Last, W. M. and Smol, J. P. (Eds.), Tracking Environmental Change Using Lake Sediments. Kluwer Academic Publishers, p. 504.

Wright, H. E., Mann, D. H., Glaser, P. H., 1984. Piston corers for peat and lake sediments. Ecology, 65: 657-659.

Zimov, S. A., Schuur, E. A. G., Chapin, F. S., 2006. Permafrost and the global carbon budget. Science, 312: 1612-1613.

2.10 Figures

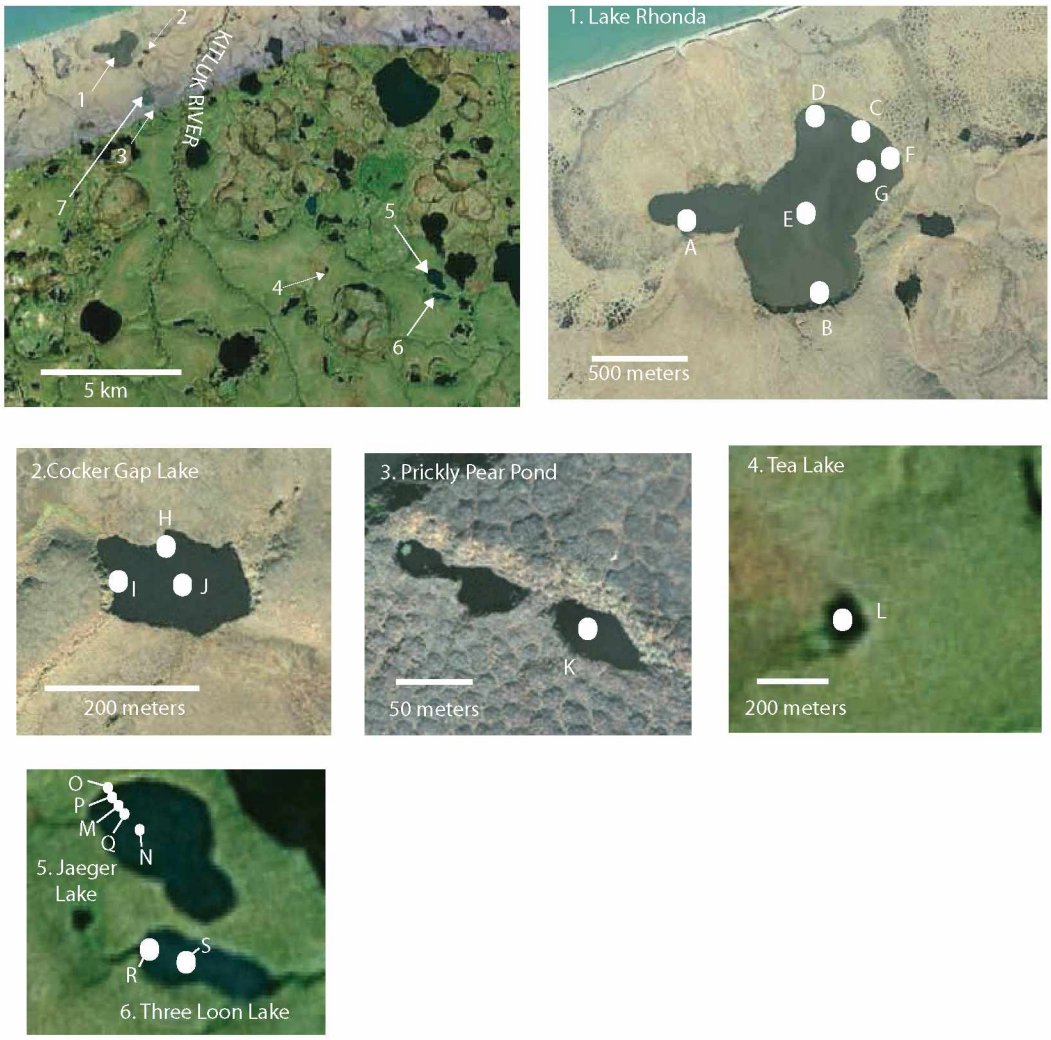

Figure 2.1: Map of lakes. The study area is shown in the top left. Numbers correspond to lakes and letters correspond to coring locations in subsequent images. White circles represent lake areas cored, some containing multiple core holes. The letters correspond to each lake's coring location. Lake Claudi (lake seven) is shown in detail in Figure 2.2. 1. Lake Rhonda. Letters correspond to the following core locations: A, SPA-RHO10-Site 1; B, SPA-RHO09- Site 2; C, SPA-RHO10-Site 3; D, SPA-RHO09- Site 4; E, SPA-RHO09-Site 5; F, SPA0RHO09-Site 1 and G SPA-RHO09-Site 2. 2. Cocker Gap Lake. Letters correspond to the following coring locations: A, SPA-COCK09-Site 1, B; SPA-COCK09-Site 2 and C, SPA-COCK09-Site 3. 3. Prickly Pear Pond. The letter K corresponds to coring location SPA-PRICK09-Site 1. 4. Tea Lake. The letter L corresponds to coring location SPA-TEA09-Site 1. 5. Lake Jaeger. Letters correspond to the following coring locations: M, SPA-JAE09-Site 1; N, SPA-JAE09-Site 2; O, SPA-JAE09-Site 3; P, SPA-JAE09-Site 4; and Q SPA-JAE09-Site 5. 6. Three Loon Lake. Letters correspond to the following coring locations: R, SPA-3LOO09-Site 1; and S, SPA-3LOO09-Site 2. All images were taken from Google Earth (Google 2011) using the Alaskan Statewide Digital Mapping Initiative high resolution overlay (http://www.alaskamapped.org/). For longitude and latitude of each lake refer to Table 2.1.

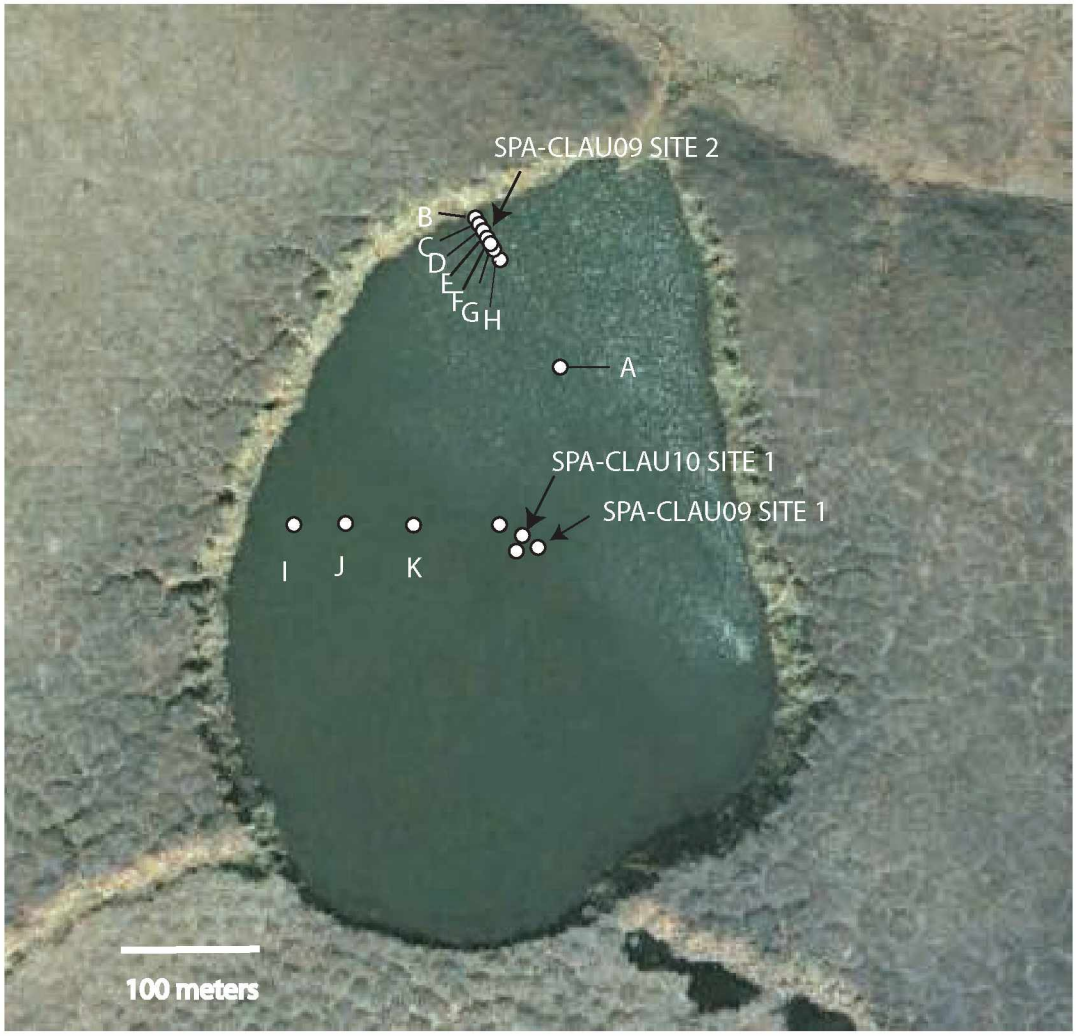

Figure 2.2: Map of Lake Claudi (lake seven in Figure 2.1) coring locations. Labeled cores correspond to those referred to within the text. Within Lake Claudi, letters correspond to the following core sights: A, SPA-CLAU09-Site 10; B, SPA-CLAU09-Site 5; C, SPA-CLAU09-Site6; D, Spa-CLAU09-Site 3; E, SPA-CLAU09-Site 2; F, SPA-CLAU09-Site 7; G, SPA-CLAU09-Site 4; H, SPA-CLAU09-Site 8; I, SPA-CLAU10-Site 3; J, SPA-CLAU10-Site 2 and K, SPA-CLAU10- Site 4. Image was taken from Google Earth(Google 2011), using the Alaskan Statewide Digital Mapping Initiative high resolution overlay (http://www.alaskamapped.org/).

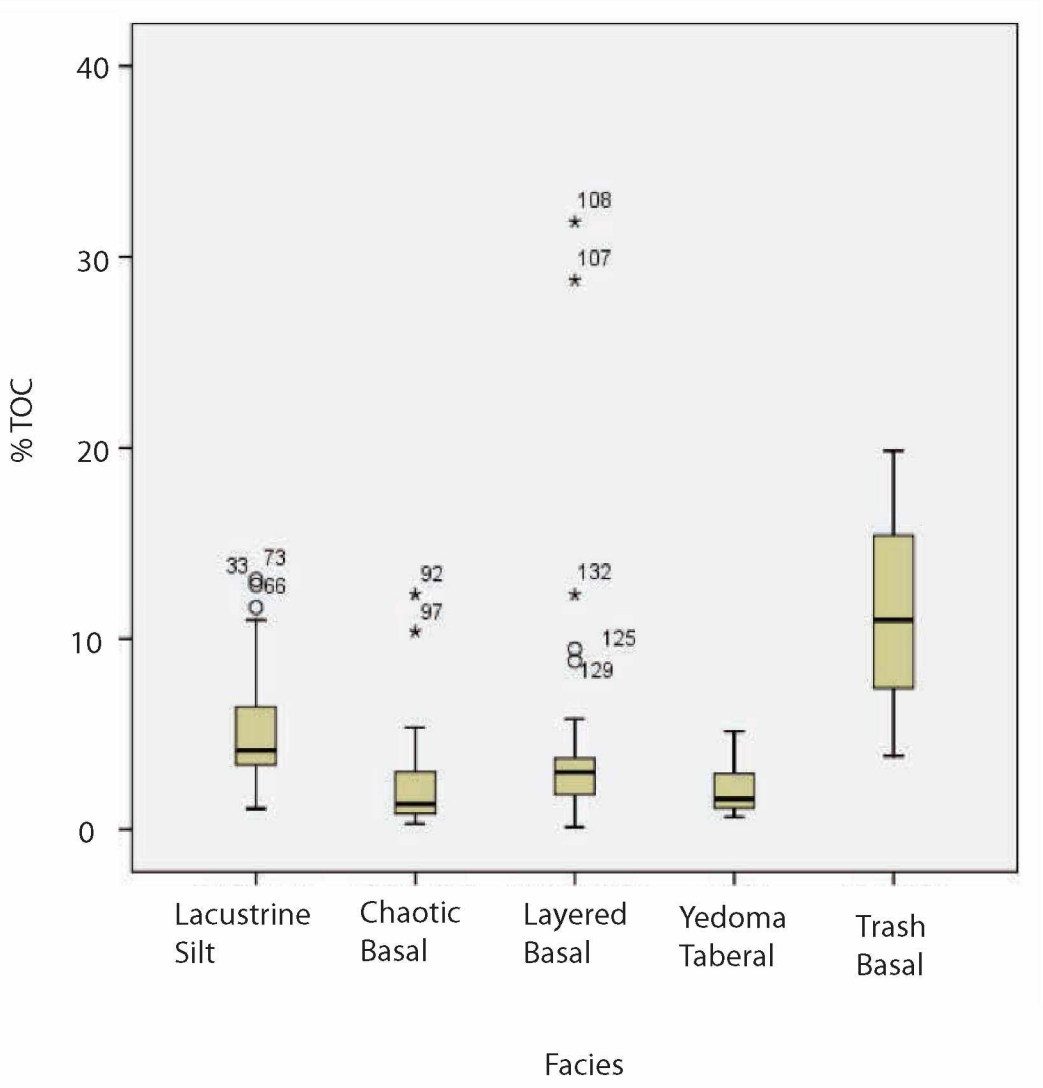

Figure 2.3: Box plot of TOC by facies. The horizontal black line shows the median value. Whiskers connect the lowest and highest values that are not considered outliers. Circles represent outliers, stars represent extreme outliers. Numbers adjacent to stars and circles indicate data point label. Outliers are defined by calculating the difference between the upper and lower quartile. Outliers are 1.5x to 3x from the upper or lower quartile. Extreme outliers are greater than 3x from the upper or lower quartile.

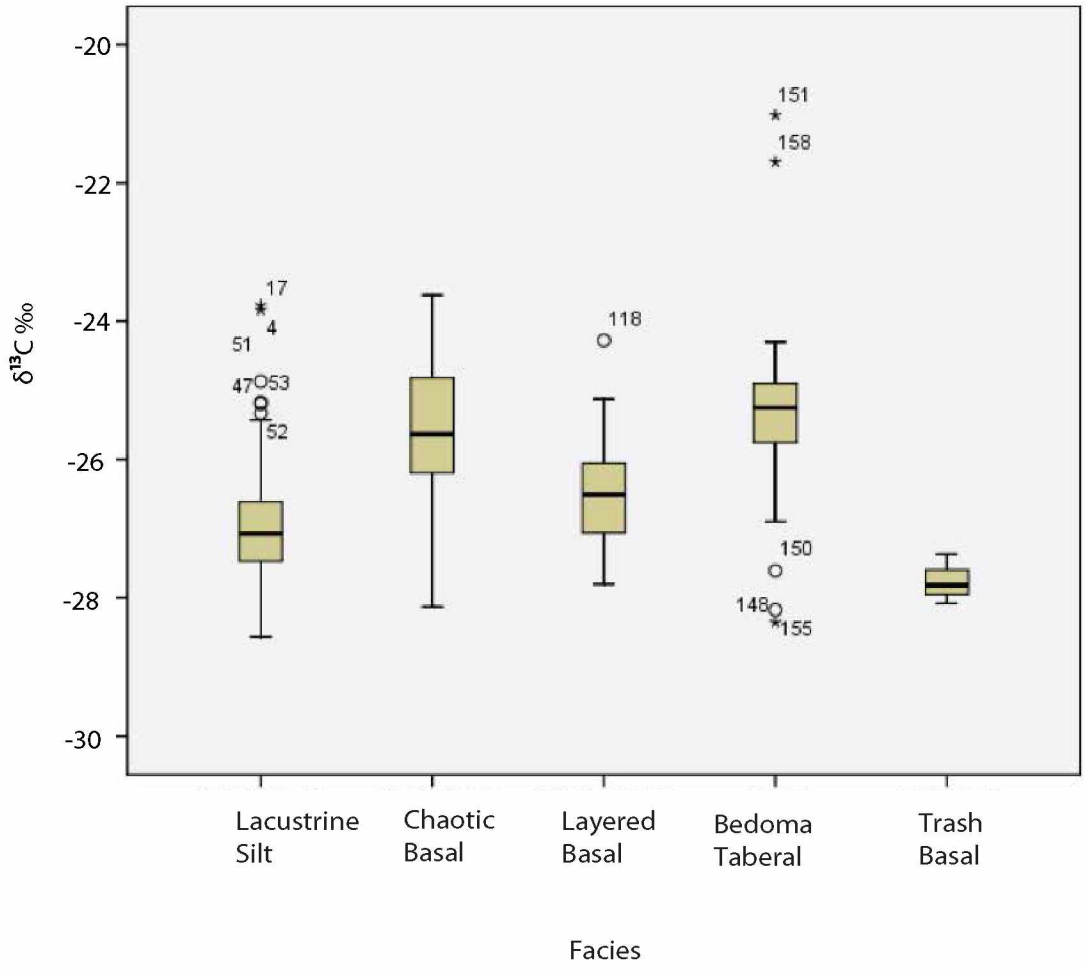

Figure 2.4: Box plot of $\delta^{13}C$ (‰) for each facies. The horizontal black line shows the median value. Whiskers connect the lowest and highest values that are not considered outliers. Circles represent outliers and stars represent extreme outliers. Numbers adjacent to stars and circles indicate a data point label. Outliers are defined by calculating the difference between the upper and lower quartile. Outliers are 1.5x to 3x from the upper or lower quartile. Extreme outliers are greater than 3x from the upper or lower quartile.

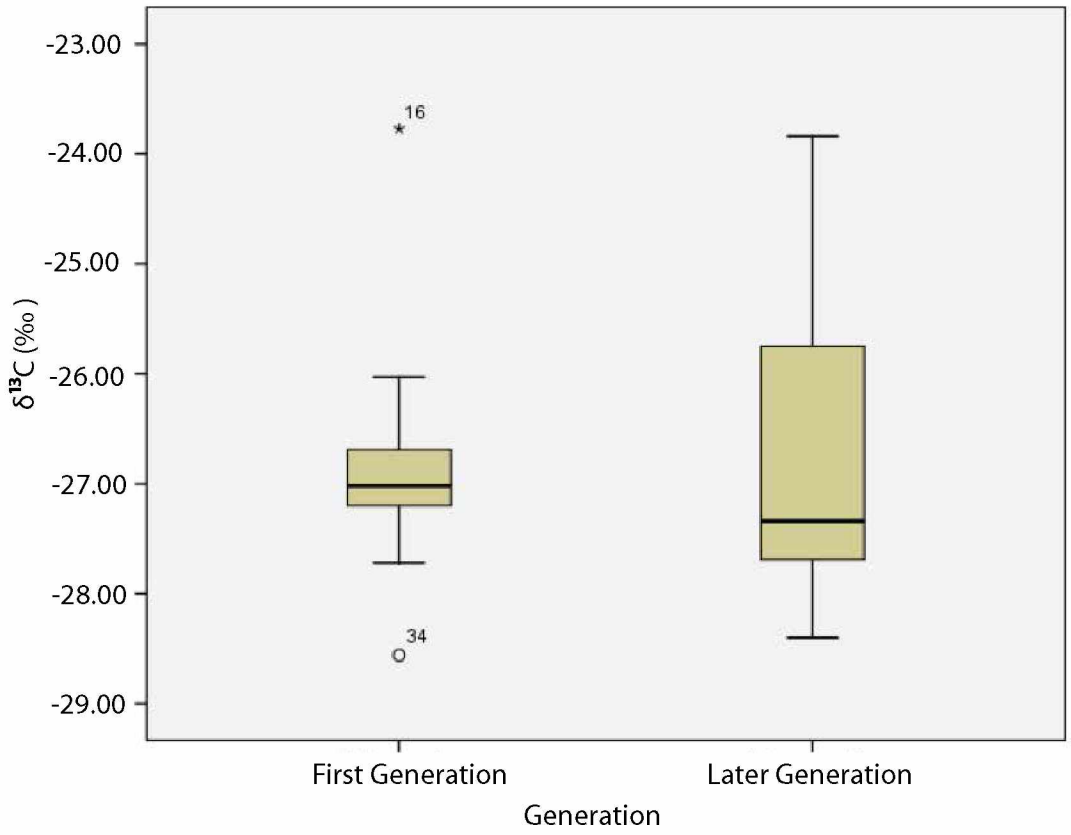

Figure 2.5: Box plot $\delta^{13}C$ (‰) for Lacustrine Silt facies, between generations. The horizontal black line shows the median value. Whiskers connect the lowest and highest values that are not considered outliers. Circles represent outliers. Stars represent extreme outliers. Numbers adjacent to stars and circles indicate a data point label. Outliers are defined by calculating the difference between the upper and lower quartile. Outliers are 1.5x to 3x from the upper or lower quartile. Extreme outliers are greater than 3x from the upper or lower quartile.

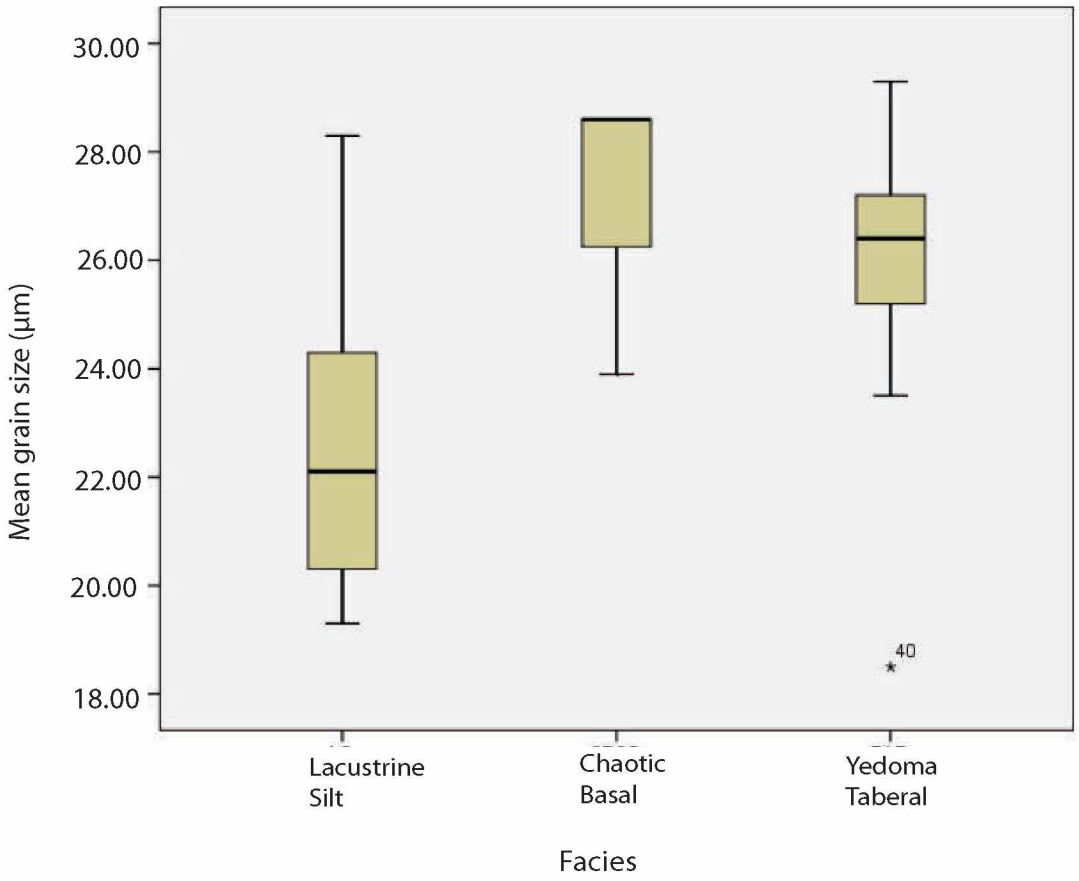

Figure 2.6: Box plot of mean grain size (µm) between facies. The horizontal black line shows the median value. Whiskers connect the lowest and highest values that are not considered outliers. Circles represent outliers. Stars represent extreme outliers. Numbers adjacent to stars and circles indicate a data point label. Outliers are defined by calculating the difference between the upper and lower quartile. Outliers are 1.5x to 3x from the upper or lower quartile. Extreme outliers are greater than 3x from the upper or lower quartile.

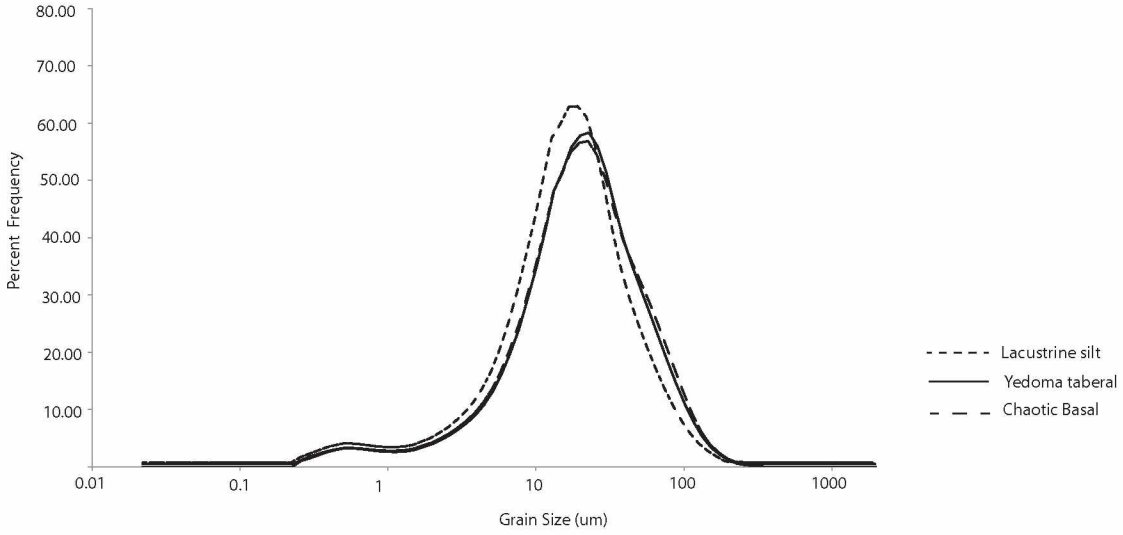

Figure 2.7: Mean grain size distribution curves. Facies analyzed: Lacustrine Silt facies (n=28), Chaotic Basal facies (n=3) and Yedoma Taberal Silt facies (n=10). These data are from Lake Claudi, coring location, Site 1. Samples were only run for the Lacustrine Silt facies, Yedoma Taberal Silt facies and the Chaotic Basal facies. The area under the curve is equal to 100%.

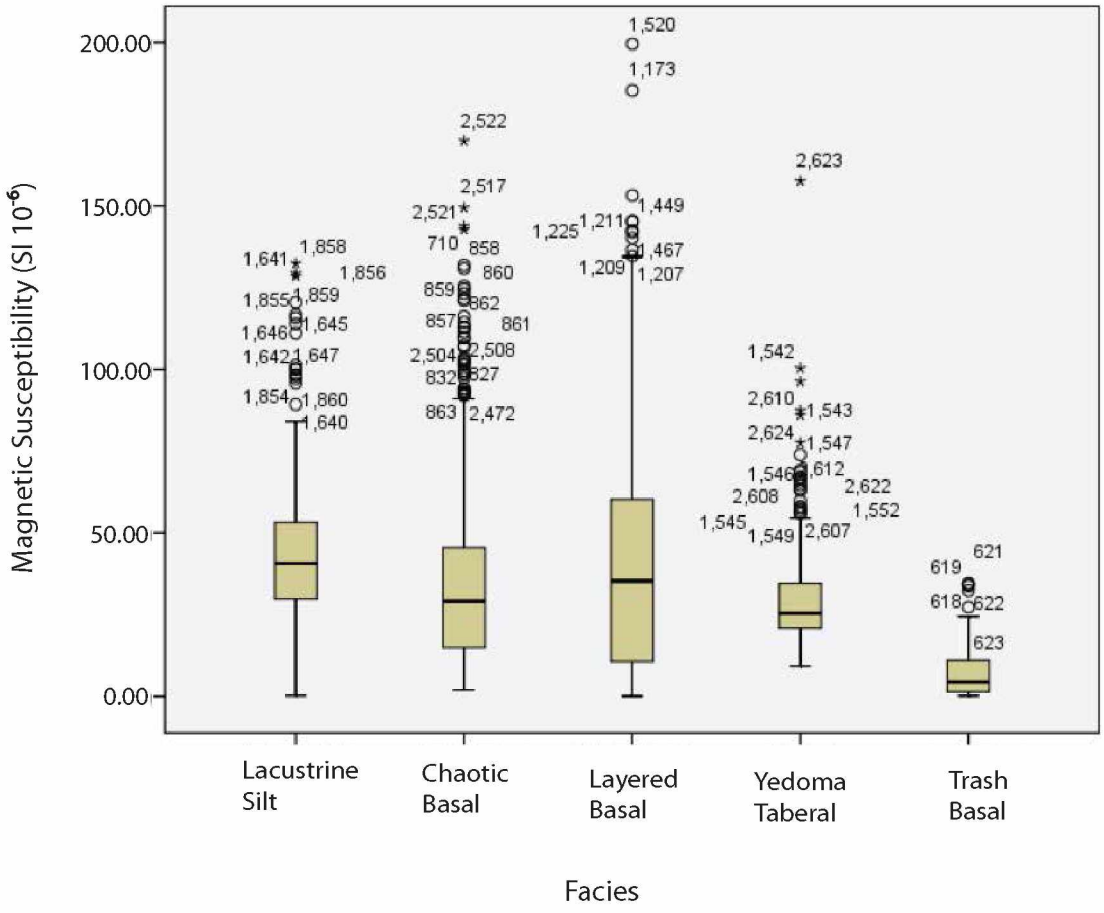

Figure 2.8: Box plot of magnetic susceptibility between facies. The horizontal black line shows the median value. Whiskers connect the lowest and highest values that are not considered outliers. Circles represent outliers. Stars represent extreme outliers. Numbers adjacent to stars and circles indicate a data point label. Outliers are defined by calculating the difference between the upper and lower quartile. Outliers are 1.5x to 3x from the upper or lower quartile. Extreme outliers are greater than 3x from the upper or lower quartile.

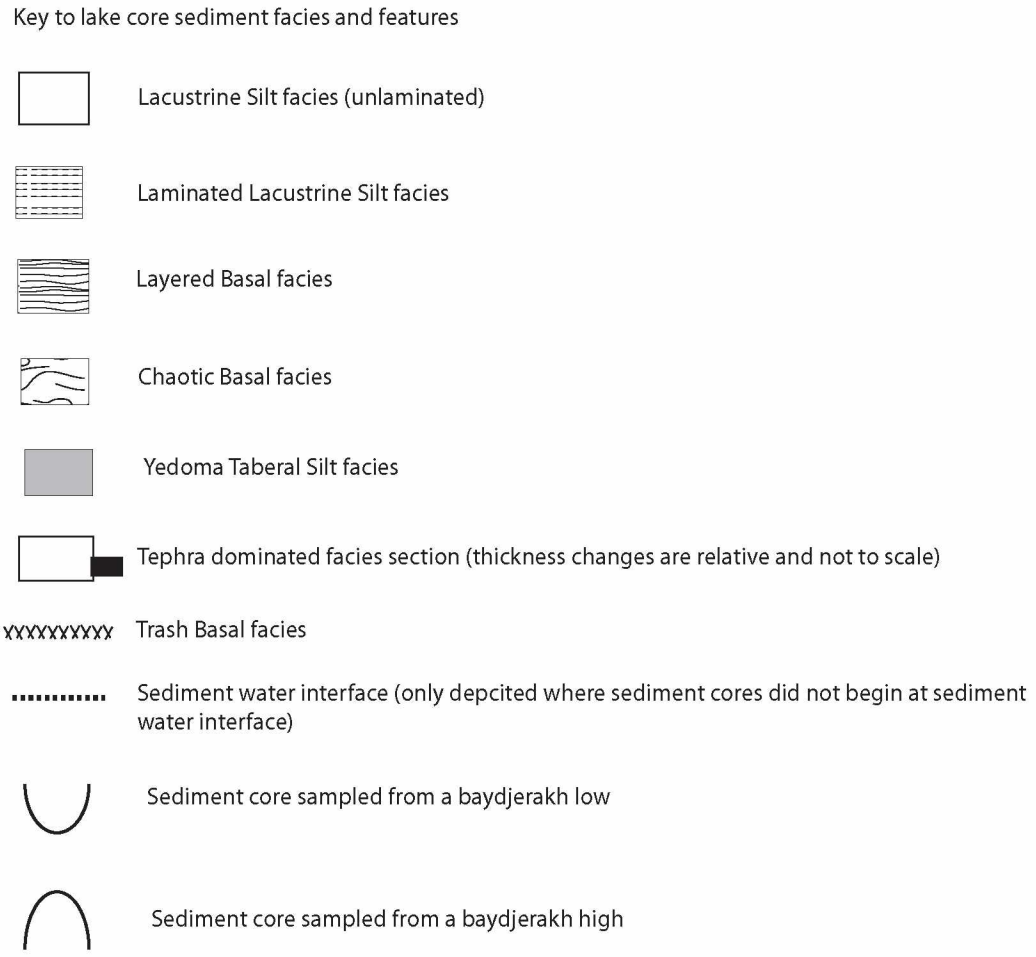

Figure 2.9: Key for schematics and diagrams.

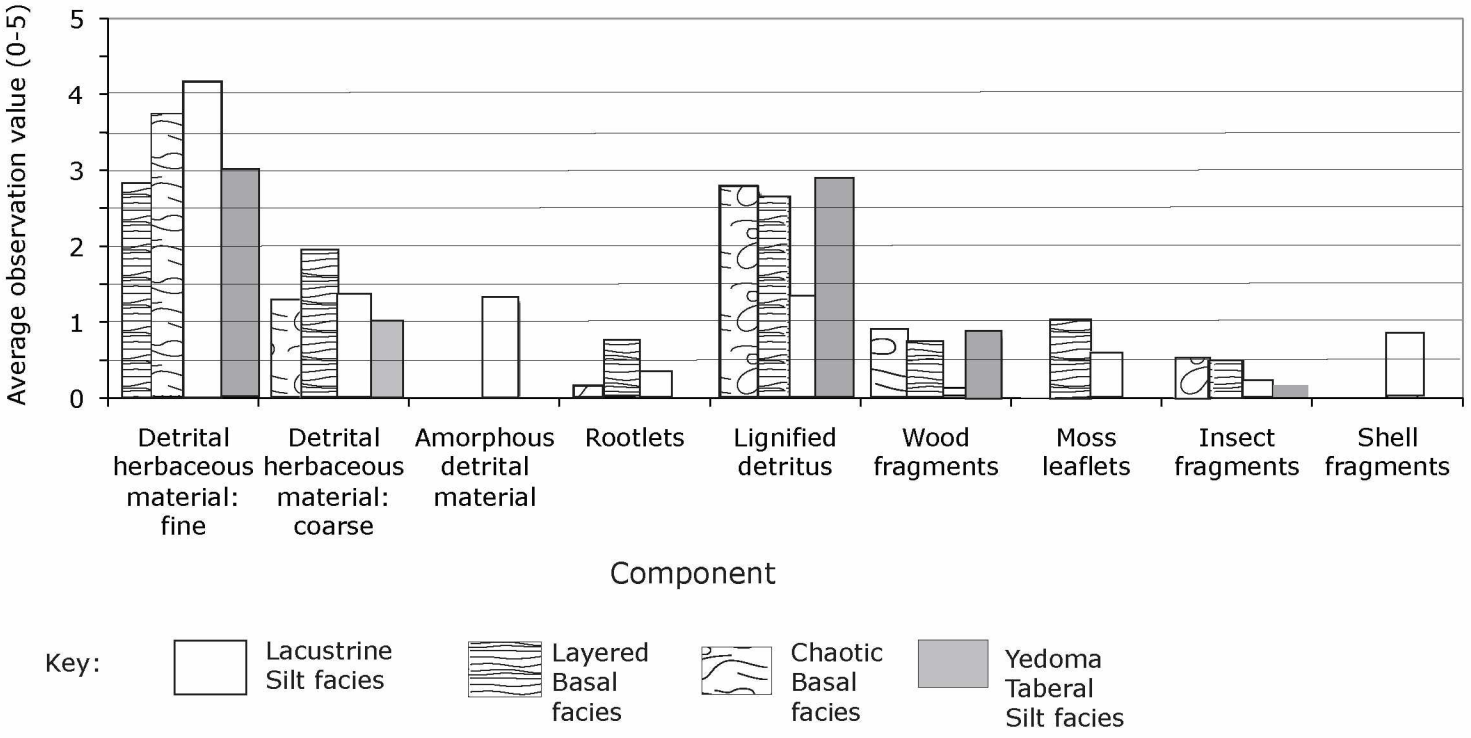

Figure 2.10: Qualitative observations on >250 um fraction of lake sediment, between facies. Average observation value: 5 = 80-100%; 4=50-80; 3 = 30-50%; 2= 5-20%; 1=<5%, 0=0.

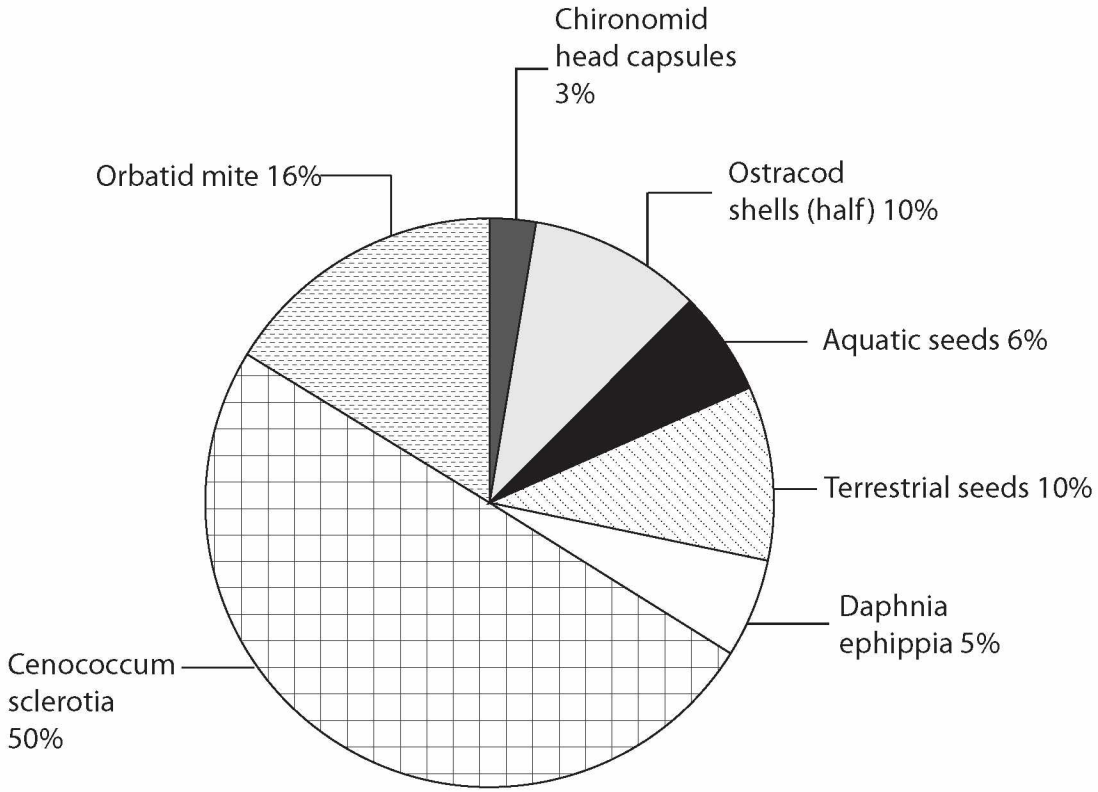

Figure 2.11: Pie chart of discrete macrofossils observed within the Trash Basal facies.

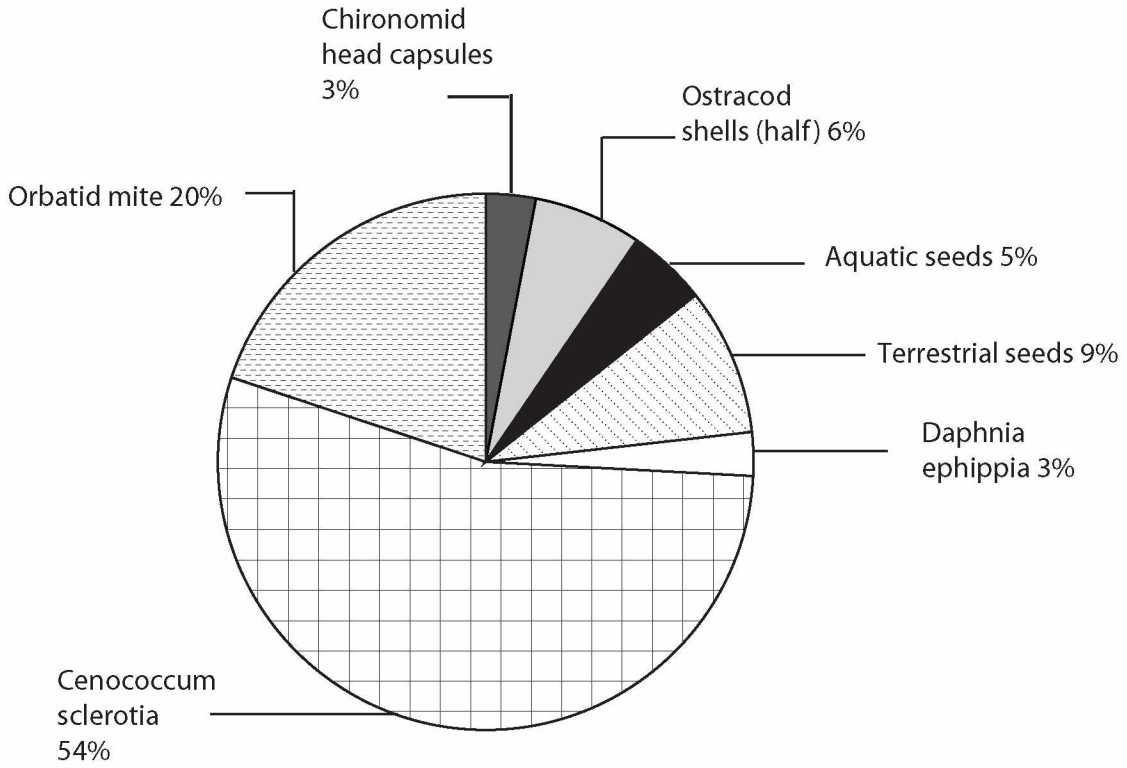

Figure 2.12: Pie chart of discrete macrofossils observed within the Layered Basal facies.

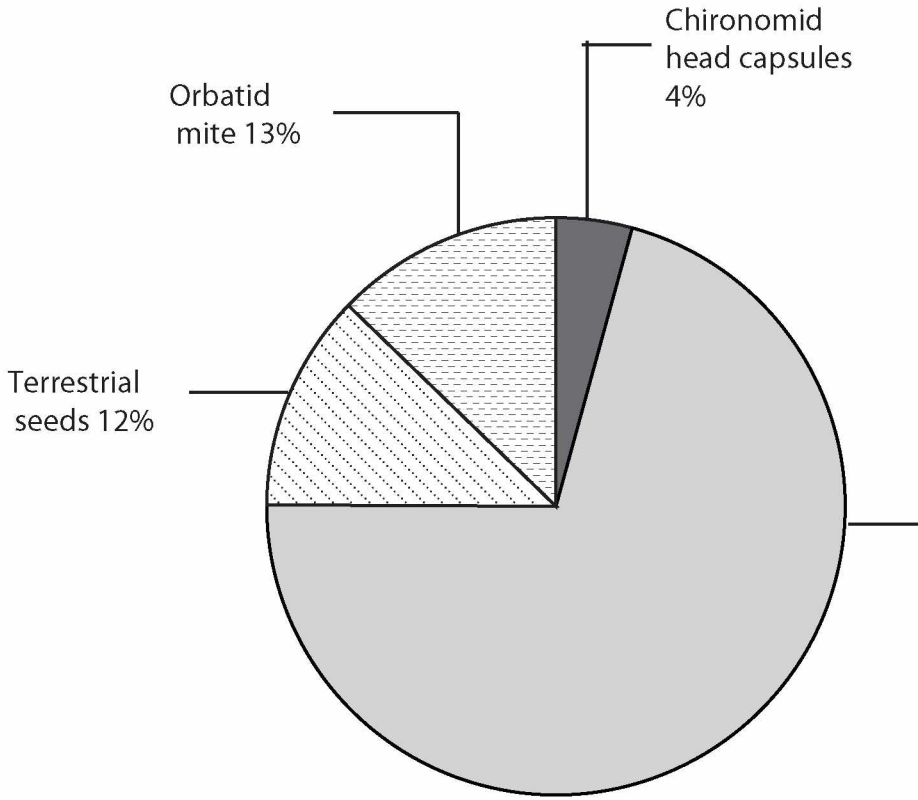

Figure 2.13: Pie chart of discrete macrofossils observed within the Chaotic Basal facies.

Ostracod
shells (half) 71%

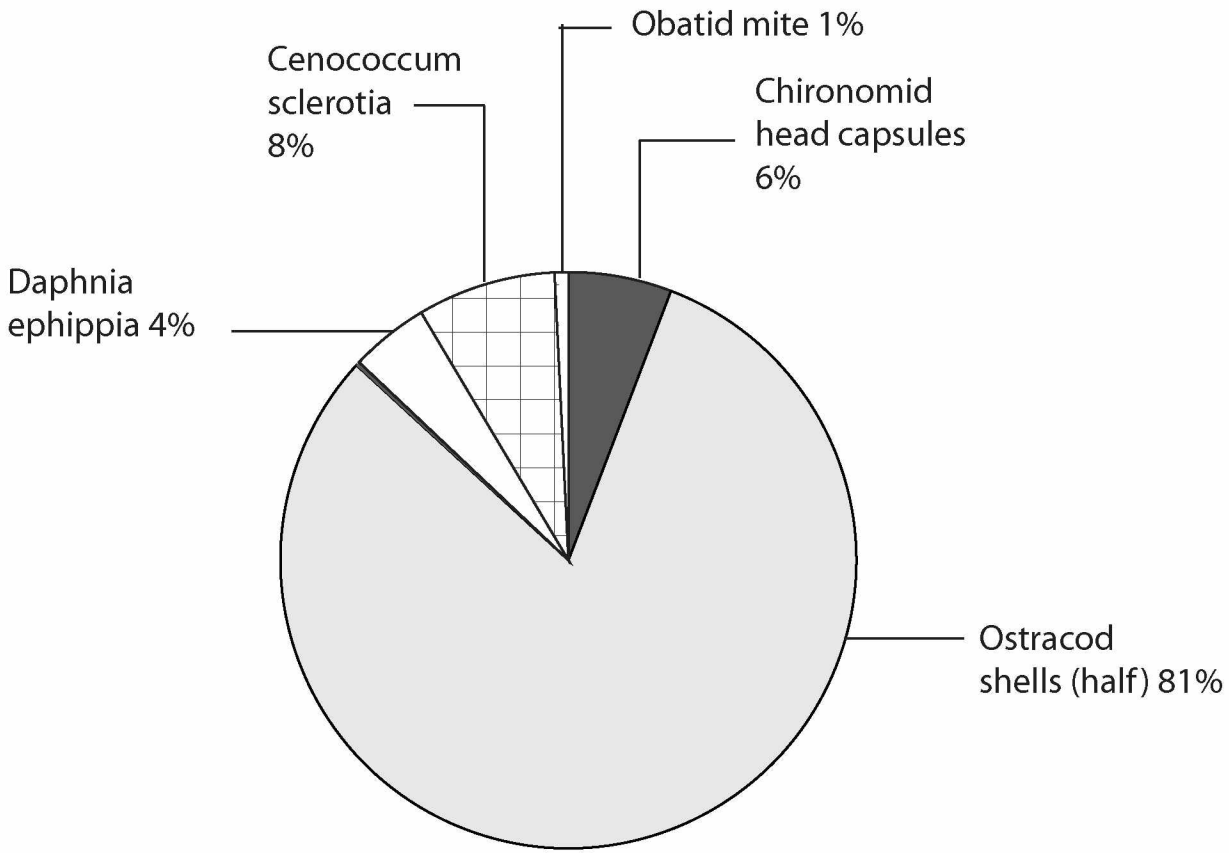

Figure 2.14: Pie chart of discrete macrofossils observed within the Lacustrine Silt facies.

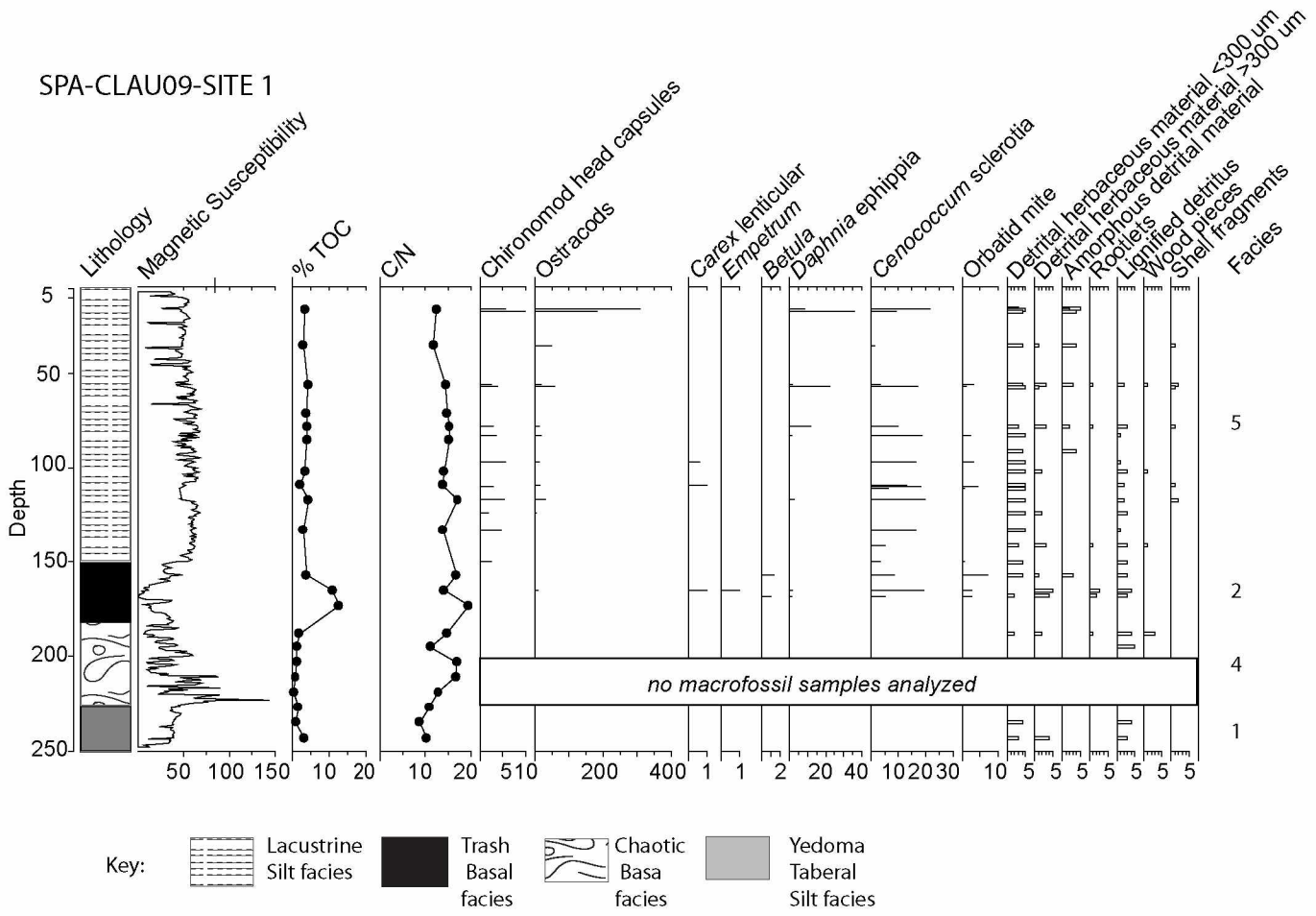

Figure 2.15: Downcore analysis of lake Claudi, SPA-CLAU09--Site 1. For lithology key see Figure 2.7. Macrofossil analysis standardized to 7 cm^3. Scale bars marked 0-5 are qualitative macrofossil observations.

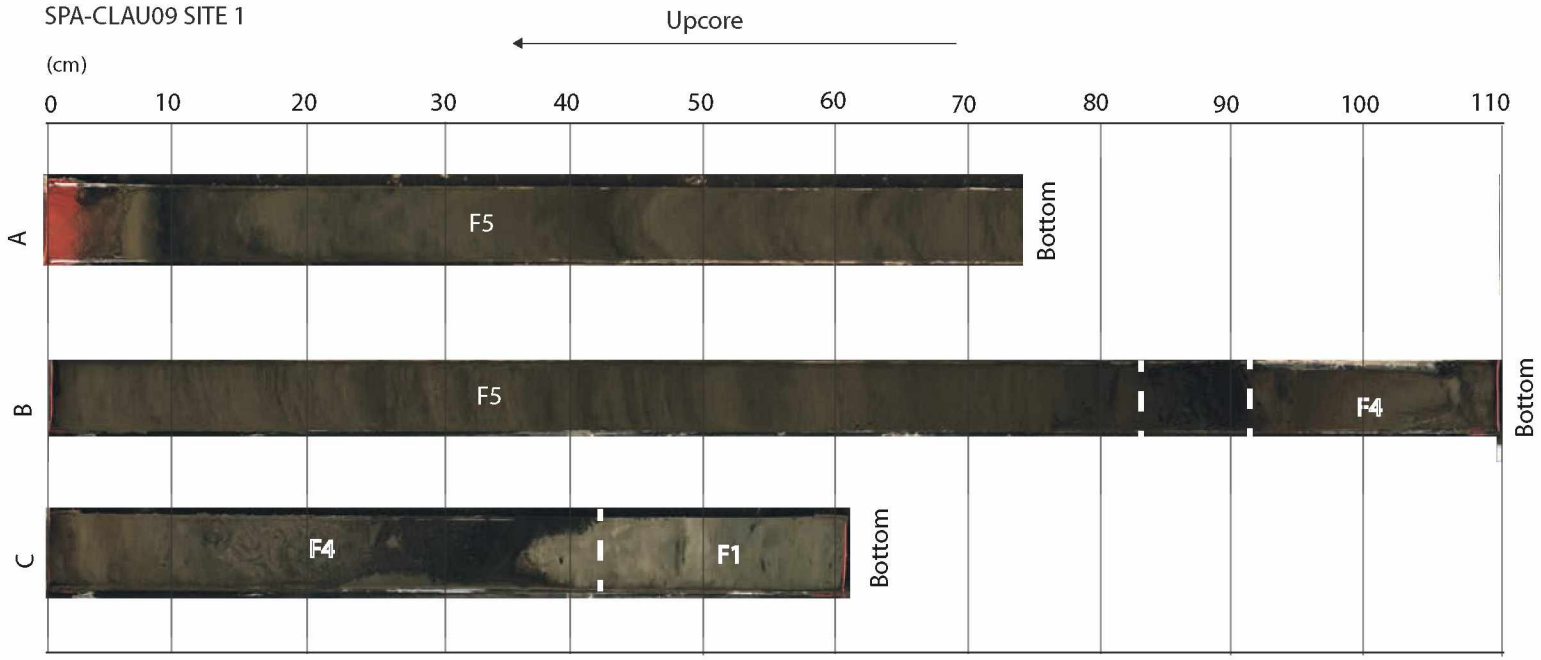

Figure 2.16: High-resolution images of SPA-CLAU09-Site 1. The top of the lake core lies to the left, while the bottom of the core lies to the right. Core A is the one taken closest to the sediment-water interface.

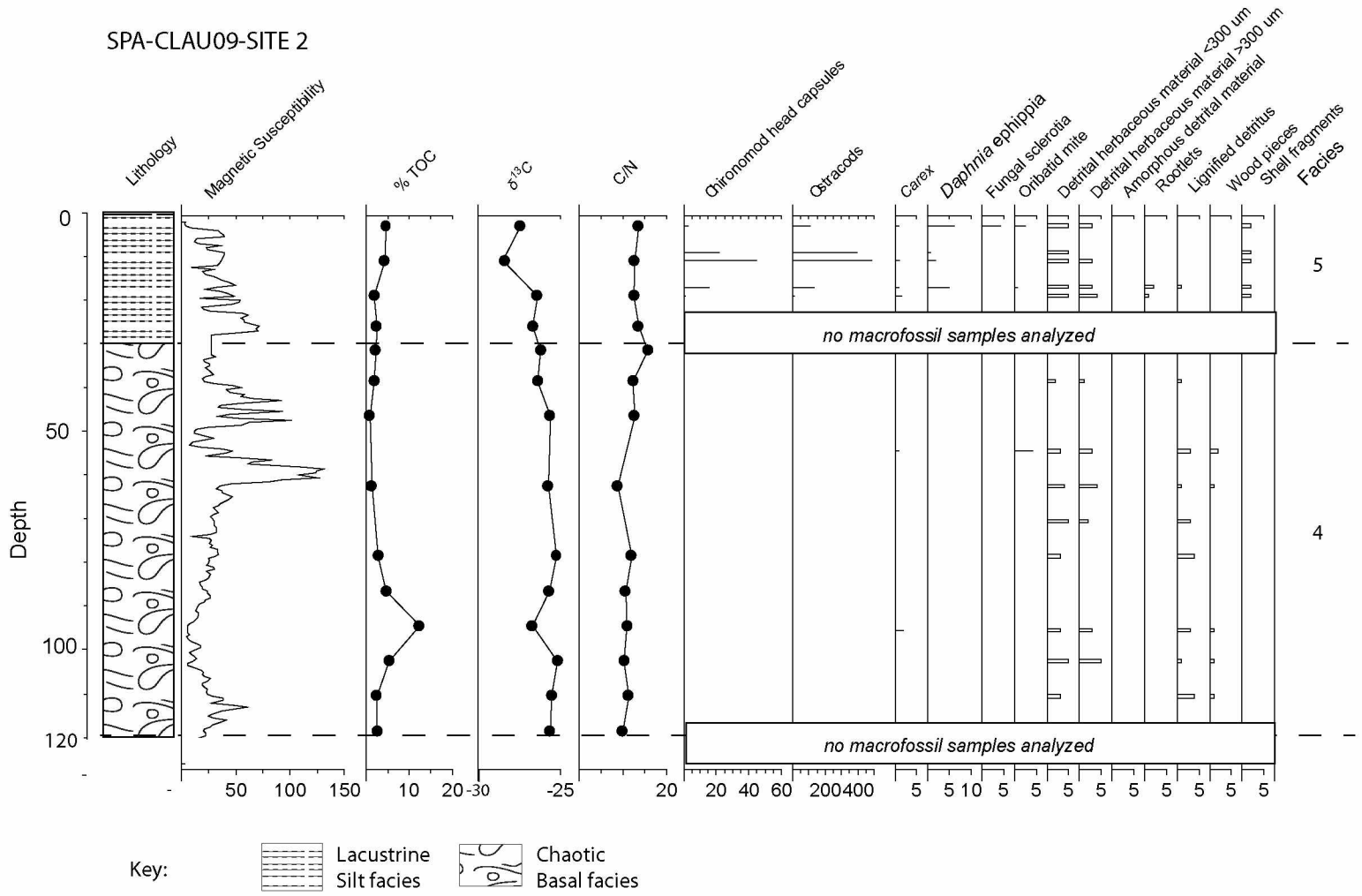

Figure 2.17: Downcore analysis of Lake Claudi site SPA-CLAU09-SITE 2. Macrofossil analysis standardized to 7 cm^3. Scale bars marked 0-5 are qualitative macrofossil observations.

Figure 2.18: High-resolution image of SPA-CLAU09 Site 2 from Lake Claudi. The top of the lake core lies to the left, while the bottom of the core lies to the right. Core A is taken closest to the sediment-water interface.

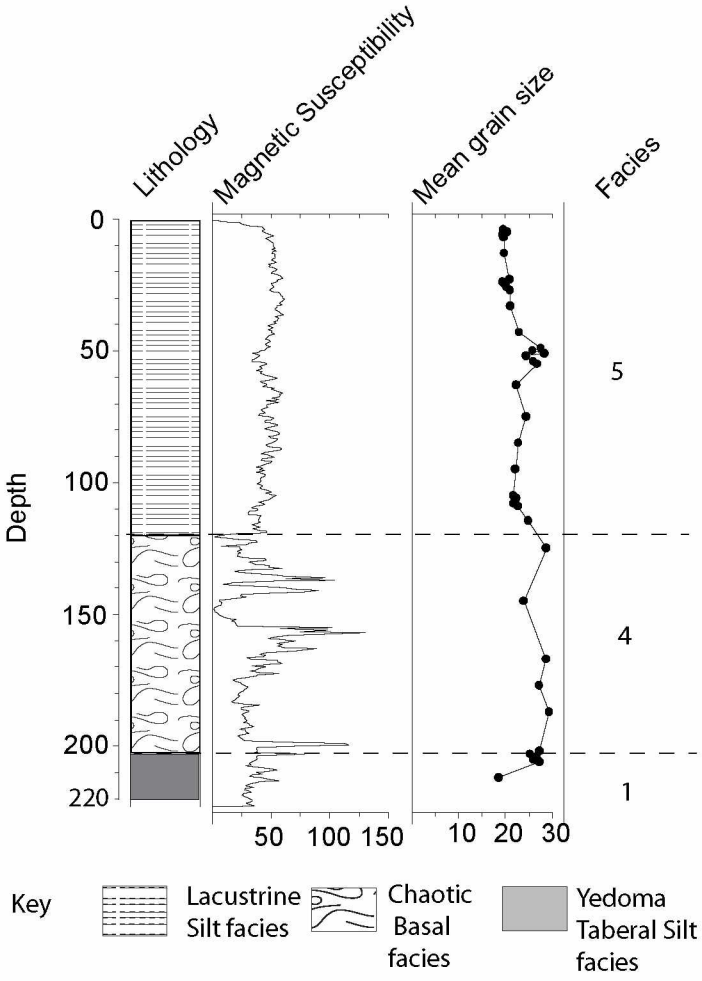

Figure 2.19: Downcore analysis of Lake Claudi, SPA-CLAU10-SITE 2.

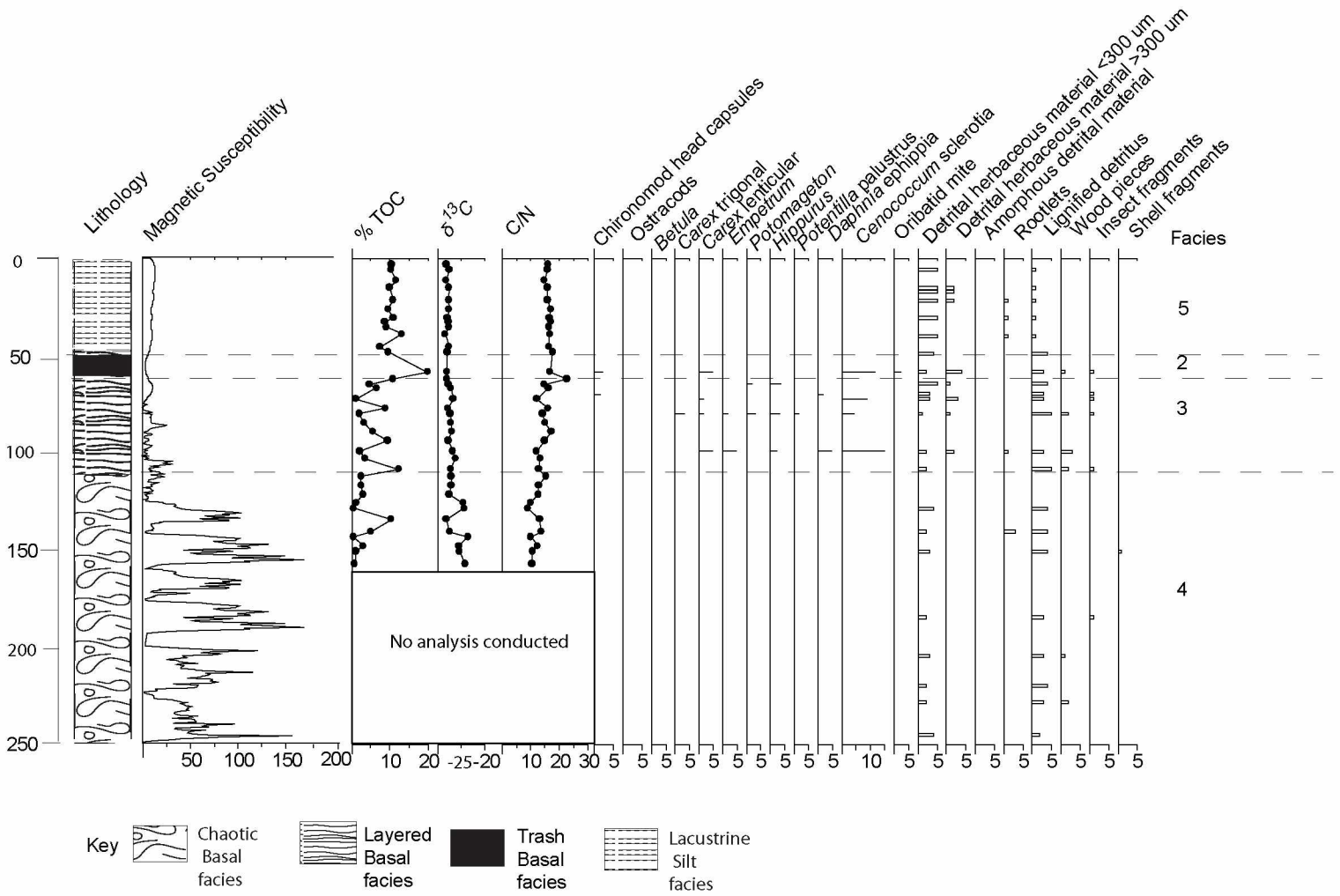

Figure 2.20: Downcore analysis of lake Rhonda, SPA-RHO09 SITE 2. Macrofossil analysis standardized to 7 cm^3. Scale bars marked 0-5 are qualitative macrofossil observations.

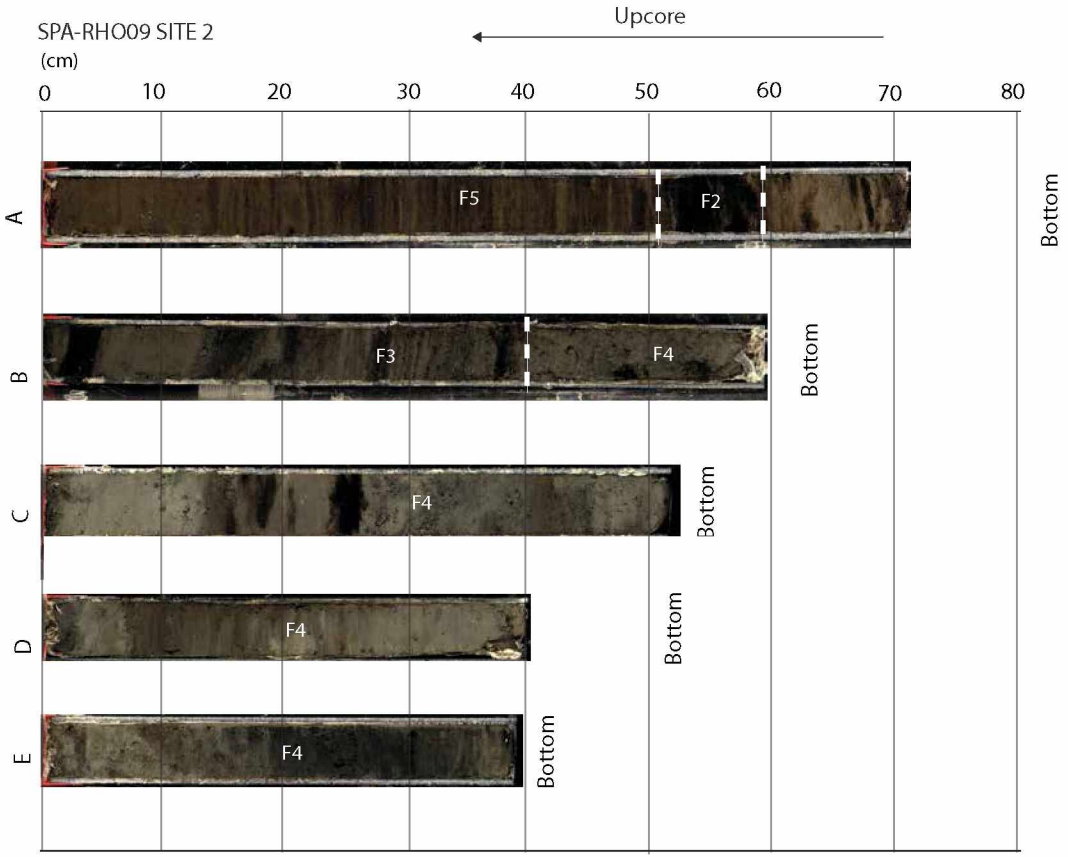

Figure 2.21: High-resolution images of SPA-RHO09 Site 2 from Lake Rhonda. The top of the lake core lies to the left, while the bottom of the core lies to the right. Core A is taken closest to the sediment-water interface. There was no overlap between the cores displayed.

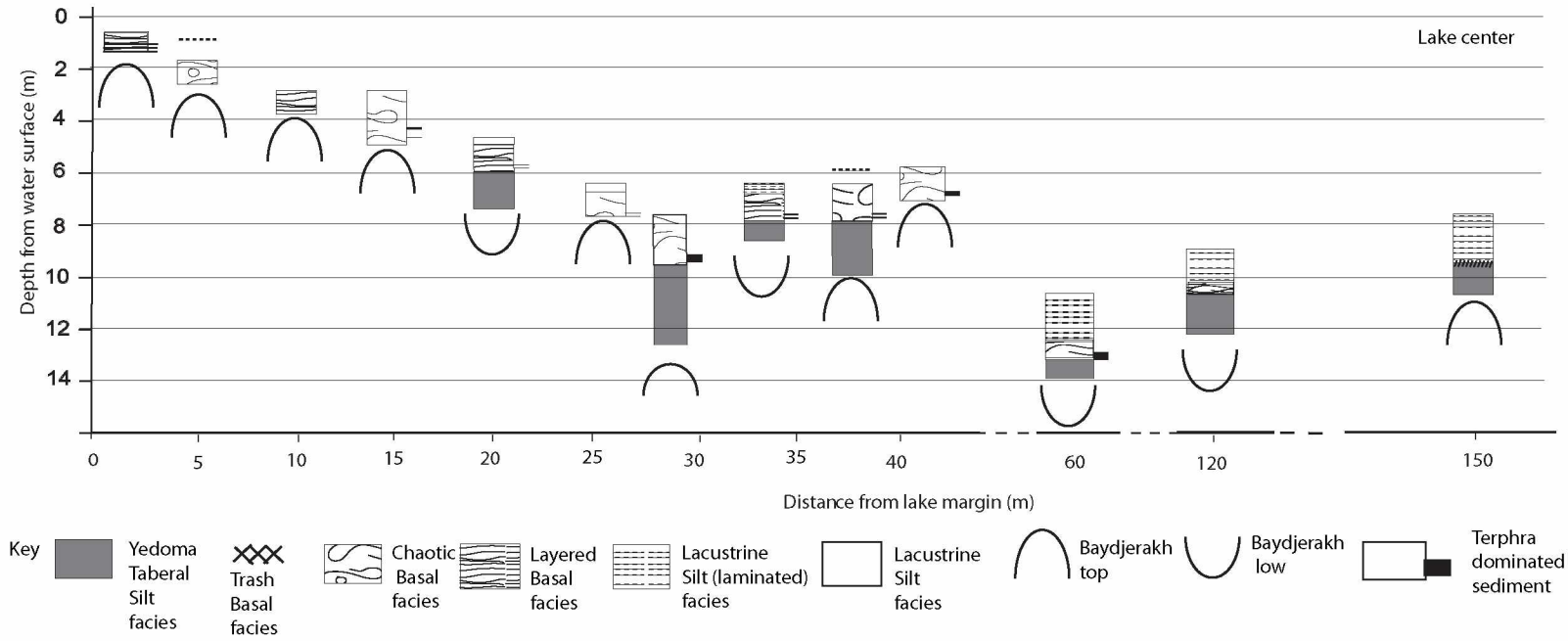

Figure 2.22: Schematic of facies distribution within Lake Claudi from the margin to the lake center. The dashed lines indicates a change in scale.

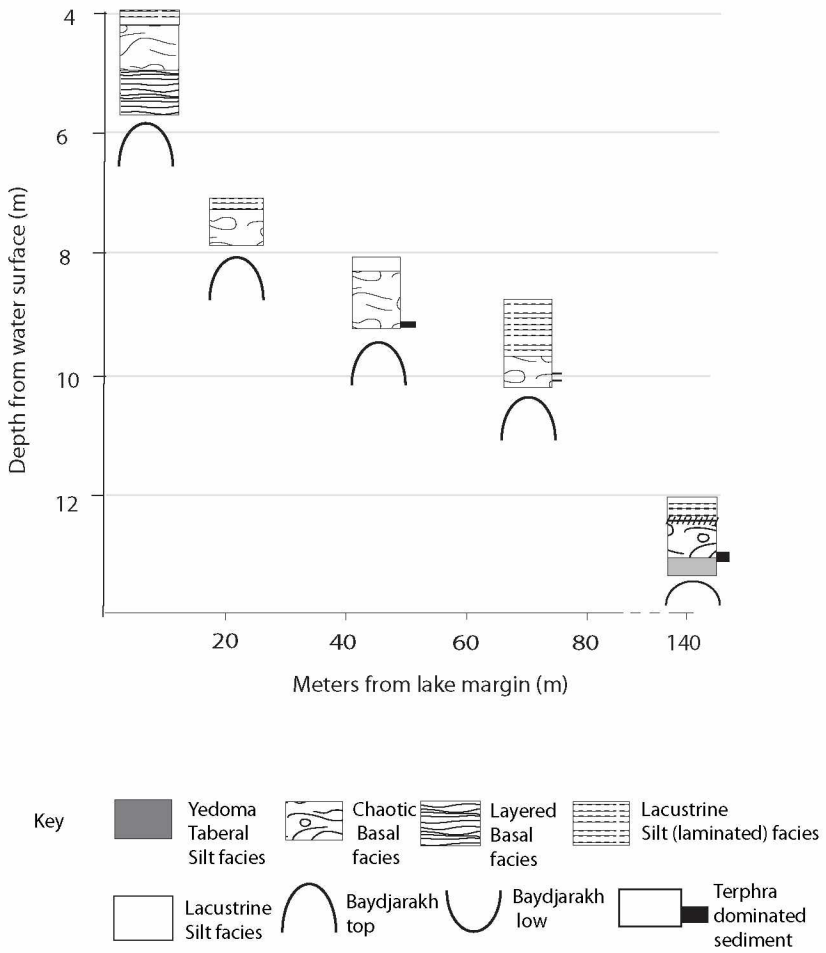

Figure 2.23: Schematic of Lake Jaeger facies distribution from the margin (left), towards the lake center (right). The dashed line indicates a change in scale.

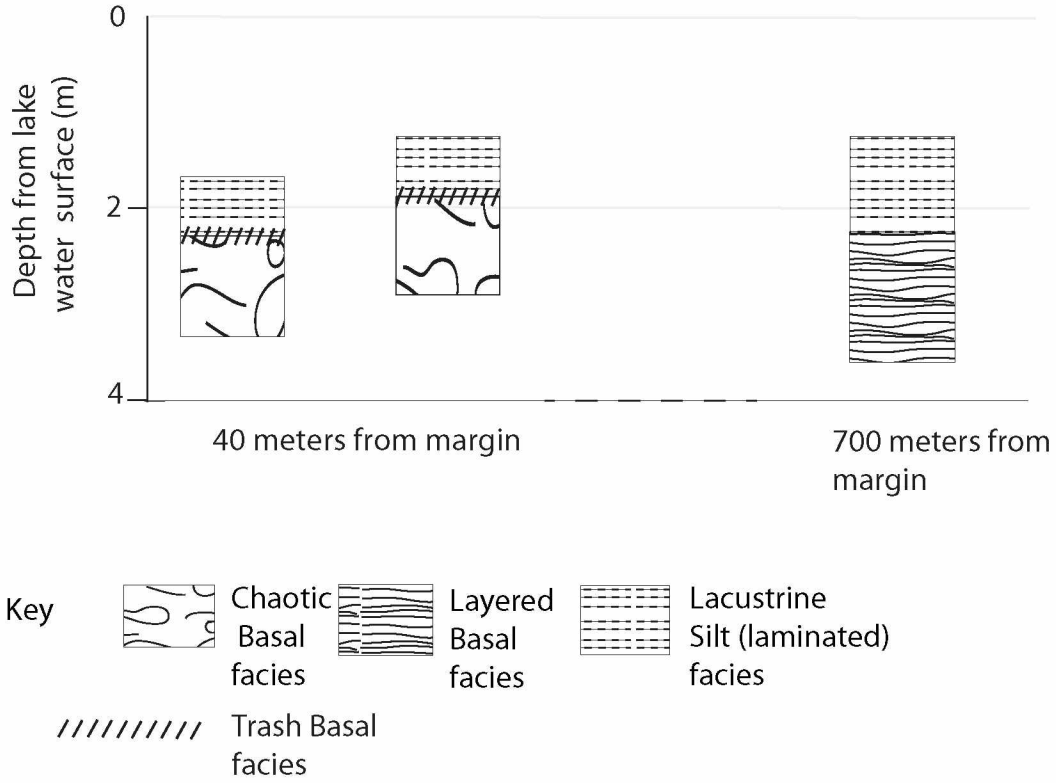

Figure 2.24: Schematic of facies distribution in lake Rhonda. The dashed line indicates a change in scale.

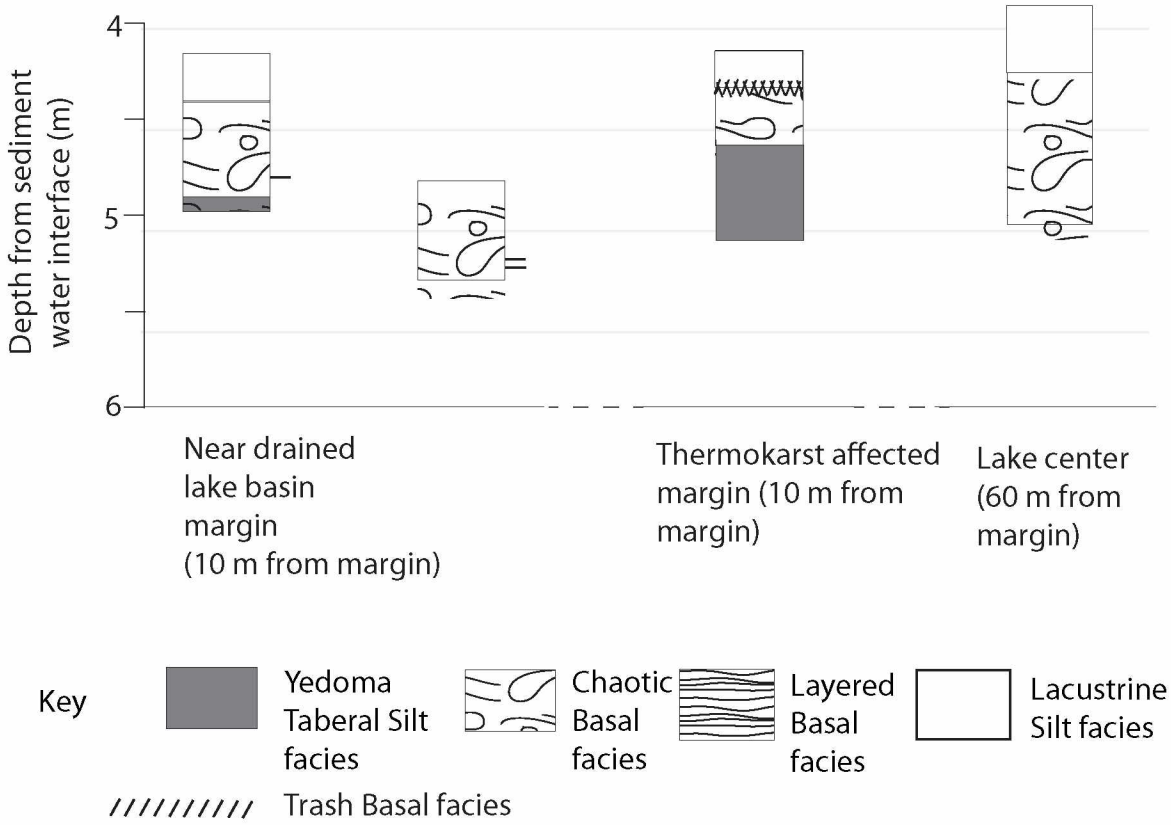

Figure 2.25: Schematic of facies distribution in Cocker Gap Lake. The dashed lines indicate a significant distance (>30 m) between sampling locations.

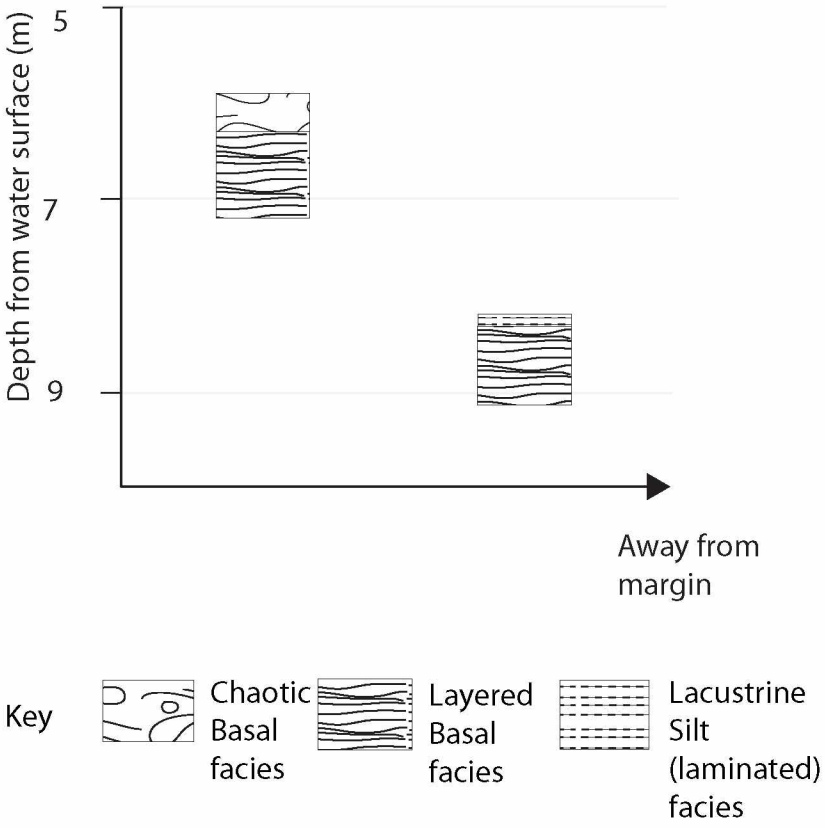

Figure 2.26: Schematic of facies distribution in Three Loon Lake.

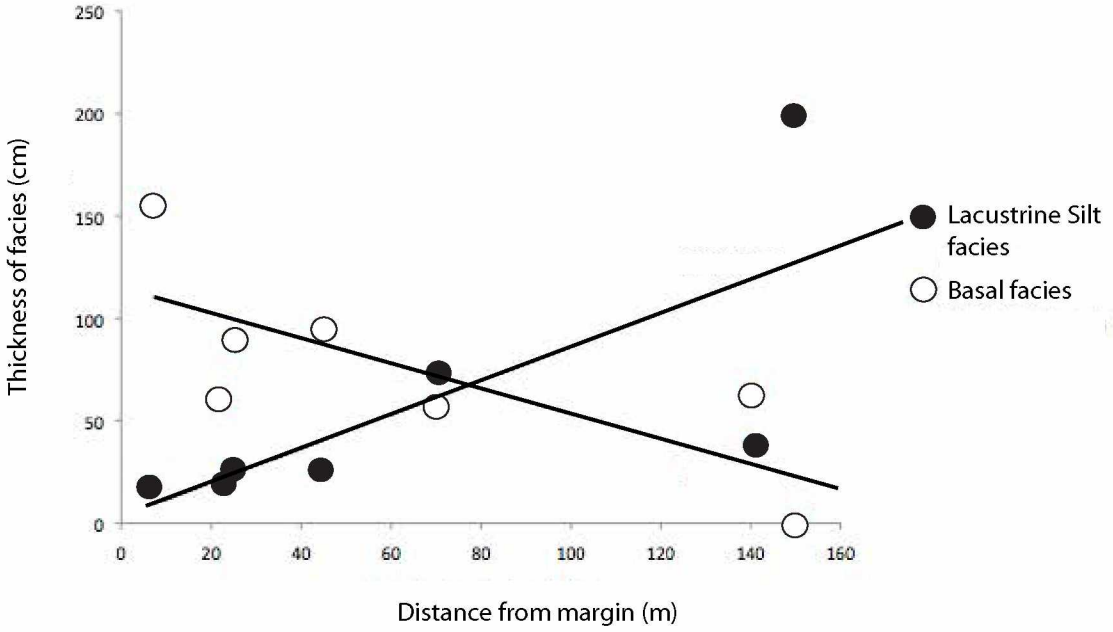

Figure 2.27: Thickness of Lacustrine Silt and combined basal facies versus distance from margin. Basal facies = F3 and F4, Lacustrine Silt = F5. Insufficient data were available to include the Trash Basal facies, F2. Measurements were only taken from baydjarakh highs in lakes Claudi and Jaeger. The relationship between distance from the lake margin and thickness of facies was calculated using the Pearson Correlation test. For basal facies y = -0.6137x + 114.81, for Lacustrine Silt, y = 0.8272x + 3.3314. For basal facies, r= -0.754, N=7, $p<0.02$. For Lacustrine Silt, r=0.731, N=7, $p<0.03$.

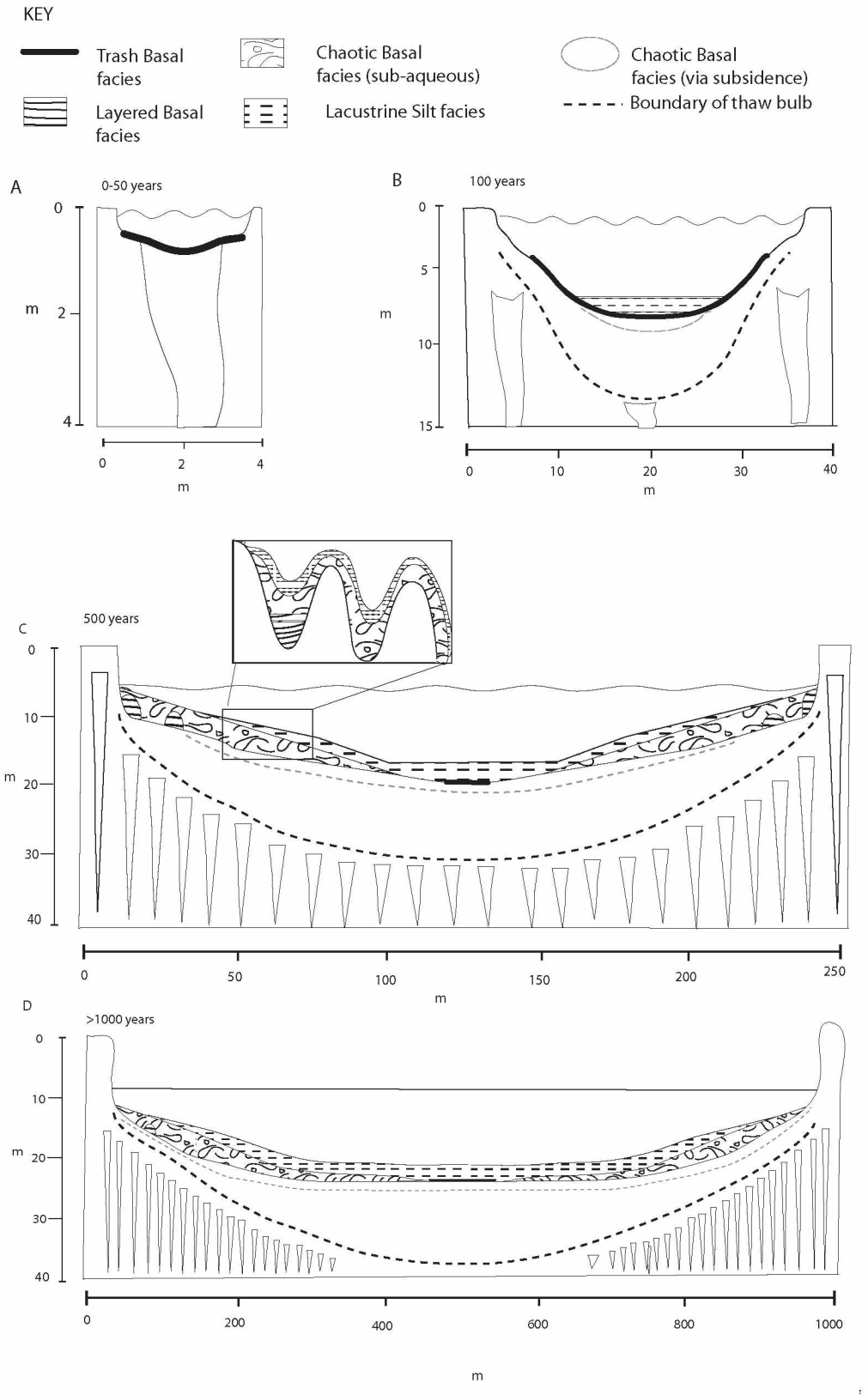
KEY
Trash Basal facies
Layered Basal facies
Chaotic Basal facies (sub-aqueous)
Lacustrine Silt facies
Chaotic Basal facies (via subsidence)
Boundary of thaw bulb
A
0-50 years
B
100 years
C
500 years
D
>1000 years
m

Figure 2.28: Facies distribution at different stages of lake development. Note that both horizontal and vertical scales change. A) Initial thaw and collapse results in Trash Basal facies formation. B) Further subsidence results in lake deepening and taberal deposits beneath the Trash Basal facies becoming distorted as ice thaws. Deposition of Lacustrine Silt in a low energy depositional environment begins. Margin expansion occurs via thermo-erosion. C) Vertical and horizontal lake expansion continues. Baydjarakh topography emerges as ice wedge thaw progresses. Bluff height increases and Chaotic and Layered Basal facies appear due to both an increase in bluff height and deformation of underlying sediment within the thaw bulb. Central, deeper areas of the lake continue to accumulate Lacustrine Silt. D) Excess ice becomes completely depleted beneath the lake center and downward thaw bulb growth continues. The lake bottom begins to flatten in the center. Please note the difference between opaque and solid black lines in the key. The increase in thaw bulb depth through time was taken from Kessler et al. (2011). Expansion rates were taken from B.M.Jones et al. (2011).

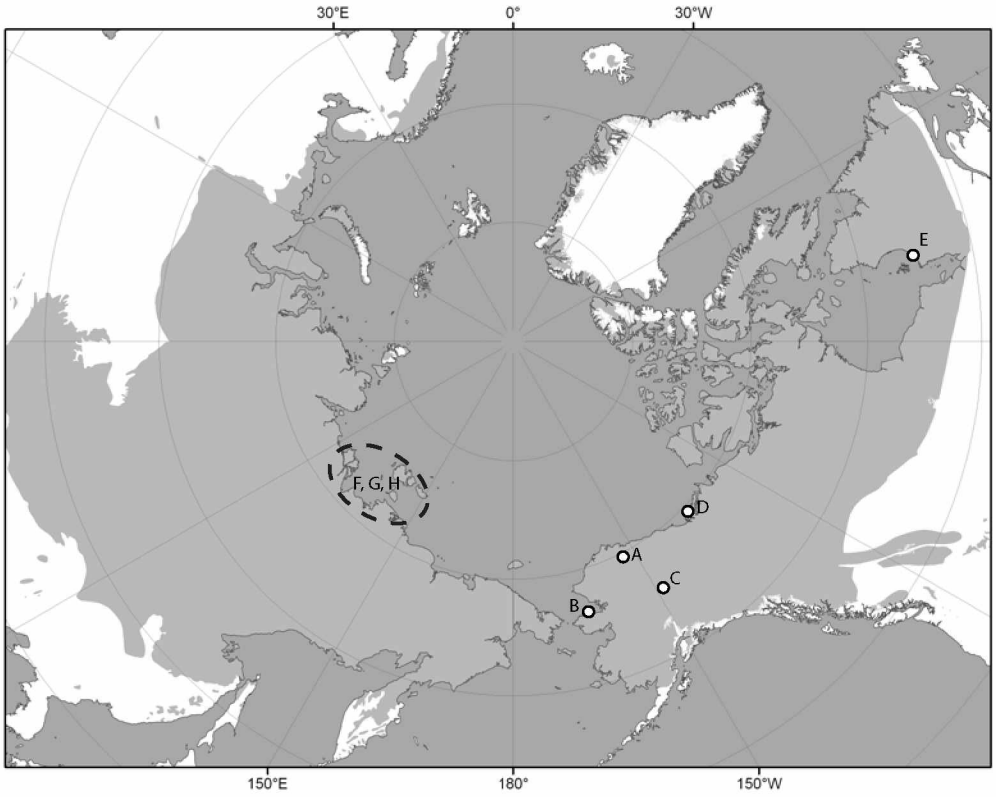

Figure 2.29: Map of pan-arctic showing locations discussed in section 2.6.5 and 2.6.6 on Yedoma and non-yedoma lake comparison: Brooks Range Foothills (A, Rawlinson 1990); Seward Peninsula (B, Charron 1995); Interior Alaska (C, (Brosius 2010); the Tuktoyaktuk Peninsula (D, Murton 1996); Hudson Bay Lowlands (E, Bouchard et al. 2011); Arga Island, Lena River Delta (F, Schwamborn et al. 2000); and northeast Siberia (G, Schirrmeister et al. 2008a and 2011 and H, Wetterich et al. 2009). Shaded areas designate extent of permafrost-affected soils. Map courtesy of G. Grosse 2011.

2.11 Tables

Table 2.1: Lake metadata. Dashes indicate that no data were available. Lake area values based on 2006 Ikonos imagery (supplied by G.Grosse, unpublished data). The maximum depths are those measured during field campaigns, therefore true maximum depths within the lakes are unknown due to limited field surveys. Asterisks indicate first-generation lakes.

Lake name	Lake depth (max, m.)	Secchi disk reading (m)	Long axis (m)	Short axies (m)	Area (ha)	Freeze to bottom	Latitude	Longitude
Jaeger*	12.73	-	732	217	24.06	no	66° 30'1.27"N	164° 15'21.35"W
Claudi*	9.2	3.4	575	397	16.27	no	66° 33'05.80"N	164° 27'01.37"W
Tea*	5.75	-	157	105	1.28	no	66° 30'09.35"N	164° 19' 47.5"W
Rhonda	1.01	0.9	1247	1162	79.77	yes	66° 33'40"N	164° 28' 20"W
Cocker Gap	7.76	-	225	120	2.18	no	66° 33'42.38"N	164° 27' 10.88"W
Three Loon	5.75	-	560	134	9.37	no	66° 29'44.2"N	164° 15' 06.46"W
Prickly	5.75	-	72	32	1.80	no	66° 32'48.19"N	164° 26'48.03"W

Table 2.2: Statistical relationships between measurements of TOC, C/N, $\delta^{13}C$, magnetic susceptibility and mean grain size between facies, lakes and generations. Asterisks indicate that only Lacustrine Silt facies only were compared. A cross indicates that only facies from Lake Claudi were analyzed and compared for grain size. 'Lake' is a comparison of all lakes sampled. 'Generation' is the comparison of first- and later-generation lake Lacustrine Silt facies. 'First-generation lakes' compares only Lake Claudi and Lake Jaeger. 'Later-generation lakes' compares lakes Rhonda, Three Loon and Cocker Gap.

Dependent	Variable	Results	Significant difference?
Facies	% TOC	χ^2 = 51.221, *df* =4, p *<0.001*	Yes
Generation*	% TOC	χ^2 = 0.147, *df* =1, p*<0.701*	No
Lake (Claudi, Jaeger, Three Loon, Cocker Gap and Rhonda)*	% TOC	χ^2 = 11.243, *df* =4, p *<0.024*	Yes
First generation lakes*	% TOC	χ^2 = 0.480, *df* =1, p*<0.489*	No
Later generation lakes*	% TOC	χ^2 = 1.033, *df* =2, p*<0.597*	No
Facies	C/N	χ^2 = 43.311, *df* =4, p *<0.001*	Yes
Lake (Claudi, Jaeger, Three Loon, Cocker Gap and Rhonda)*	C/N	χ^2 =21.269 , *df* =4, p *<0.001*	Yes
Generation*	C/N	χ^2 = 5.902, *df* =1, p*<0.015*	Yes
First generation lakes*	C/N	χ^2 = 1.039, *df* =1, p*<0.308*	No
Later generation lakes*	C/N	χ^2 = 8.962, *df* =2, p*<0.011*	Yes
Facies	δ13C	χ^2 = 48.635, *df* =4, p *<0.001*	Yes
Lake (Claudi, Jaeger, Three Loon, Cocker Gap and Rhonda)*	δ13C	χ^2 = 20.405, *df* =4, p *<0.001*	Yes
Generation*	δ13C	χ^2 = 10.181, *df* =1, p*<0.001*	Yes
First generation lakes*	δ13C	χ^2 = 13.576, *df* =1, p*<0.001*	Yes
Later generation lakes*	δ13C	χ^2 = 4.718, *df* =2, p*<0.095*	No
Facies	MS	χ^2 = 193.897, df =4, p<0.001	Yes
Lake (Claudi, Jaeger, Three Loon, Cocker Gap and Rhonda)*	MS	χ^2 = 14.492, *df* =4, p *<0.006*	Yes
Generation*	MS	χ^2 = 5.902, *df* =1, p*<0.152*	No
First generation lakes*	MS	χ^2 = 76.393, *df* =1, p*<0.001*	Yes
Later generation lakes*	MS	χ^2 = 134.493, *df* =2, p*<0.001*	Yes
Facies+	grain	χ^2 = 134.493, *df* =2, p*<0.001*	Yes

Table 2.3: Games Howell pairwise comparison of TOC for each facies. Sample populations were significantly different when $p<0.05$. Asterisks indicate where there was a significant difference between facies.

Facies	Facies	Sig.
*	Chaotic basal	0.018
	Laminated basal	0.997
*	Taberal	0.000
Lacustrine silt	Trash basal	0.695
*	Lacustrine silt	0.018
	Laminated basal	0.539
	Taberal	0.894
Chaotic basal	Trash basal	0.505
	Lacustrine silt	0.997
	Chaotic basal	0.539
	Taberal	0.168
Laminated basal	Trash basal	0.671
*	Lacustrine silt	0.000
	Chaotic basal	0.894
	Laminated basal	0.168
Taberal	Trash basal	0.463
	Lacustrine silt	0.695
	Chaotic basal	0.505
	Laminated basal	0.671
Trash basal	Taberal	0.463

Table 2.4: Median values and visual characteristics of facies identified. Dashes indicate where data were not available. No mean values or standard deviations are stated, as data were not found to have a normal distribution.

Facies	% TOC	C/N	$\delta^{13}C$	Grain size (um)	MS SI 10^{-6}	Visual characteristics
Taberal (F1)	1.582 (n=27)	10.864 (n=27)	-25.250 (n=27)	26.40 (n=10)	25.45 (n=242)	Massive grey (5 Y 4/1) silt matrix containing occasional peat and tephra balls, lenses or distorted bands
Trash basal (F2)	11.85 (n=2)	18 (n=2)	-27.756 (n=2)	-	4.40 (n=41)	Distinct dark brown (5Y 3/1) band >5cm thickness composed of poorly decomposed detrital organic material
Layered basal (F3)	2.998 (n=35)	13.531 (n=35)	-26.506 (n=33)	-	35.3 (n=396)	Alternate bedding of silt, organic detrital material and tephra, bands range in thickness from
Chaotic basal (F4)	1.323 n=22)	12.150 (n=22)	-25.633 (n=21)	28.60 (n=3)	29.2 (n=537)	A silt matrix of either brown or grey (5Y 3/1, 5 Y 4/3), showing signs of disturbance, with tephra and peat inclusions
Lacustrine silt (F5)	3.91 (n=65)	13.746 (n=80)	-27.071 (n= 80)	22.1 (n=29)	40.700 (n=1396)	Fine brown silt (2.5Y 3/1, 2.5Y 3/2, 5Y 3/1 or 5Y 3/2), often displaying darker laminations (and10YR 2/1 to 10YR 3/2) <2mm thickness

Table 2.5: Pairwise comparison of $\delta^{13}C$ values (n=167) for each facies. Sample populations were significantly different when $p<0.05$. Asterisks indicate where there was a significant difference between facies. Samples were analyzed for Lake Claudi, Lake Rhonda, Lake Three Loon, Lake Jaeger and Lake Cocker Gap.

Facies	Facies		Sig
Lacustrine silt	Chaotic basal	*	0.000
	Laminated basal		0.074
	Taberal	*	0.000
	Trash basal		0.121
Chaotic basal	Lacustrine silt	*	0.000
	Laminated basal	*	0.025
	Taberal		0.956
	Trash basal	*	0.000
Laminated basal	Lacustrine silt		0.074
	Chaotic basal	*	0.025
	Taberal	*	0.012
	Trash basal	*	0.029
Taberal	Lacustrine silt	*	0.000
	Chaotic basal		0.956
	Laminated basal	*	0.012
	Trash basal	*	0.000
Trash basal	Lacustrine silt		0.121
	Chaotic basal	*	0.000
	Laminated basal	*	0.029
	Taberal	*	0.000

Table 2.6: Pairwise comparison of C/N values (n=167) for each facies. Sample populations were significantly different when $p<0.05$. Asterisks indicate where there was a significant difference between facies. Samples were analyzed for Lake Claudi, Lake Rhonda, Three Loon Lake, Lake Jaeger and Cocker Gap Lake.

Facies	**Facies**		Sig.
Lacustrine silt	Chaotic basal	*	0.069
	Laminated basal		0.999
	Taberal	*	0.000
	Trash basal		0.461
Chaotic basal	Lacustrine silt		0.069
	Laminated basal		0.117
	Taberal		0.170
	Trash basal		0.139
Laminated basal	Lacustrine silt		0.999
	Chaotic basal		0.117
	Taberal	*	0.000
	Trash basal		0.528
Taberal	Lacustrine silt	*	0.000
	Chaotic basal		0.170
	Laminated basal	*	0.000
	Trash basal		0.088
Trash basal	Lacustrine silt		0.461
	Chaotic basal		0.139
	Laminated basal		0.528
	Taberal		0.088

Table 2.7: Pairwise comparison of mean grain size values for each facies (no samples were run from Trash or Layered Basal facies). Sample populations were significantly different when $p<0.05$. Asterisks indicate where there was a significant difference between facies. Samples (n=42) were taken from a central core from Lake Claudi.

Facies		Facies	Sig.
		Chaotic basal	0.162
Lacustrine silt	*	Taberal	0.020
		Lacustrine silt	0.162
Chaotic basal		Taberal	0.755
	*	Lacustrine silt	0.020
Taberal		Chaotic basal	0.755

Table 2.8: Pairwise comparison of magnetic susceptibility values (n=2630) between facies. Sample populations were significantly different when $p<0.05$. Asterisks indicate where there was a significant difference between facies. Samples were analyzed for Lake Claudi, Lake Rhonda, Three Loon Lake, Lake Jaeger and Cocker Gap Lake.

Facies		**Facies**	Sig.
	*	Chaotic basal	0.032
		Laminated basal	0.571
	*	Taberal	0.000
Lacustrine silt	*	Trash basal	0.000
	*	Lacustrine silt	0.032
	*	Laminated basal	0.025
	*	Taberal	0.006
Chaotic basal	*	Trash basal	0.000
		Lacustrine silt	0.571
	*	Chaotic basal	0.025
Laminated	*	Taberal	0.000
basal	*	Trash basal	0.000
	*	Lacustrine silt	0.000
	*	Chaotic basal	0.006
	*	Laminated basal	0.000
Taberal	*	Trash basal	0.000
	*	Lacustrine silt	0.000
	*	Chaotic basal	0.000
	*	Laminated basal	0.000
Trash basal	*	Taberal	0.000

Table 2.9: Key characteristics described for yedoma thermokarst lakes forming in Alaska. Dashed lines indicate no data were available.

Loaction	Facies	Seward peninsula yedoma thermokarst lake facies equivalent (this study)	% TOC	C/N	$\delta^{13}C$	Mean grain size (phi)	MS 10-8m3/kg	Visual characteristics	Reference
Seward Peninsula, Alaska	Basal unit	Chaotic and layered basal	-	-	-	-	-	Detrital unit of sand and organic detrital material, between 0,1 and 1.0 meters thick.	Hopkins and Kidd (1988)
Seward Peninsula, Alaska	Infill	Lacustrine silt	-	-	-	-	-	Fine-grained, thin-bedded deposit, between one and ten m thick	Hopkins and Kidd (1988)
Seward Peninsula, Alaska	Setion 3, unit A	Chaotic basal	8.4 % (LOI)	-	-	8.6 phi	-	Inorganic silt matrix with organic silt inclusions	Charron 1995
Seward Peninsula, Alaska	Section 3, unit B	-	20.9 - 24.9 % (LOI)	-	-	8.2 phi	-	Organic rich silt - no bedding visible due to abundant organics	Charron 1995
Seward Peninsula, Alaska	Section 3, unit C	Trash basal	-	-	-	-	-	Peat, 14 cm thick, flat lying twigs and moss	Charron 1995
Seward Peninsula, Alaska	Section 3, unit D	Layered basal	20.0 - 25.8 %(LOI)	-	-	silty clay	-	Alternating beds of peat (3-4 cm)and organic silt (5-6), below an organic rich silt, no visible bedding due to abundant organics	Charron 1995
Seward Peninsula, Alaska	Section 4, unit A	Taberal	-	-	-	-	-	Massive sand containing 2-cm thick lag deposits of fossil marine mollusks	Charron 1995
Seward Peninsula, Alaska	Section 4, unit B	Lacustrine silt with laminations	4.0 - 5.6 % (LOI)	-	-	7.3 phi (very fine silt)	-	Horizontally bedded silt with fossil mollusks	Charron 1995
Seward Peninsula, Alaska	Section 4, unit C	Layered basal	3.0 - 5.0 % (LOI)	-	-	-	-	Two alternating packages of laminated silt and x0stratified sand	Charron 1995
Seward Peninsula, Alaska	Section 4, unit D	Layered basal	3.9-3.8 % (LOI)	-	-	6.9 phi (very fine silt) for the mineral bands only	-	Alternating bads of coarse silt and very fine sand,	Charron 1995
Brooks Range Foothills, Alaska	Lake sediments	Lacustrine silt, possibly layered basal	-	-	-	-	-	i) 0.6 meters thick, overlie and fill two ice wedge pseudomorphs ii)organic bedded silt	Rawlinson 1990
Brooks Range Foothills, Alaska	Thin organic bed	Trash basal	-	-	-	-	-	0.3 m thick organic bed, containing freshwater gastropods	Rawlinson 1990

Table 2.10: Key characteristics described for yedoma thermokarst lakes forming in northeast Siberia. Dashed lines indicate no data were available.

Loaction	Facies	Seward peninsula yedoma thermokarst lake facies equivalent (this study)	% TOC	C/N	$\delta^{13}C$	Mean grain size (um)	MS 10-8m3/kg	Visual characteristics	Reference
Dmitry Laptev Straight , northeast Siberia	Lacustrine	i) Chaotic basal, ii) layered basal	2 to 6	2 to 8	-26 to -29	15 to 50	15 to 35	i) Cryotubrated, poorly decomposed peat in a sand silt matrix, ii) alternating beds of dark gray clayish silt with 2mm layers of plant detritus	Wetterich et al. 2009
Dmitry Laptev Straight, northeast Siberia	Taberal	Taberal	1 to 6	4 to 13	-31 to -28	15 to 40	10 to 30	Greenish grey with peat lenses of 5-10 cm in length	Wetterich et al. 2009
Duvanny Yar, northeast Siberia	Lacustrine (all)	i) Chaotic basal, ii) lacustrine silt	-	-	-	-	-	i) Peat inclusions in a silty matrix , ii) disturbed, bedded dark grey, silty fine sand	Schirrmeister et al. 2008
North east Siberia, various locations	Late glacial/Holocene thermoakrst lacustrine (all)	Not applicable	5.9 +/-9 (n= 148)	10.0 +/-5.4 (n=133)	-27.93+/-1.33 (n=139)	-	-	-	Schirrmeister et al. 2011 (includes data from Wetterich et. al 2009)
North east Siberia, various locations	Taberal	Taberal	2.7 +/- 4 (n=9)	7.3 +/-3.4 (n=9)	-29.47 +/-1.55 (n=9)	-	-	-	Schirrmeister et al. 2011 (includes data from Wetterich et. al 2009)
Central Yakutia	Organic rich silt	Lacustrine infill	-	-	-	-	-	-	Katamura et al. 2006
Central Yakutia	Sand	Taberal	-	-	-	-	-	-	Katamura et al. 2006

Table 2.11: Key characteristics of Interior Alaska, yedoma-type thermokarst lakes. Dashed lines indicate no data were available.

Location	Facies	Seward peninsula yedoma thermokarst lake facies equivalent	% TOC	C/N	$\delta^{13}C$	Mean grain size	MS SI	Visual characteristics	Reference
Interior Alaska, Goldstream Lake	Lake infill	Lacustrine silt and basal facies	19.1 +/- 1.4	20.3 +/- 0.4	-	-	-	Extremely thin (<5 cm) organic sediment layer, composed of aquatic detritus	Brosius 2010
Interior Alaska, Goldstream Lake	Taberal	Taberal	0.6 - 0.9	10.8 +/- 1.2	-	-	-	Thick, dense silt	Brosius 2010
Interior Alaska, Killarney Lake	Lake infill	Lacustrine silt and basal facies	1.0 - 9.3	12.4 +/- 1.8	-	-	-	Visible layering	Brosius 2010
Interior Alaska, Killarney Lake	10 cm thick detritus rich layer	Trash basal	-	-	-	-	-	Composed of well preserved terrestrial organic material	Brosius 2010
Interior Alaska, Killarney Lake	Taberal	Taberal	-	-	-	-	-	Massive mineral layer	Brosius 2010

Table 2.12: Key characteristics of non-yedoma thermokarst lakes in the Hudson Bay Lowlands, the Tuktoyaktuk Peninsula and the Lena River Delta. Dashed lines indicate no data were available.

Location	Facies	Seward peninsula yedoma thermokarst lake facies equivalent	% TOC	C/N	$\delta^{13}C$	Mean grain size (um)	MS SI	Visual characteristics	Reference
Hudson Bay Lowlands	upper facies (lake infill)	lacustrine silt	<5% (LOI)	-	-	0.5 to 4	-	massive structure, dry, grey (Munsell color scale 2.5 Y 4/1) to lighter grey (2.5 Y 5/1)	Bouchard et al. 2011
Hudson Bay Lowlands	lower facies	taberal	6 to 10% (LOI)	-	-	4.2 to 4.8	-	generally finely laminated, laminations <1mm, soft, wet, dark grayish brown (2.5 Y 4/2) to a lighter grayish brown (2.5 Y5/2)	Bouchard et al. 2011
Hudson Bay Lowlands	transitional facies	trash basal	-	-	-	-	-	dark grayish brown (2.5 Y3/2), macroscopic peat/plant remains.	Bouchard et al. 2011
Tuktoyaktuk Peninsula, Northwest Territories	central infill	lacustrine silt	-	-	-	-	-	mud/muddy peat forms by suspension settling of fine and/or low-density material, typically in the deep-water zone of thermokarst lakes	Murton 1996
Tuktoyaktuk Peninsula, Northwest Territories	basal unit	chaotic basal	-	-	-	-	-	mix of diamicton and impure sand, inclusions of woody fibrous peat. Facies displays foresets.	Murton 1996
Tuktoyaktuk Peninsula, Northwest Territories	basin margin fills	layered basal	-	-	-	-	-	waves and currents winnow mud and detrital peat from underlying impure sand and diamicton, leaving a veneer of well-sorted and rippled fine sand and/or lenses or sheets of pebbly sand/sandy gravel	Murton 1996
Arga Comples, Lena River Delta	sandy infill	lacustrine silt	3.90%		-25 to -27	64		organic rich fine sand	Andreev et al. 2004

Chapter 3: Overall conclusions

In Chapter 1, I identified key knowledge gaps related to thermokarst lake sedimentology, which I developed into the following hypotheses: 1) yedoma thermokarst lakes consist of a suite of facies, each representing a different depositional environment; 2) first-generation yedoma thermokarst lakes will exhibit a change in facies distribution through time; 3) facies distribution will be different between first- and later-generation yedoma thermokarst lakes; 4) Yedoma lakes in regions other than the Seward Peninsula will exhibit similar facies and facies distribution; and 5) differences in parent material, excess ice volume and cryostructure will result in differences between yedoma and non-yedoma thermokarst lakes.

3.1 Key findings

I found that five key facies were present within yedoma thermokarst lakes forming on the Seward Peninsula. First-generation facies distribution changes through time as a function of lake expansion via margin erosion and deepening via subsidence. First-generation lake sedimentology is more consistent than that of later-generation thermokarst lakes, which showed greater variability. The sediment in later-generation lakes is similar to first-generation lakes where the lakes erode into upland yedoma, but markedly different when eroding into other margin types. Therefore, position within the landscape should be taken into account when determining lake generation using aerial imagery.

Similarities were found between the sedimentology of northeast Siberian and Seward Peninsula lakes. This includes the presence of a Yedoma Taberal Silt facies beneath first-generation lake deposits, and the presence of a Layered Basal facies, a Chaotic Basal facies, and a fine-grained fill. A key difference between lakes forming on the Seward Peninsula and those forming in Siberia is the presence of tephra.

I found consistent similarities between thermokarst lake regions, including the presence of a Yedoma Taberal Silt facies (thawed permafrost below an sub-lacustrine

unconformity) and detrital basal units. Sediment distribution and composition varies between regions due to differences in cryostructure and parent material.

3.2 Further research

Further information on the formation of the Chaotic Basal facies is needed. Within this study I was unable to differentiate between Chaotic Basal facies forming from material deposited at the lake margin and that forming from the deformation of taberal sediment during thaw and settlement. In addition radiocarbon dating would have enhanced understanding of temporal scales of sediment accumulation and changes in facies distribution.

Within this study, dating of thermokarst lake activity was challenging. Further research on how to date thermokarst lake activity is necessary. This will enable a fuller understanding of thermokarst lake chronology during the Late Pleistocene and Holocene and identification of what drives thermokarst lake activity.

Comparisons of the sedimentary facies present in yedoma and non-yedoma thermokarst lakes in other regions could be improved by more detailed studies of lake sediments. This would facilitate a more reliable identification of thermokarst lake types within periglacial deposits, leading to a more accurate reconstruction of landscape evolution. Literature on yedoma thermokarst lakes in northeast Siberia focuses on the yedoma ice complex and thermokarst lakes are considered as a single facies. To gain a better understanding of how yedoma thermokarst lake sediment composition and distribution varies, Siberian yedoma thermokarst lakes need to be analyzed at a higher sampling resolution at both tundra and boreal forest locations. Comparisons with non-yedoma thermokarst lakes are similarly restricted.

Appendix 1: Bulk density data

Bulk Density Methods:

Bulk density measurements were taken with a Geotek Multisensor Core Logger-S. Measurements were taken on whole, unsplit cores every 0.5 cm and bulk density values are given in grams of wet sediment per cubic centimeter (g/cc).

Table A.1.1: Descriptive statistics for bulk density (n=4761).

Facies	Mean bulk density (g/cc)	Variance	Range
Taberal	1.83	0.069	2.33
Trash basal	1.38	0.030	.69
Chaotic basal	1.79	0.072	1.36
Layered basal	1.65	0.094	2.02
Lacustrine silt	1.56	0.062	1.82

Table A.1.2: Analysis of variance output for bulk density. Due to the non-normal distribution of bulk density data, the non-parametric Kruskal Wallis test was used.

Dependent	Variable	Results	Significant difference?
Bulk Density	Facies	$\chi^2 = 930.47$, $df = 4$, $p < 0.001$	Yes

Table A.1.3: Games Howell pairwise comparison of bulk density between facies. All pairwise comparisons were found to be significantly different.

Dependent Variable: Bulk Density (gm/cc)

		Sig.
lacustrine silt	chaotic basal	.000
	layered basal	.004
	taberal	.000
	trash basal	.000
chaotic basal	lacustrine silt	.000
	layered basal	.000
	taberal	.000
	trash basal	.000
layered basal	lacustrine silt	.004
	chaotic basal	.000
	taberal	.000
	trash basal	.000
taberal	lacustrine silt	.000
	chaotic basal	.000
	layered basal	.000
	trash basal	.000
trash basal	lacustrine silt	.000
	chaotic basal	.000
	layered basal	.000
	taberal	.000

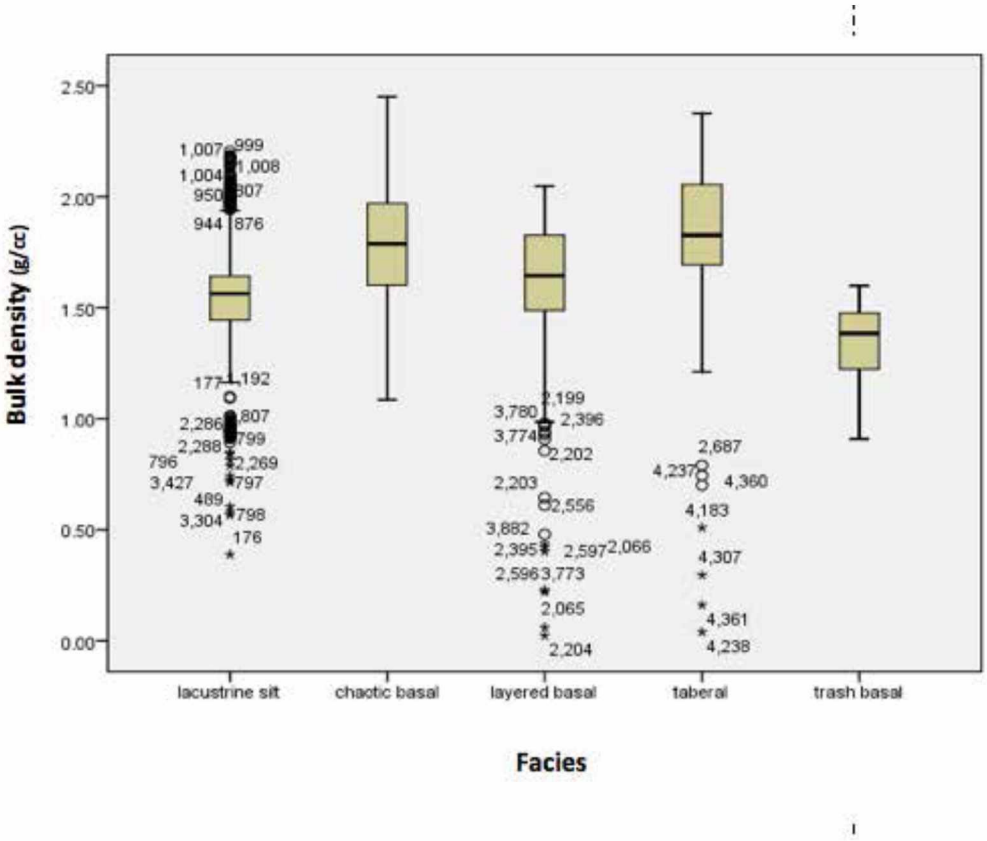

Figure A.1.1: Box plots of bulk density between facies. The horizontal black line shows the median value. Whiskers connect the lowest and highest values that are not considered outliers. Circles represent outliers. Stars represent extreme outliers. Numbers adjacent to stars and circles indicate data point label. Outliers are defined by calculating the difference between the upper and lower quartile (x). Outliers are $1.5x$ to $3x$ from the upper or lower quartile. Extreme outliers are greater than 3x from the upper or lower quartile.

Table A.1.4: Smear slide observations. Obse1rvation percentages based on single smear slide and percent cover of entire smear slide.

total	core	colour/feature	Facies	depth cm	calcite (and high-Mg calcite	muscovite	quartz/feldspar clay size indeterminate	diatoms	amorphous algal OM	vascualr OM	charcoal	pollen/spores/plant bodies	tephra	rounding	sorting	sediment name	comments
100	SPA_CLAU09-1C-1N-1	bottom of darkbrown to black band	LS	10-11	0	2	50	5	3	30	10	0	trace	0	sub-angular	medium-poor	quartz dominated clayey silt	lots of microscopic detrital material, round diatoms well preserved
100	SPA_CLAU09-1C-1N-1	unlaminated, just below darker band with diffuse boundaries	LS	29-30	0	trace	50	20	5	20	5	0	trace	0	sub-angular	medium-poor	quartz dominated clayey silt	round diatoms
100	SPA_CLAU09-1C-1N-1	unlaminated band, medium brown	LS	50-51	0	2	25	35	3	20	15	0	trace	trace	sub-angular	medium-poor	quartz dominated clayey silt	round diatoms
100	SPA_CLAU09-1C-1N-1	unlaminated, lighter band	LS	70-71	0	2	45	20	5	18	10	0	trace	0	angular	medium-poor	quartz dominated clayey	round diatoms, organic material very detrital
100	SPA-CLAU09-1D-1U-1	darker band with very diffuse boundaries	LS	25-26	3	2	50	10	5	15	15	0	0	0	sub-angular	poor	quartz dominated clayey silt	circales diatoms, sponge spicules
100	SPA-CLAU09-1D-1U-1	unlaminted, lighter band	LS	32-33	0	2	45	15	5	23	10	0	trace		sub-angular	medium-poor	quartz dominated clayey silt	mostly centrales, few pennate diatom
105	SPA-CLAU09-1D-1U-1	slightly darker brown band	LS	48-49	trace	0	50	15	5	30	5	0	0	0	sub-angular	medium-poor	quartz dominated clayey silt	pennate and centrales diatoms
100	SPA-CLAU09-1D-1U-1	unlaminated band, medium brown	LS	56-57	trace	0	80	8	trace	10	2	0	0	0	sub-angular	medium	quartz dominated clayey silt	
100	SPA-CLAU09-1D-1U-1	unlaminated section above organic rich band	LS	64-65	0	1	37	20	2	35	5	0	0	0	sub-angular	medum-well	quartz dominated silt	trace sponge spicules, centrale diatom
100	SPA-CLAU09-1D-1U-1	darker ssection, 3cm above organic rich band.	trash	80-81	0	trace	47	5	8	20	20	0	0	0	sub-angular	medium	quartz dominated silt	square diatom chain, pennate diatoms (many different types).

Table A.1.4: Continued.

total	core	colour/feature	Facies	depth cm	calcite (and high-Mg calcite	muscovite	quartz/feldspar	clay size indeterminate	diatoms	amorphous algal OM	vascualr OM
100	SPA-CLAU09-1D-1U-1	tan silt below detrital band	trash	104-105	2	trace	83	10	trace	trace	5
100	SPA-CLAU09-1D-1U-2	grey silty mud	cb	8-9	trace	2	85	13	0	trace	trace
100	SPA-CLAU09-1D-1U-2	grey silty mud	cb	1-2	0	0	94	1	0	0	5
100	SPA-CLAU09-1D-1U-2	massive tan fine silty mud	taberal	56-57	0	0	55	35	0	5	5
100	SPA-CLAU09-1D-1U-2	massive tan fine silty mud	taberal	48-49	2	0	53	35	0	5	5
100	SPA-RHO09-2C-1L-1	faint lamination	LS	4-5	0	0	15	15	10	30	30
100	SPA-RHO09-2C-1L-1	unlaminated band, medium brown	LS	5-6	0	0	65	10	0	10	15
100	SPA-RHO09-2C-1L-1	faint lamination	LS	6-7	0	0	50	10	10	20	10
100	SPA-RHO09-2C-1L-1	unlaminated band, medium brown	LS	14-15	0	0	25	25	8	10	32

charcoal	pollen/spores/plant bodies	tephra	rounding	sorting	sediment name	comments
0	trace	0	sub-angular	medum-well	quartz dominated silt	
0	0	0	sub-angular	medum-well	quartz dominated clayey silt	
0	0	0	sub-angular	well	quartz dominated silt	
0	0	0	sub-angular	medium-poor	quartz dominated clayey silt	
0	0	0	sub-angular	medium-poor	quartz dominated clayey silt	
0	0	0	sub-angular	poor	organic dominated, quartzy, clayey silt	large variety of diatoms, some not symmetrical. Range of cascular organic material
0	0	0	sub-angular	medium	organic dominated, quartzy, clayey silt	chironomid jaw found, 4-5 huge chunks of vascular plant material - if this was considered then these take up 60% of material - compared to only 20 % quartz
0	0	0	sub-angular	medium-well	organic dominated, quartzy, clayey silt	
0	0	trace	sub-angular	poor	organic dominated, quartzy, clayey silt	

Table A.1.4: Continued.

total	core	colour/feature	Facies	depth cm	calcite (and high-Mg calcite	muscovite	quartz/feldspar	clay size indeterminate	diatoms	amorphous algal OM	vascualr OM
100	SPA-RHO09-2C-1L-1	tan silt with some organic inclusions	layered basal	76-77	0	0	90	trace	0	0	10
100	SPA-RHO09-2C-3L-1	tan silt	chaotic basal	4-5	15	0	40	45	0	0	0
100	SPA-RHO09-2C-3L-1	organic detriatal inclusion	chaotic basal	17-18	trace	1	25	30	trace	10	34
100	SPA-RHO09-2C-3L-1	tan fine silty mud	chaotic basal	28-29	trace	0	20	0	0	0	0
100	SPA-RHO09-2C-4L-1	tan fine silty mud	chaotic basal	6-7	3	trace	87	0	0	0	5
100	SPA-RHO09-2C-4L-1	tan fine silty mud	chaotic basal	23-24	2	trace	78	20	0	0	0
101	SPA-RHO09-2C-5L-1	medium brown fine silty mud with small (1x1mm) tephra pieces	chaotic basal	6-7	1	trace	55	35	0	0	5
100	SPA-RHO09-2C-5L-1	horizontal band of black material with indistinct boundaries	chaotic basal	24-25	4	trace	45	38	2	5	1

charcoal	pollen/spores/plant bodies	tephra	rounding	sorting	sediment name	comments
0	0	0	sub-angular to rounded	well	quartz dominated silt	no diatoms
0	0	0	sub-angular to rounded	poor	quartz dominated clayey silt	no diatoms
0	0	0	sub-angular	poor	quartz dominated clayey silt	
0	0	80	sub-angular	medium	silty tephra	small grain size, some tephra fragments ?
0	0	5	sub-angular	medium-poor	quartz dominated clayey silt	angular fragments - likely tephra
0	0	0	sub-angular	poor	quartz dominated clayey silt	
0	0	5	sub-angular	poor	quartz dominated clayey silt	
0	0	5	sub-angular	poor	quartz dominated clayey silt	diatoms present. Interesting when combined with image - looks as though this section of the core may have experienced ponding/ anaerobic environments.

Table A.1.4: Continued.

total	core	colour/feature	Facies	depth cm	calcite (and high-Mg calcite	muscovite	quartz/feldspar	clay size indeterminate	diatoms	amorphous algal OM
100	SPA-CLAU09-10A-1N-1	unlaminated band, medium brown	LS	24-25	trace	1	45	15	1	25
100	SPA-CLAU09-10A-1N-1	dark, thin laminations	LS	34-35	1	1	20	40	5	20
100	SPA-CLAU09-10A-1N-1	unlaminated band, medium brown	LS	4-5	1	1	30	31	1	25
100	SPA-CLAU09-10A-1N-1	dark band 6-8	LS	7-8	0	trace	20	44	10	25
100	SPA-JAE09-2A-1N-1	medium brown fine silty mud	LS	4-5	2	1	20	50	0	27
100	SPA-JAE09-2A-1N-1	finely laminated brown fine silty mud	LS	16-17	2	1	60	10	2	23
103	SPA-JAE09-2A-1N-1	finely laminated brown fine silty mud	LS	25-26	2	1	25	50	5	15
100	SPA-JAE09-2A-1N-1	dark band of tephra dominated material	chaotic basal	48-49	0	0	80	10	0	0
100	SPA-JAE09-5A-1N-1	medium brown fine silty mud, laminations absent	LS	1-2	1	1	25	15	1	55
100	SPA-JAE09-5A-1N-1	medium brown fine silty mud, laminations absent	LS	9-10	2	1	60	20	1	12

vascualr OM	charcoal	pollen/spores/plant bodies	tephra	rounding	sorting	sediment name	comments
10	0	0	3	sub-angular	poor	quartz dominated clayey silt	
8	0	0	5	sub-angular	poor	quartz dominated clayey silt	circales diatoms
8	0	0	3	sub-angular	poor	quartz dominated clayey silt	
0	?	0	1	sub-angular	poor	quartz dominated clayey silt	
0	0	0	trace	sub-angular	poor	quartz dominated clayey silt	
0	0	0	2	sub-angular	medium	quartz dominated clayey silt	
4	0	0	1	sub-angular	poor	quartz dominated clayey silt	
0	0	0	10	rounded	well	quartz dominated silt	
2	0	0	0	sub-angular	poor	quartz dominated clayey silt	
4	0	0	n/o	sub-angular	poor	quartz dominated clayey silt	

Table A.1.4: Continued.

total	core	colour/feature	Facies	depth cm	calcite (and high-Mg calcite	muscovite	quartz/feldspar clay size indeterminate	diatoms	amorphous algal OM	vascualr OM
100	SPA-JAE09-5A-1N-1	dark lamination in medium brown fine silty mud	LS	17-18	3	1	15	10	0	60	10
100	SPA-JAE09-5A-1N-1	faintly laminated medium brown fine silty mud	LS	25-26	3	1	15	10	0	60	10
100	SPA-JAE09-5A-1N-1	lamination in medium brown fine silty mud	LS	33-34	3	1	35	10	0	40	10
100	SPA-JAE09-5A-1N-1	faintly laminated medium brown fine silty mud	LS	49-50	1	3	40	11	5	30	10
100	SPA-JAE09-5A-1N-1	unlaminated band, medium brown fine silty mud	LS	57-58	2	2	51	10	5	15	15
100	SPA-CLAU09-2A-1N-1	medium brown file silty mud, no visible laminations	LS	1-2	1	0	15	6	8	60	10
101	SPA-CLAU09-2A-1N-1	medium brown fine silty mud with darker brown motteling	LS	9-10	1	0	10	10	10	60	10
100	SPA-CLAU09-2A-1N-1	medium brown fine silty mud	LS	17-18	0	1	89	5	0	5	0

charcoal	pollen/spores/plant bodies	tephra	rounding	sorting	sediment name	comments
0	0	1	sub-angular	poor	quartz dominated clayey silt	
0	0	1	sub-angular	poor	quartz dominated clayey silt	
0	0	1	sub-angular	poor	quartz dominated clayey silt	
0	0	1	sub-angular	medium-poor	quartz dominated clayey silt	
0	0	n/o	sub-angular	poor	quartz dominated clayey silt	mix of diatom types - mostly centric
0	0	0	sub-angular	poor	quartz dominated clayey silt	mix of diatom types - pennate and centric
0	0	0	sub-angular	poor	quartz dominated clayey silt	
0	0	0	sub-angular to rounded	medium-well	quartz dominated silt	

Table A.1.4: Continued.

total	core	colour/feature	Facies	depth cm	calcite (and high-Mg calcite	muscovite	quartz/feldspar clay size indeterminate	diatoms	amorphous algal OM	vascualr OM
100	SPA-CLAU09-2A-1N-1	medium brown fine silty mud	LS	24-25	1	2	57	20	0	20	0
100	SPA-CLAU09-2A-1N-2	massive mid brown silt	chaotic basal	8-9	0	3	80	7	0	5	5
100	SPA-CLAU09-2A-1N-2	brown silt with some gritty tephra	chaotic basal	16-17	0	3	80	7	0	5	5
100	SPA-CLAU09-2A-1N-2	mid brown silt	chaotic basal	24-25	0	1	40	7	0	2	50
100	SPA-CLAU09-2A-1N-2	tan silt	chaotic basal	32-33	5	1	70	24	0	0	0
100	SPA-CLAU09-2A-1N-2	tan silt	chaotic basal	40-41	5	1	70	24	0	0	0
100	SPA-CLAU09-2A-1N-2	tan silt	chaotic basal	48-49	4	1	55	30	0	5	5
100	SPA-CLAU09-2A-1N-2	dark silt	chaotic basal	72-73	3	1	50	10	0	18	18
100	SPA-CLAU09-2A-1N-2	tan silt	chaotic basal	80-81	5	2	58	5	0	20	10
100	SPA-CLAU09-2A-1N-2	tan silt	chaotic basal	88-89	5	2	69	10	0	10	4

charcoal	pollen/spores/plant bodies	tephra	rounding	sorting	sediment name	comments
0	0	0	sub-angular	poor	quartz dominated clayey silt	
0	0	0	sub-angular	poor	quartz dominated clayey silt	
0	0	0	sub-angular	poor	quartz dominated clayey silt	
0	0	0	sub-angular	poor	quartz dominated clayey silt	organic rich - beat up vasular material
0	0	0	sub-angular to rounded	medium	quartz dominated clayey silt	abundant calcite fragments
0	0	0	sub-angular to rounded	medium	quartz dominated clayey silt	abundant calcite fragments
0	0	0	sub-angular to rounded	medium	quartz dominated clayey silt	abundant calcite fragments
0	0	0	sub-angular	medium-poor	quartz dominated clayey silt	
0	0	0	sub-angular	poor	quartz dominated clayey silt	
0	0	0	sub-angular	poor	quartz dominated clayey silt	

Table A.1.4: Continued.

total	core	colour/feature	Facies	depth cm	calcite (and high-Mg calcite	muscovite	quartz/feldspar clay size indeterminate
100	SPA-CLAU09-2A-1N-2	tan silt	chaotic basal	96-97	5	2	69	10
100	SPA-JAE09-2A-1N-2	gritty tephra	chaotic basal	8-9	0	0	50	0
100	SPA-JAE09-2A-1N-2	tan silt	taberal	48-49	0	0	70	15
100	SPA-CLAU09-5A-1L-1	mid brown silt with organic detrital bands	layered basal	1-2	0	1	80	4
100	SPA-CLAU09-5A-1L-1	mid brown silt with organic detrital bands	layered basal	16-17	1	1	73	15
100	SPA-CLAU09-5A-1L-1	mid brown silt with organic detrital bands	layered basal	24-25	1	1	38	10
100	SPA-CLAU09-5A-1L-1	mid brown silt with tephra band	layered basal	32-33	0	0	80	0
100	SPA-CLAU09-5A-1L-1	coasrse tephra	layered basal	48-49	0	0	10	3

diatoms	amorphous algal OM	vascualr OM	charcoal	pollen/spores/plant bodies	tephra	rounding	sorting	sediment name	comments
0	10	4	0	0	0	sub-angular	medium	quartz dominated clayey silt	
0	0	0	0	0	50	sub-angular	poor	quartz dominated clayey silt	
0	5	10	0	0	0	sub-angular	poor	quartz dominated clayey silt	
0	0	15	0	0	0	sub-angular	poor	quartz dominated clayey silt	
0	5	5	0	0	0	sub-angular	medium-poor	quartz dominated clayey silt	
0	0	50	0	0	0	sub-angular	medium-poor	quartz dominated clayey silt	
0	0	0	0	0	20	sub-angular to rounded	well	quartz dominated silt	
0	10	77	0	0	0	sub-angular	medium	organic rich silt	

Appendix 2: Sediment core field metadata

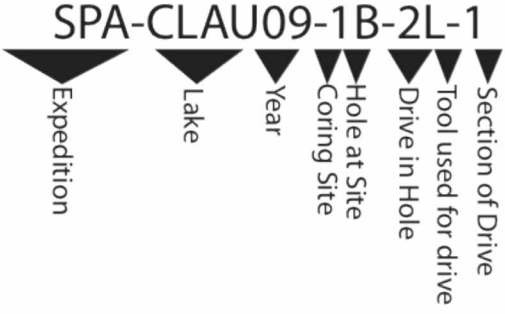

Figure A.2.1: National Lacustrine Core Facility labeling nomenclature.

Table A.2.1: Sediment core metadata for 2009, part 1. Core ID follows the nomenclature given in Figure A.3.1. 'Ice to sed. (m)', provides the depth from the top of the ice to the sediment-water interface. 'Coring equipment used' provides the common name for the coring device used to extract sediment from the lake. 'Depth to Drive (m)' gives the depth at which sampling of sediment began. If 'Depth to drive (m)' is greater than 'Ice to sediment (m)' this indicates that the top of the core drive was below the sediment-water interface. 'Section length (cm)' gives the length in cm of sediment retrieved from the lake during that drive. Water depth gives the depth of water to the sediment-water interface once a hole had been augured through the ice. Baydjarakh high or low indicates whether the core was retrieved on a baydjarakh top or within a baydjarakh low.

Core ID	Ice to sed (m)	Coring equiptment used	Depth to drive (m)	section length (cm)	Water depth (m)	Baydjarakh high or low	Distance from shore (m)	Lat/Long
SPA-3LOO09-1A-1N	5.75	Universal	8.23	0.88	5.75	-	-	
SPA-3LOO09-2A-1N-1	5.75	Universal	5.75	1.3	5.75	-	-	
SPA-3LOO09-2A-1N-2	5.75	Universal	-	61.2	5.75	-	-	
SPA-CLAU09-1A-1P-1	7.66	Piston corer	7.66	0.53	7.66	high	120	66° 33' 00.42718" N, 164° 27' 08.35937" W
SPA-CLAU09-1A-2B-1	7.66	Bolivia	8.27	1	7.66	high	120	66° 33' 00.42718" N, 164° 27' 08.35937" W
SPA-CLAU09-1A-3B-1	7.66	Bolivia	9.27	0.69	7.66	high	120	66° 33' 00.42718" N, 164° 27' 08.35937" W
SPA-CLAU09-1A-4L-1	7.66	Livingston	9.95	0.26	7.66	high	120	66° 33' 00.42718" N, 164° 27' 08.35937" W
SPA-CLAU09-1B-1N-1	7.66	Universal	7.66	0.753	7.66	high	120	66° 33' 00.45162" N, 164° 27' 08.27657" W
SPA-CLAU09-1C-1N-1	7.66	Universal	7.66	1.512	7.66	high	120	66° 33' 00.49142" N,164° 27' 08.33551" W
SPA-CLAU09-1C-1N-2	7.66	Universal	-	41.2	7.66	high	120	66° 33' 00.49142" N,164° 27' 08.33551" W
SPA-CLAU09-1D-1U-1	7.66	Uwitech	8.43	2	7.66	high	120	66° 33' 00.50074" N, 164° 27' 08.40772" W
SPA-CLAU09-1D-1U-2	7.66	Uwitech	-	60.4	7.66	high	120	66° 33' 00.50074" N, 164° 27' 08.40772" W
SPA-CLAU09-1D-2U-1	7.65	Uwitech	10.43	1.6	7.66	high	120	66° 33' 00.50074" N, 164° 27' 08.40772" W
SPA-CLAU09-1E-1N-1	7.66	Universal	7.7	1.15	7.66	high	120	66° 33' 00.54478" N, 164° 27' 08.44289" W
SPA-CLAU09-2A-1N-1	3.66	Universal	3.66	1.37	3.66	high	20	66° 33' 07.21323" N, 164° 27' 07.73663" W
SPA-CLAU09-2B-1P-1	4.9	Piston corer	4.7	0.2	3.66	slope	20	66° 33' 07.16721" N, 164° 27' 07.60976" W
SPA-CLAU09-2B-2L-1	4.9	Livingston	4.9	1	3.66	slope	20	66° 33' 07.16721" N, 164° 27' 07.60976" W
SPA-CLAU09-2B-3L-1	4.9	Livingston	5.9	0.6	3.66	slope	20	66° 33' 07.16721" N, 164° 27' 07.60976" W
SPA-CLAU09-2C-1N-1	4.9	Universal	3.7	1.24	3.66	high	20	66° 33' 07.20124" N, 164° 27' 07.77503" W
SPA-CLAU09-2C-1N-2	4.9	Universal	3.7	1.24	3.66	high	20	66° 33' 07.20124" N, 164° 27' 07.77503" W

Table A.2.1 continued.

Core ID	Ice to sed (m)	Coring equiptment used	Depth to drive (m)	section length (cm)	Water depth (m)	Baydjarakh high or low	Distance from shore (m)	Lat/Long
SPA-CLAU09-3A-1N-1	2.74	Universal	2.74	2.11	2.74	high	14	66° 33' 07.41169" N,164° 27' 07.93133" W
SPA-CLAU09-4A-1N-1	5.66	Universal	5.66	1.31	5.83	high	28	66° 33' 06.69810" N, 164° 27' 07.03888" W
SPA-CLAU09-4B-1U-1	5.83	Bolivia	6.33	2	5.83	high	28	66° 33' 06.69810" N, 164° 27' 07.03888" W
SPA-CLAU09-4B-2U-1	5.83	Bolivia	8.33	2	5.83	high	28	66° 33' 06.69810" N, 164° 27' 07.03888" W
SPA-CLAU09-5A-1L-1	1.1	Livingston	1.66	0.885	1.1	high	3	66° 33' 07.67125" N, 164° 27' 08.23110" W
SPA-CLAU09-6A-1N-1	2.77	Universal	2.77	0.88	2.77	high	10	66° 33' 07.58720" N, 164° 27' 08.11732" W
SPA-CLAU09-7A-1P-1	6.36	Piston corer	6.3	0.15	6.36	high	25	66° 33' 07.09128" N, 164° 27' 07.51059" W
SPA-CLAU09-7A-2L-1	6.36	Livingston	6.51	1	6.36	high	25	66° 33' 07.09128" N, 164° 27' 07.51059" W
SPA-CLAU09-7A-3L-1	6.36	Livingston	7.47	0.11	6.36	high	25	66° 33' 07.09128" N, 164° 27' 07.51059" W
SPA-CLAU09-8A-1P-1	6.5	Piston corer	6.3	0.41	6.5	high	34	66° 33' 06.80753" N, 164° 27' 06.80949" W
SPA-CLAU09-8A-2L-1	6.5	Livingston	6.71	1	6.5	high	34	66° 33' 06.80753" N, 164° 27' 06.80949" W
SPA-CLAU09-8A-3L-1	6.5	Livingston	7.71	0.4	6.5	high	34	66° 33' 06.80753" N, 164° 27' 06.80949" W
SPA-CLAU09-10A-1N-1	7.05	Universal	7.05	1.8	7.1	high	75	66°33'5.39"N, 164°27'3.62"W
SPA-COCK09-1A-1B-1	7.66	Bolivia	4.31	0.98	7.55	-	-	-
SPA-COCK09-1B-1L-1	4.4	Livingston	5	0.74	7.55	-	-	-
SPA-COCK09-2A-1N-1	4.3	Universal	4.3	1.06	7.55	-	-	-

Table A.2.2: Sediment core metadata for 2010. For an explanation of column headings, see Table A.2.1.

Core ID	Coring equiptment used	Depth to drive (m)	section length (m)	Water depth (m)	Baydjarakh high or low	Distance from shore (m)	Lat/Long
SPA-CLAU10-1A-1B-1	Bolivia	8.2	0.79	8.4	low	150	66°32'59.58"N, 164°27'8.12"W
SPA-CLAU10-1A-2L-1	Livingston	10.05	0.9	8.4	low	150	66°32'59.58"N, 164°27'8.12"W
SPA-CLAU10-1A-3L-1	Livingston	11.05	0.3	8.4	low	150	66°32'59.58"N, 164°27'8.12"W
SPA-CLAU10-1C-1B-1	Bolivia	11.39	0.4	8.4	low	150	66°32'59.58"N, 164°27'8.12"W
SPA-CLAU10-2A-1L-1	Livingston	9.82	0.75	8.8	low	120	66°32'58.88"N, 164°27'14.96"W
SPA-CLAU10-2A-2L-1	Livingston	10.82	0.41	8.8	low	120	66°32'58.88"N, 164°27'14.96"W
SPA-CLAU10-2A-3L-1	Livingston	11.17	0.45	8.8	low	120	66°32'58.88"N, 164°27'14.96"W
SPA-CLAU10-2A-4L-1	Livingston	11.67	0.22	8.8	low	120	66°32'58.88"N, 164°27'14.96"W
SPA-CLAU10-2B-1B-1	Bolivia	9.32	0.78	8.8	low	120	66°32'58.88"N, 164°27'14.96"W
SPA-CLAU10-4A-1B-1	Bolivia	6.95	0.76	7.15	low	40	66°32'59.24"N, 164°27'11.33"W
SPA-CLAU10-4A-2L-1	Livingston	8.17	0.8	7.15	low	40	66°32'59.24"N, 164°27'11.33"W
SPA-CLAU10-4A-3L-1	Livingston	9.14	0.38	7.15	low	40	66°32'59.24"N, 164°27'11.33"W
SPA-CLAU10-4A-4L-1	Livingston	9.48	0.34	7.15	low	40	66°32'59.24"N, 164°27'11.33"W
SPA-CLAU10-3A-1B-1	Bolivia	10.83	0.8	10.2	low	65	66°32'58.60"N, 164°27'19.04"W
SPA-CLAU10-3B-2L-1	Livingston	11.2	0.54	10.2	low	65	66°32'58.60"N, 164°27'19.04"W
SPA-CLAU10-3B-3L-1	Livingston	12.1	0.26	10.2	low	65	66°32'58.60"N, 164°27'19.04"W
SPA-CLAU10-3B-4L-1	Livingston	13.05	0.42	10.2	low	65	66°32'58.60"N, 164°27'19.04"W
SPA-CLAU10-3B-5L-1	Livingston	13.45	0.68	10.2	low	65	66°32'58.60"N, 164°27'19.04"W
SPA-CLAU10-3B-6L-1	Livingston	14.23	0.5	10.2	low	65	66°32'58.60"N, 164°27'19.04"W
SPA-CLAU10-3B-7L-1	Livingston	14.44	0.23	10.2	low	65	66°32'58.60"N, 164°27'19.04"W
SPA-CLAU10-3B-8L-1	Livingston	14.72	0.31	10.2	low	65	66°32'58.60"N, 164°27'19.04"W
SPA-CLAU10-3B-9L-1	Livingston	15.03	0.3	10.2	low	65	66°32'58.60"N, 164°27'19.04"W
SPA-RHO10-1A-1B-1	Bolivia	1.15	0.82	1.15	-	10	66°33'41.76"N, 164°29'7.55"W
SPA-RHO10-2A-1B-1	Bolivia	1.25	0.58	1.25	-	10	66°33'32.08"N, 164°27'51.73"W
SPA-RHO10-3A-1B-1	Bolivia	0.9	0.7	0.9	-	10	66°34'0.39"N, 164°27'41.88"W
SPA-RHO10-4A-1B-1	Bolivia	1	0.55	1	-	10	66°34'3.79"N, 164°28'1.11"W
SPA-RHO10-5A-1L-1	Livingston	1.03	0.64	1.03	-	700	66°33'45.48"N, 164°28'9.04"W
SPA-RHO10-5A-2L-1	Livingston	1.67	0.58	1.03	-	700	66°33'45.48"N, 164°28'9.04"W
SPA-RHO10-5A-3L-1	Livingston	2.25	0.29	1.03	-	700	66°33'45.48"N, 164°28'9.04"W
SPA-RHO10-5A-4L-1	Livingston	2.54	0.24	1.03	-	700	66°33'45.48"N, 164°28'9.04"W
SPA-RHO10-5A-5L-1	Livingston	2.78	0.26	1.03	-	700	66°33'45.48"N, 164°28'9.04"W
SPA-RHO10-5A-6L-1	Livingston	3.04	0.25	1.03	-	700	66°33'45.48"N, 164°28'9.04"W

Appendix 3: Additional data on Tea Lake and Prickly Pond, sediment core description sheets and sample locations

Sedimentology of Tea Lake and Prickly Pond

Tea Lake, first-generation (Figure A.3.2): Only one location within Tea lake was sampled. The upper sediment was interpreted as a Trash Basal facies, 0.3 m thick. A 1.2 cm thick Chaotic Basal facies was present beneath the Trash Basal facies.

Prickly Pond, later-generation (Figure A.3.3): Prickly Pond sediment was sampled towards the lake center. The Yedoma Taberal Silt, Layered Basal and Trash Basal facies were absent. The Chaotic Basal facies is 1.37 m thick and overlain by unlaminated Lacustrine Silt facies, 0.23 m thick.

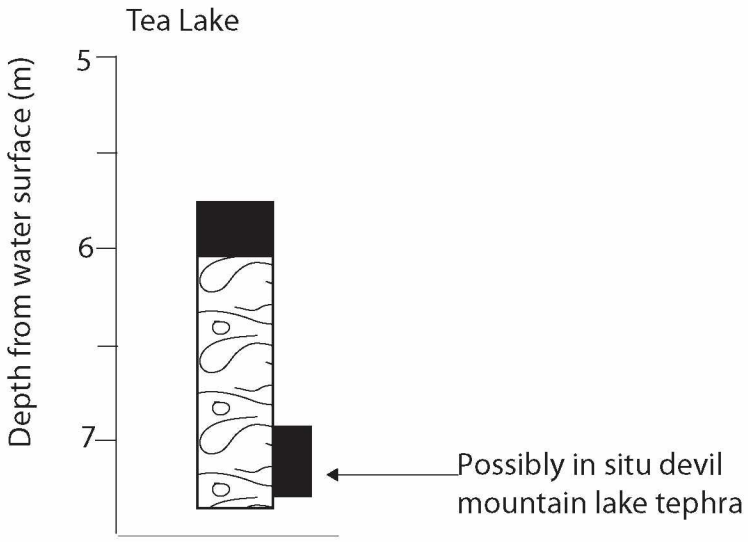

Figure A.3.2: Schematic of sediment core taken from Tea Lake. For key see Figure 2.7

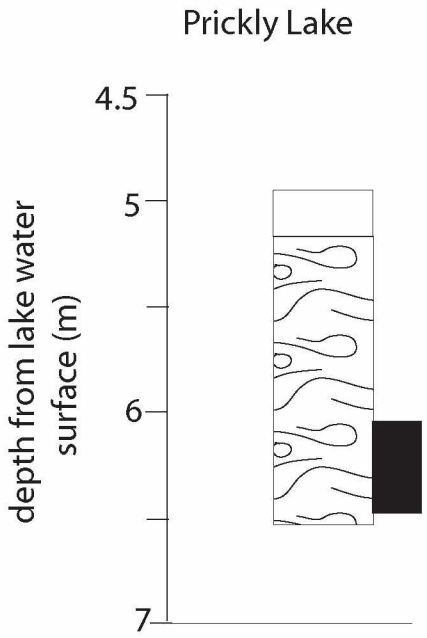

Figure A.3.3: Schematic of sediment core taken from Prickly Pond. For key see Figure 2.7.

Table A.3.1: AMS radiocarbon dates for Three Loon Lake, Lake Claudi, Lake Jaeger and Lake Rhonda.

Lab ID	Project sample name	Material dated	Facies	^{14}C age (BP)	+/-	Comments
UCIT21193	3loo09-2A-1N-1 5-7cm	herbaceous	trash basal	4615	20	Old carbon
UCIT21196	Clau09-1d-1u-2 47-48cm	herbaceous		18170	80	Old carbon
UCIT21210	CLAUDI: modern	drepanocladus	n/a	2495	20	modern aquatics
UCIT21209	CLAUDI:modern	potamogeton	n/a	2260	20	modern aquatics
UCIT21194	Jae09-5a-1n-1 42-44cm	herbaceous	lacustrine silt	4825	20	minimum lake age
UCIT21195	Rho09-2c-1l-1 61.5	plant stem	trash basal	4660	20	minimum lake age

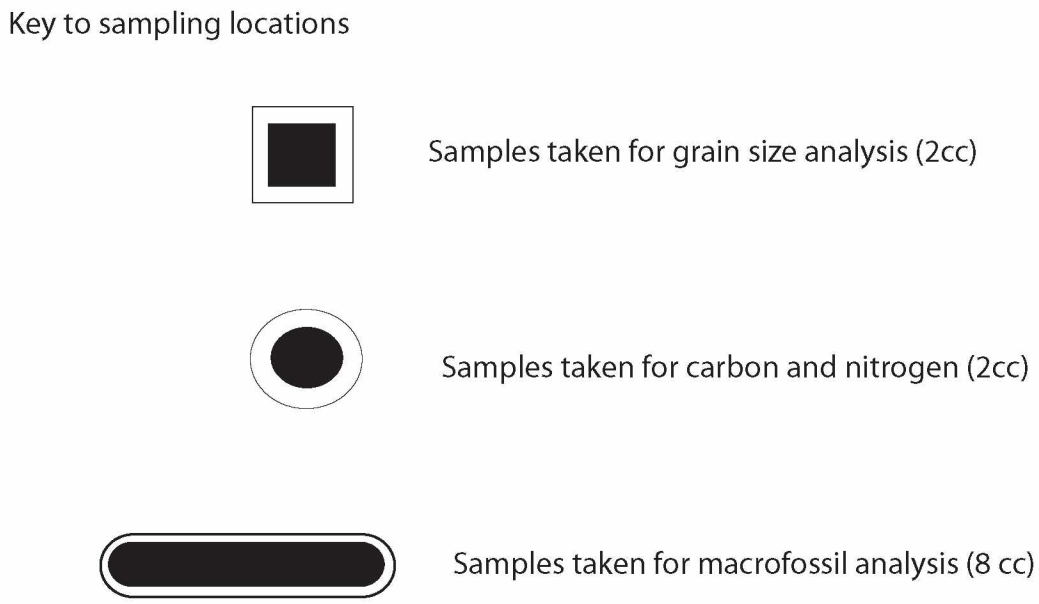

Figure A.3.4: Key to sampling locations within core description sheets.

Figure A.3.5: Initial core description sheets for cores sub-sampled.

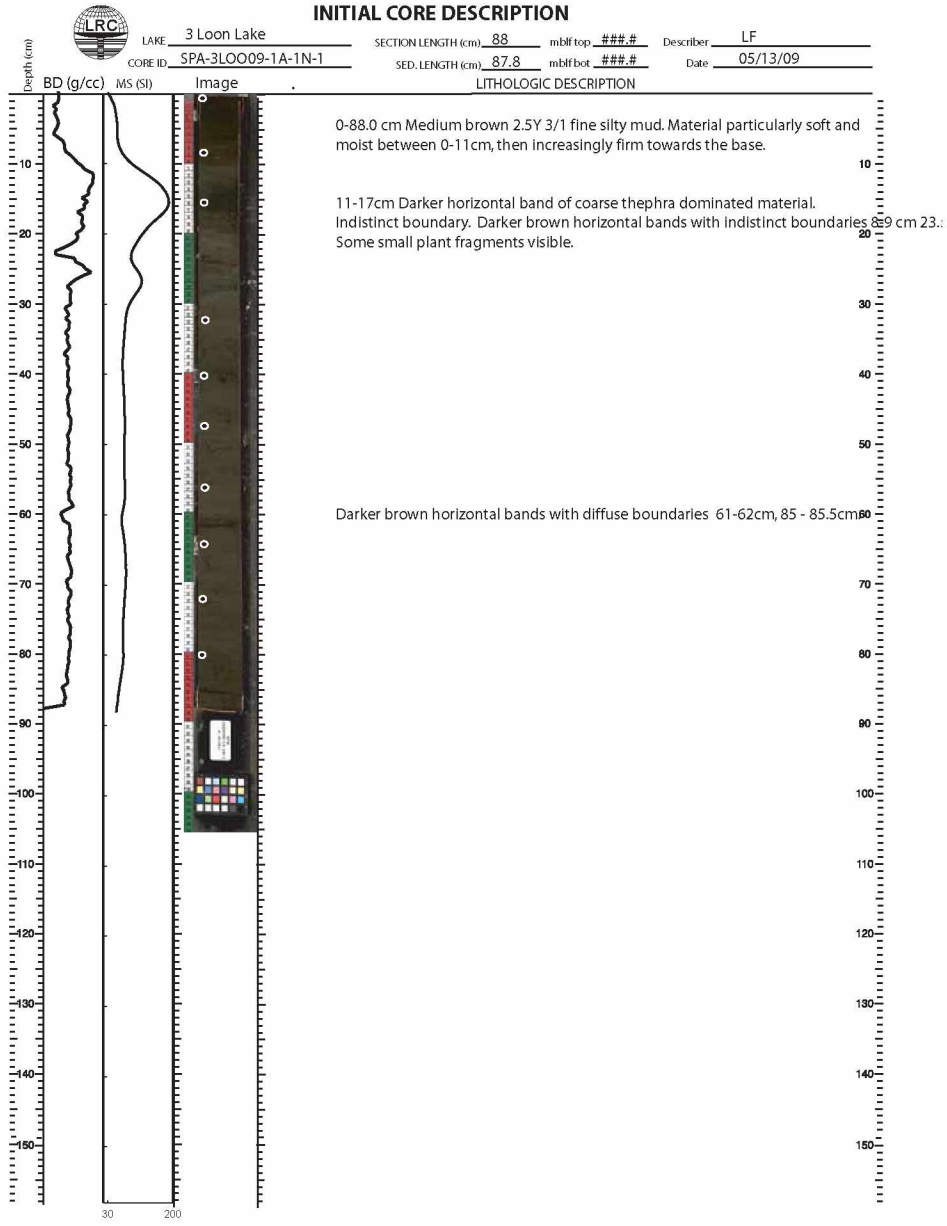

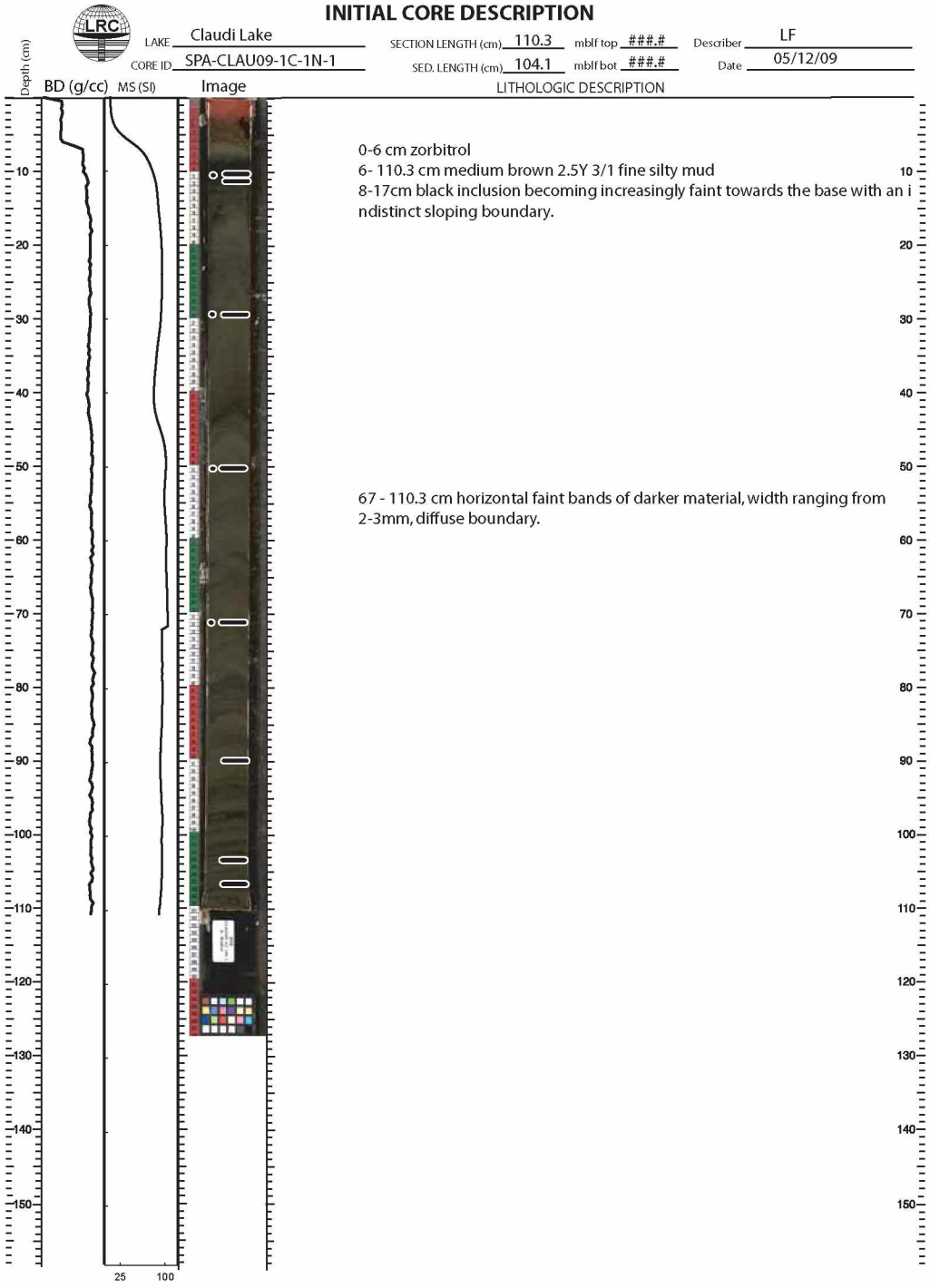
INITIAL CORE DESCRIPTION
LRC
LAKE Claudi Lake
CORE ID SPA-CLAU09-1C-1N-1
SECTION LENGTH (cm) 110.3
SED. LENGTH (cm) 104.1
mblf top ###.#
mblf bot ###.#
Describer LF
Date 05/12/09
Depth (cm)
BD (g/cc)
MS (SI)
Image
LITHOLOGIC DESCRIPTION
0-6 cm zorbitrol
6- 110.3 cm medium brown 2.5Y 3/1 fine silty mud
8-17cm black inclusion becoming increasingly faint towards the base with an indistinct sloping boundary.
67 - 110.3 cm horizontal faint bands of darker material, width ranging from 2-3mm, diffuse boundary.
25
100

INITIAL CORE DESCRIPTION

LAKE Claudi Lake
CORE ID SPA-CLAU09-1D-1U-1
SECTION LENGTH (cm) 110.5 mblf top ###.#
SED. LENGTH (cm) 110.3 mblf bot ###.#
Describer ME/LF
Date 5/3/09

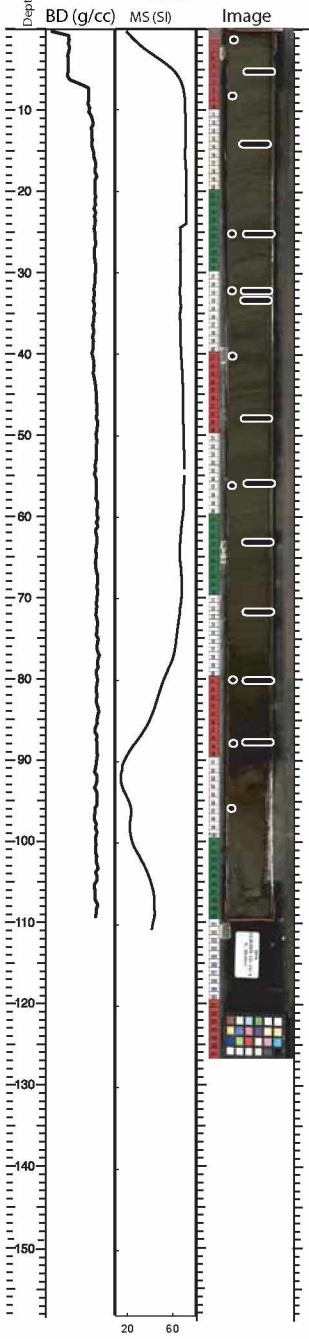

LITHOLOGIC DESCRIPTION

Core length 110.5 cm; 95-110 volume reduced and gap at 106-108 (core material pulled from barrel??)

0-80 cm: Soft, mid-brown silty mud with faint sub-horizontal darker banding 1-3 mm, indistinct contacts. 5YR 3/1. Few mollisc shell fragments.

80 cm: large pieces of plant material (sedge?), including piece protruding upward to 76 cm.

80-95 cm organic-rich layer with large pieces of graminoid stems and leaves and small, thin woody pieces (rootlets?)

95-110 cm: gradual transition to less organic brown silty mud, some material appears lost from base of core (see above).

Smear slides: 7.5 cm silty mud; 16.0 cm darker thin band; 85.5 cm organic layer; 109.5 base.

INITIAL CORE DESCRIPTION

LAKE Claudi Lake
CORE ID SPA-CLAU09-1D-1U-2
SECTION LENGTH (cm) 60.6 mblf top ###.#
SED. LENGTH (cm) 60.4 mblf bot ###.#
Describer ME/LF
Date 5/3/09

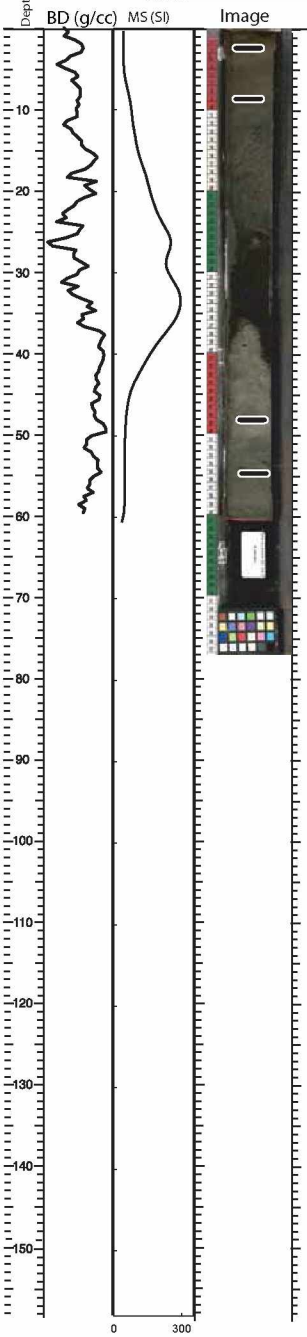

LITHOLOGIC DESCRIPTION

Core length 60.6cm; sed length 60.4cm

0-12cm Medium brown (5Y 3/1) gritty silty mud with some very faint horizontal banding.

12 - 35 Medium brown tephra dominated material. Diffuse transition from medium to dark brown at 26cm. Relatively large piece of tephra at 14.5 cm (1.5 x 1.5 cm). Tephra dragged down side of core 35-41cm

35- 60.6 Tan (5Y 4/1) fine silty mud with dark inclusions (1-5mm) not banded or tephra.

INITIAL CORE DESCRIPTION

LAKE Claudi Lake
CORE ID SPA-CLAU09-2A-1N-1
SECTION LENGTH (cm) 28 mblf top ###.#
SED. LENGTH (cm) 28.2 mblf bot ###.#
Describer LF
Date 05/28/09

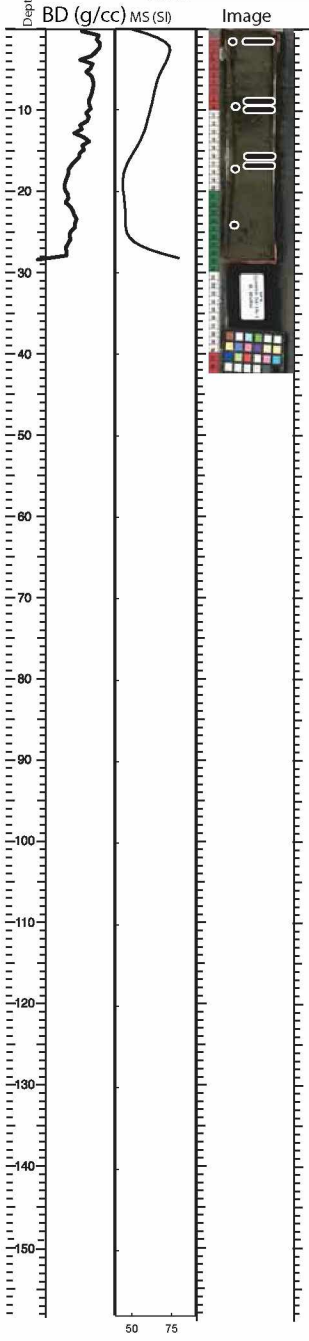

LITHOLOGIC DESCRIPTION

0-5 Medium brown 5Y 3/1 fine silty mud with shell fragments at2.3cm. undecomposed plant fragments (possibly drepanocladus) present.v

5-12.2 Medium brown fine silty mud with some darker brown to black mottling. Undecomposed plant fregments (possibly drepanocladus) present. Small shell fragments at 9.5

12.2 - 28.2 Medium brown fine silty mud. 15 - 15.5 and 27 - 28cm faint horizontal band of small shell fragments.

Smear slides: darker mottles (8.1cm), very dark (9.3cm), dark (11.3cm) , lighter band (13.6cm)

.

INITIAL CORE DESCRIPTION

LAKE Claudi Lake SECTION LENGTH (cm) ###.# mblf top ###.# Describer

CORE ID SPA-CLAU09-2A-1N-2 SED. LENGTH (cm) ###.# mblf bot ###.# Date

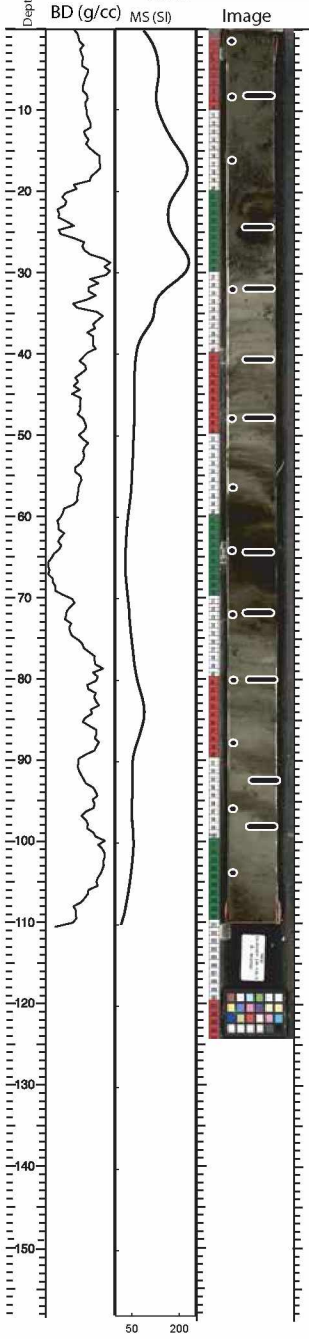

LITHOLOGIC DESCRIPTION

0-17 cm homogeneous mid-br silt 10YR 3/1with voids quite common some sand/grit

17-19 cm silt w/tephra <4mm

19-28 cm same silt with darker inclusions but not clearly banded 10YR 2/1, few voids, gritty

28-29 cm tephra as above

29-59 cm tan silt 5Y 4/3, from 29-40 cm mainly homogeneous, but below faintly to moderately strongly banded with darker bands and inclusions 10YR 3/1, very few small voids

59-69 cm predominantly darker 10YR 3/1

74 cm 8 mm tephra piece

69-110 cm tan silt 5Y 4/3 with faint to moderately strong bands at 71-75, 80-85, 89-92, 94-97, 106-110 (5Y 3/1)

INITIAL CORE DESCRIPTION

LAKE Claudi Lake
CORE ID SPA-CLAU09-4B-2U-2
SECTION LENGTH (cm) 69.8 mblf top ###.#
SED. LENGTH (cm) 69.6 mblf bot ###.#
Describer
Date

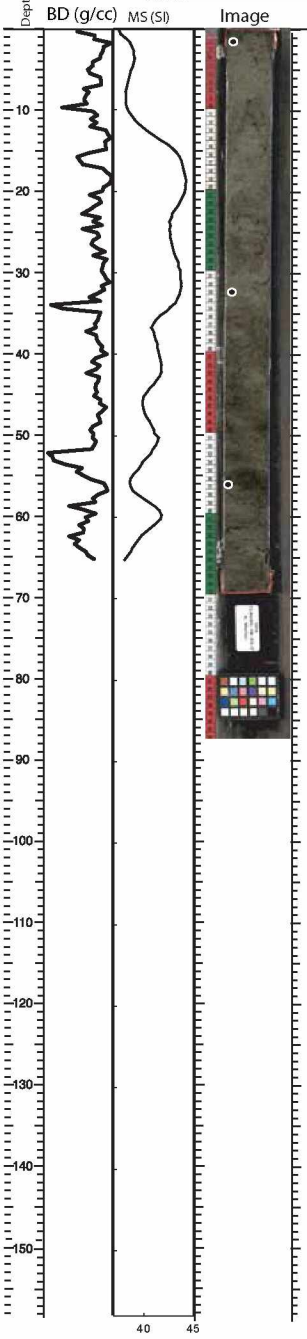

LITHOLOGIC DESCRIPTION

Core length 69.8 cm
Sed length: 69.6 cm

Whole core massive grey silt, dry, with possibly some fine sand; mica visible.

No obvious color changes (but see photo), no inclusions. Few fine organic fragments. Voids common 0-4 cm, few below.

Dating: Organic matter at 62 cm and 65.3 cm (if in situ)

Smear slides: 6.3 cm upper section with voids; 40.5 cm (mid core0; 69.2 cm (base)

INITIAL CORE DESCRIPTION

LAKE Claudi Lake
CORE ID SPA-CLAU09-5A-1L-1
SECTION LENGTH (cm) 73.5 mblf top ###.#
SED. LENGTH (cm) 69 mblf bot ###.#
Describer LF
Date 05/14/09

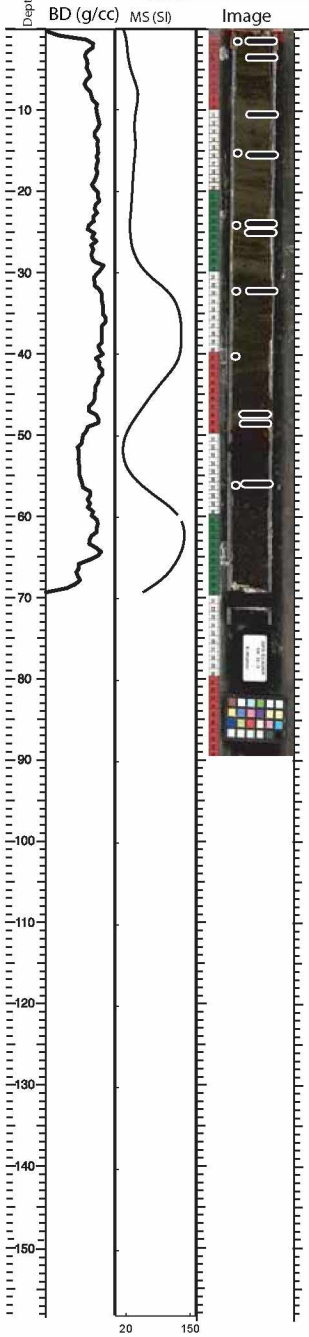

LITHOLOGIC DESCRIPTION

Number of units: 2

0-49cm Medium brown 5Y 3/1 fine silty mud
0-5.5cm Disseminated organic matter (roots?)
6-8.3cm Band of tephra-dominated material
12.5cm Large plant fragment. Root/twig.
23.5cm Large plant fragment. Twig (5cm x 3 mm)
24-30cm Numerous rootlets
31-49cm Band of tephra-dominated material becoming increasingly coarse towards base. At 34cm clump of rootlets.

49-69cm Dark brown 10 YR 2/1organic rich material. Plant fragments visible.
57.5-69cm Very coarse gritty tephra
49-52cm Small lighter 10YR 3/2 inclusion on right side of core as in image.

INITIAL CORE DESCRIPTION

LAKE Claudi Lake | SECTION LENGTH (cm) 61.4 | mblf top ###.# | Describer ME & LF

CORE ID SPA-CLAU09-8A-1P-1 | SED. LENGTH (cm) 34.3 | mblf bot ###.# | Date 03/05/09

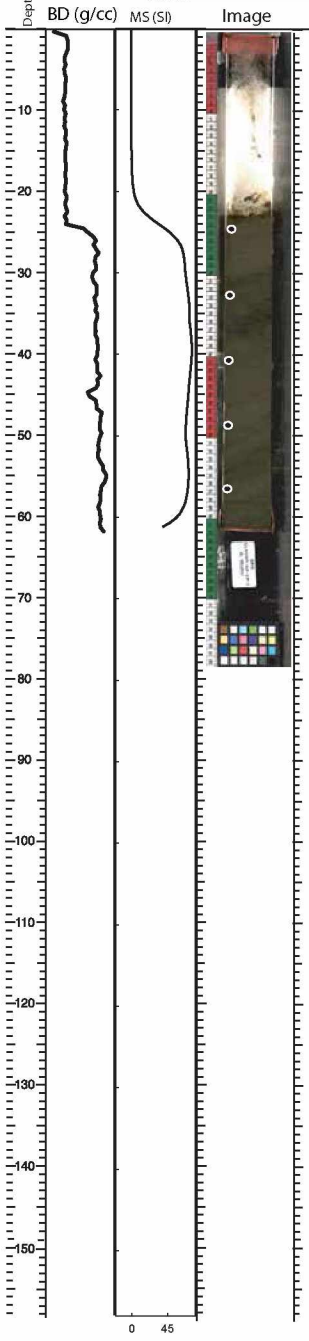

LITHOLOGIC DESCRIPTION

(zorbitrol gel in top part of tube).
Interface slightly sloping. Sediment from 22.7-61.2 cm.

Whole core is mid-brown silty moist mud (2.5Y3/1); indistinct darker banding sub-horizontal or sloping at 29.5-31.0 cm (some small plant fragments); 34-36 cm; 52-56 cm.

Band at 52-56 cm is slightly gritty.

Smear slides: 26 cm near surface; 61 cm base.

INITIAL CORE DESCRIPTION

LAKE Claudi Lake
CORE ID SPA-CLAU09-8A-2L-1
SECTION LENGTH (cm) 84.8 mblf top ###.#
SED. LENGTH (cm) 81.3 mblf bot ###.#
Describer LF
Date 05/14/09

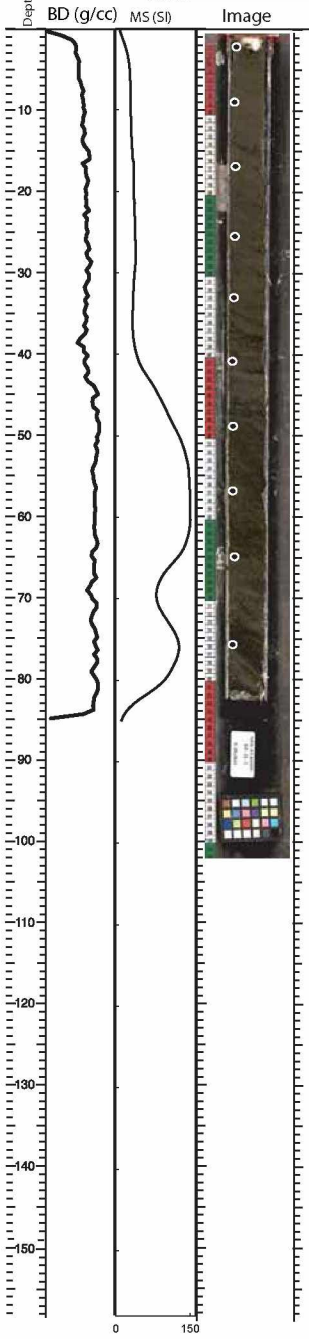

LITHOLOGIC DESCRIPTION

Number of units: 1

0-81.3cm Medium brown 5Y 3/1 fine silty mud

34.2cm Plant fragment (twig) (3cm x 2mm)

37.5cm Tephra piece (0.5cm x 0.5cm)
40.5cm Small organic inclusion (0.5x0.5cm) and tephra piece (0.5cm x 0.5cm) towards left of core as in image.
42.5-43cm Band of gritty tephra dominated material. Indistinct boundary.
45-65cm Horizontal band of gritty tephra-dominated material becoming increasingly coarse towards base of core. Diffuse boundary.

69-82cm Sloping bands of tephra-dominated material. Alternating bands of finer and coarse material with diffuse boundaries. Band width ranges from 0.5-4cm.

Smear slides: 10cm fine silty mud, 81cm base.

INITIAL CORE DESCRIPTION

LAKE Claudi Lake | SECTION LENGTH (cm) 47 | mblf top ###.# | Describer LF

CORE ID SPA-CLAU09-8A-3L-1 | SED. LENGTH (cm) 45 | mblf bot ###.# | Date 05/14/09

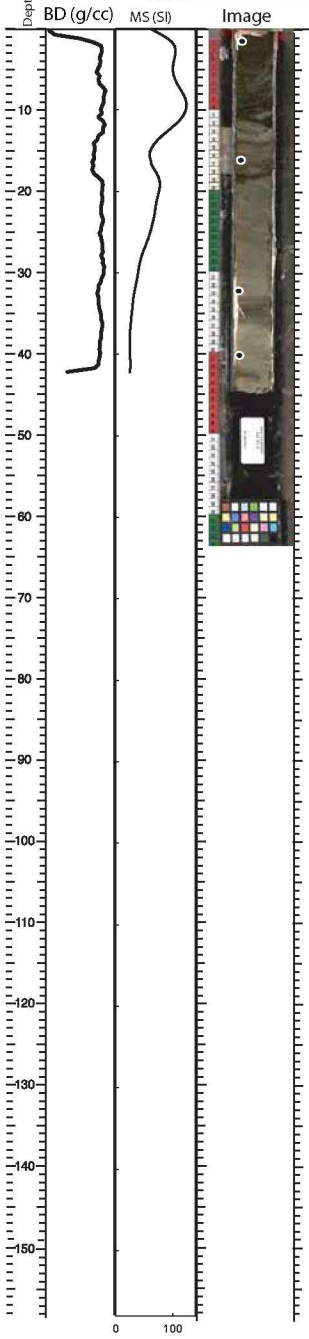

LITHOLOGIC DESCRIPTION

Number of units: 2

0-11.5 Medium brown/grey coarse gritty tephra dominated material. Finer material towards the top of the core.
4-5cm, 6-7cm Upwards curving band of fine silty mud.
10 - 10.5 cm Fine silty mud inclusion.

11.5 - 45cm Tan 5Y 4/1fine silty mud becoming increasingly lighter in color towards base of core.
12 - 12.3, 13.5 - 14cm horizontal darker band of sandy tephra with diffuse boundaries.
18-19cm horizontal abnd of gritty tephra with sharp boundary.
33-.5 - 37cm Horizontal band of darker material with diffuse boundaries.
42.8 - 43.3 cm Horizontal band of darker material spanning left side of core, as in photo, with diffuse boundaries.

Smear slides: Gritty tephra 8.5cm, dark band 35cm, base/ tan fine silty mud 44.5cm

INITIAL CORE DESCRIPTION

LAKE Claudi Lake
CORE ID SPA-CLAU09-10-1N-1
SECTION LENGTH (cm) 77cm
SED. LENGTH (cm) 74.3
mblf top ###.#
mblf bot ###.#
Describer LF
Date 05/11/09

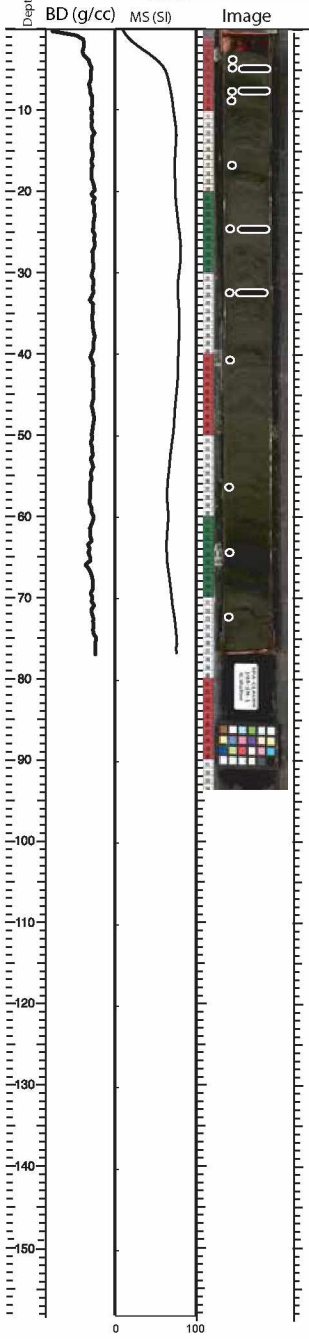

LITHOLOGIC DESCRIPTION

0-3 cm void

3-77 cm Medium brown 5Y3/1 fine silty mud.

Faint, weak horizontal darker bands with diffuse to indistinct boundaries present through core. Band width from 0.3 cm - 2 cm. Bands form upward pointing chevrons between 31- 46 cm, possibly due to sediment flexing under force of downward coring motion. Bands most prominent between 6 - 19 cm and 27-40 cm.

61 - 69 cm thick dark brown 5Y 2.5/1 band with indistinct upper and lower boundaries.

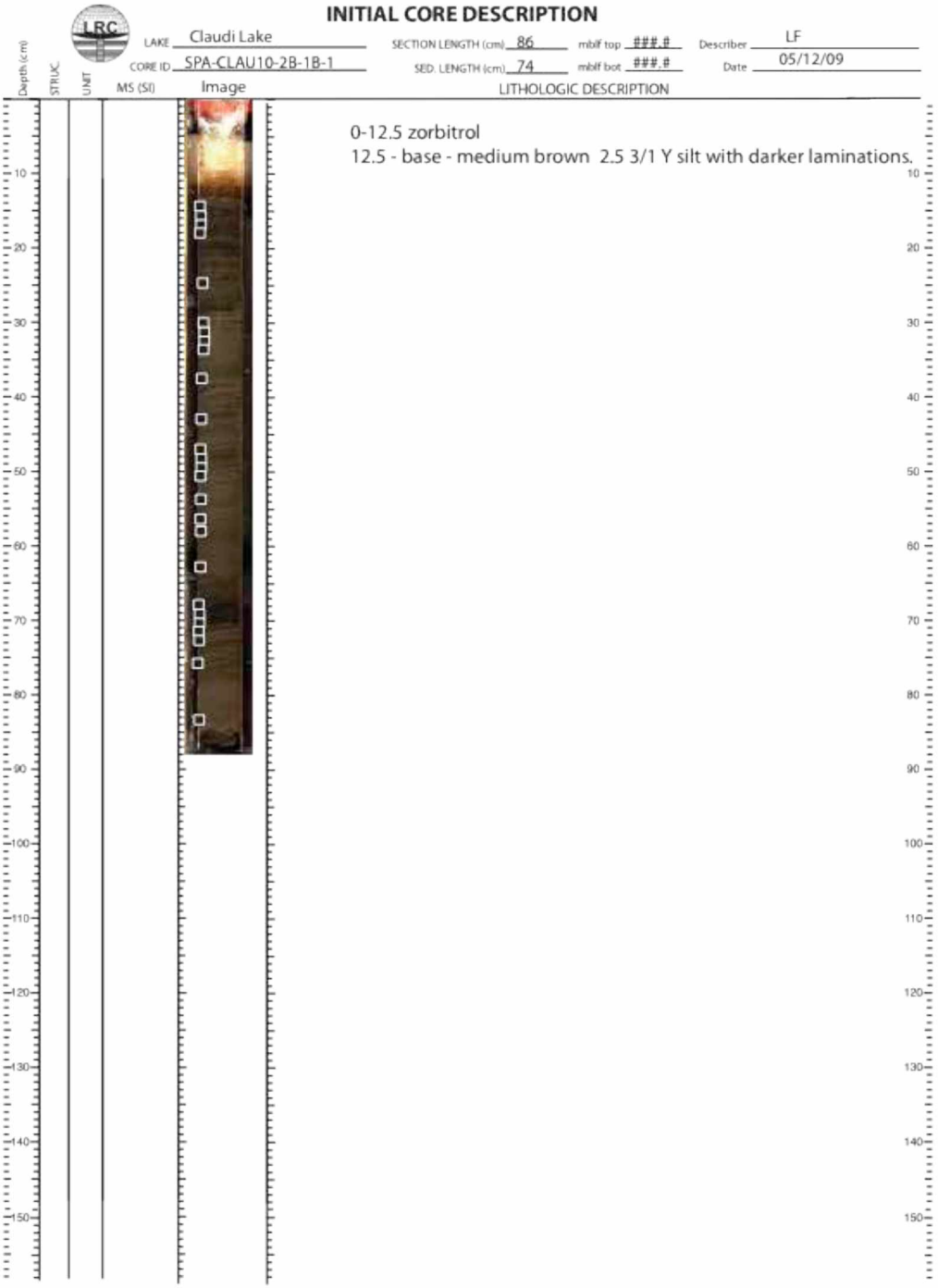
INITIAL CORE DESCRIPTION
LRC
LAKE Claudi Lake
CORE ID SPA-CLAU10-2B-1B-1
SECTION LENGTH (cm) 86
SED. LENGTH (cm) 74
mblf top ###.#
mblf bot ###.#
Describer LF
Date 05/12/09
Depth (cm)
STRUC.
UNIT
MS (SI)
Image
LITHOLOGIC DESCRIPTION
0-12.5 zorbitrol
12.5 - base - medium brown 2.5 3/1 Y silt with darker laminations.
10
20
30
40
50
60
70
80
90
100
110
120
130
140
150

INITIAL CORE DESCRIPTION

LAKE Claudi
CORE ID SPA-CLAU10-2A-1L-1
SECTION LENGTH (cm) 103 cm mblf top
SED. LENGTH (cm) 80 cm mblf bot
Describer LME
Date 9th November

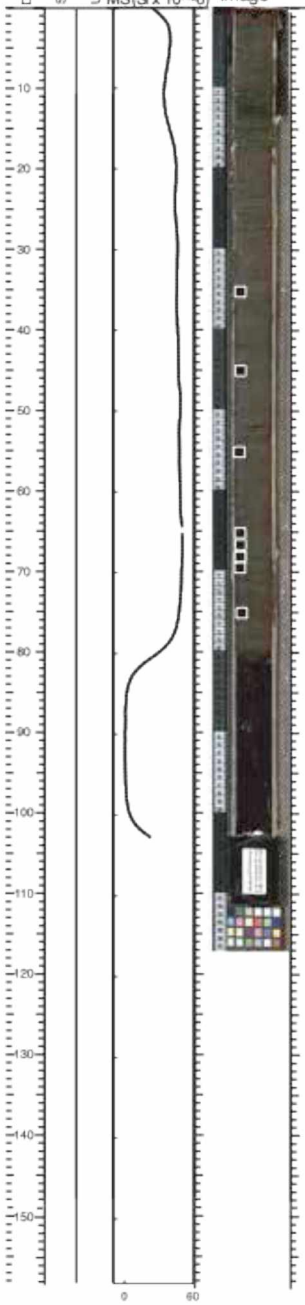

LITHOLOGIC DESCRIPTION

0-80 cm Medium brown (5Y 3/2) fine silty mud. Fine, dark brown (GLEY 1 2.5/N - 2.5Y 2.5/1) laminations down through core. Distinct to diffuse boundaries. Lamination thickness ranging from 0.1-1.5 cm in thickness. Composed of fine detrital organic material.

Laminations especially prominant between 10-18 cm depth. and decreasingly prominant down core.

Fine band of shell fragmnets at 49.9 - 50.0.

INITIAL CORE DESCRIPTION

LAKE Claudi SECTION LENGTH (cm) 41 cm mblf top _____ Describer LMF

CORE ID SPA-CLAU10-2A-2L-1 & 3L-1 SED. LENGTH (cm) 33 cm mblf bot _____ Date 9th November

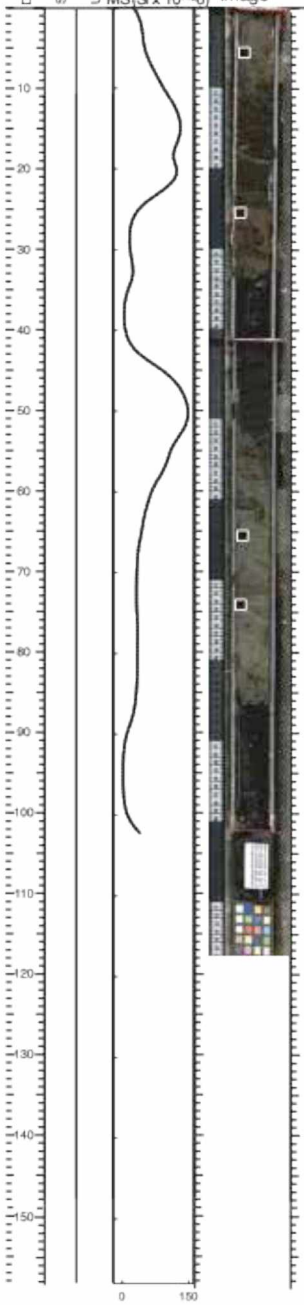

LITHOLOGIC DESCRIPTION

0-8 Medium brown (2.5 Y 3/1) fine silty mud.

8-11 Medium brown (2.5 Y 3/1) fine silty mud with tephra grains. Transition into tephra bands.
11-14 cm Gritty tephra
14-17 Gritty tephra with pieces of pumice at 16.5 - 17 cm.
17-17.5 Dark brown (10 YR 2/2) band of detrital organic material.
17.5 - 18 Medium brown (2.5 Y 3/1) silt
18-22 cm gritty tephra
22-23 cm Medium brown (2.5 Y 3/1) fine silty mud with tephra grains.
23-24 Dark brown (5Y 2.5/1) band of organic detrital material, partially decomposed to fine.
24-33 Medium brown (5Y 3/1) fine silty mud with darker inclusions with diffuse boundaries. ABUNDANT, large (0.25 x 0.25) detriatal plant fragments.

3L

0-10 gritty tephra. Possibly rediposited upon Livingston removal, from SPA-CLAU10-2A-2L-1 10-22.

10-44 cm Tan (5Y 4/1), fine silty mud, some small tephra pieces.
Large (2.5 cm x 0.2 cm) stalk, no other clearly visible macros. Darker patches with indistinct boundaries.

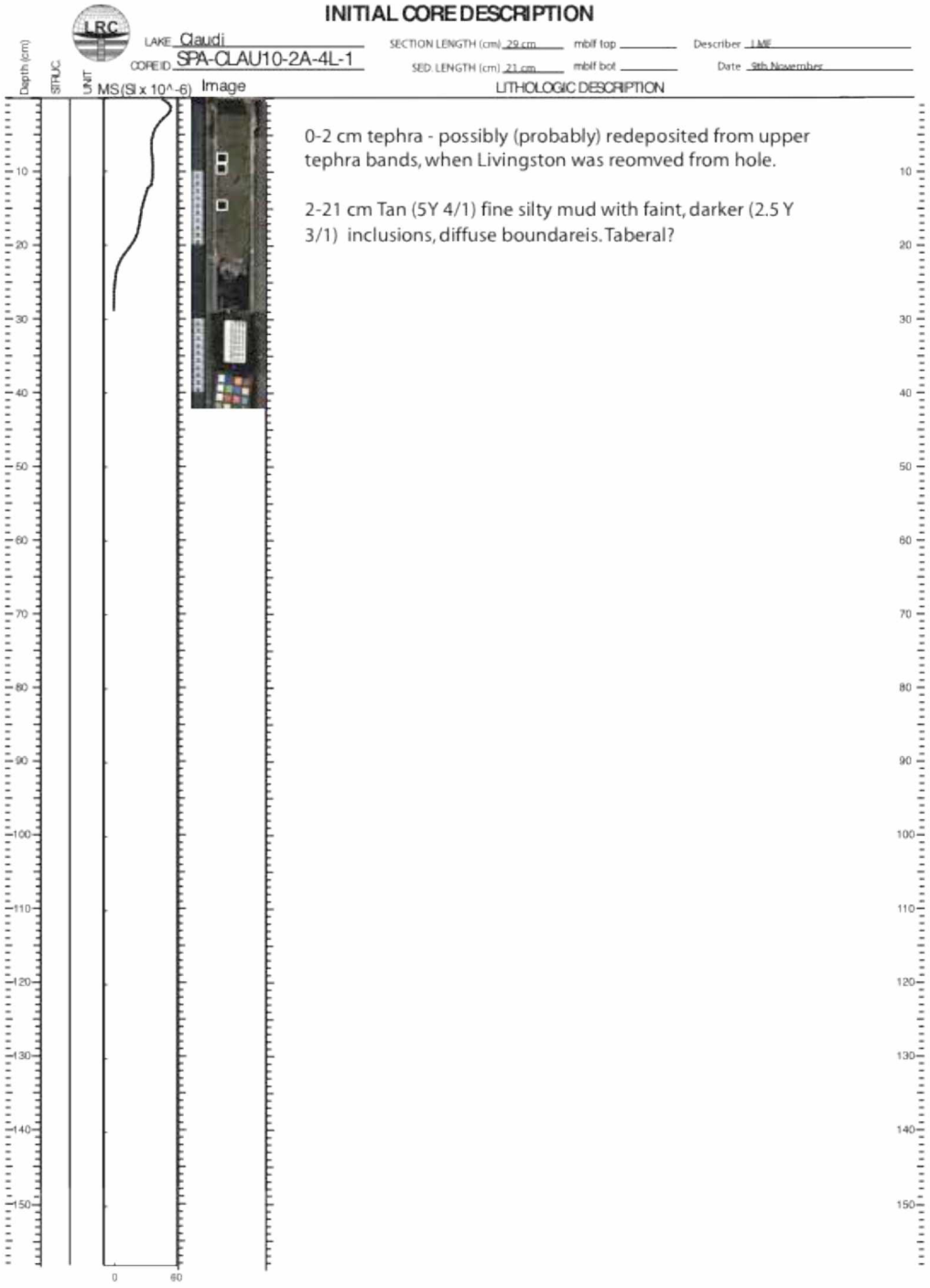
INITIAL CORE DESCRIPTION
LRC
LAKE Claudi
CORE ID SPA-CLAU10-2A-4L-1
SECTION LENGTH (cm) 29 cm
mblf top
SED. LENGTH (cm) 21 cm
mblf bot
Describer LME
Date 9th November
Depth (cm)
STRUC.
UNIT
MS (SI x 10^-6)
Image
LITHOLOGIC DESCRIPTION
0-2 cm tephra - possibly (probably) redeposited from upper tephra bands, when Livingston was reomved from hole.
2-21 cm Tan (5Y 4/1) fine silty mud with faint, darker (2.5 Y 3/1) inclusions, diffuse boundareis. Taberal?
0
60

INITIAL CORE DESCRIPTION

LAKE Cocker Gap SECTION LENGTH (cm) 110 mblf top ###.# Describer LF

CORE ID SPA-COCK09-2A-1N-1 SED. LENGTH (cm) 104.8 mblf bot ###.# Date 05/09/09

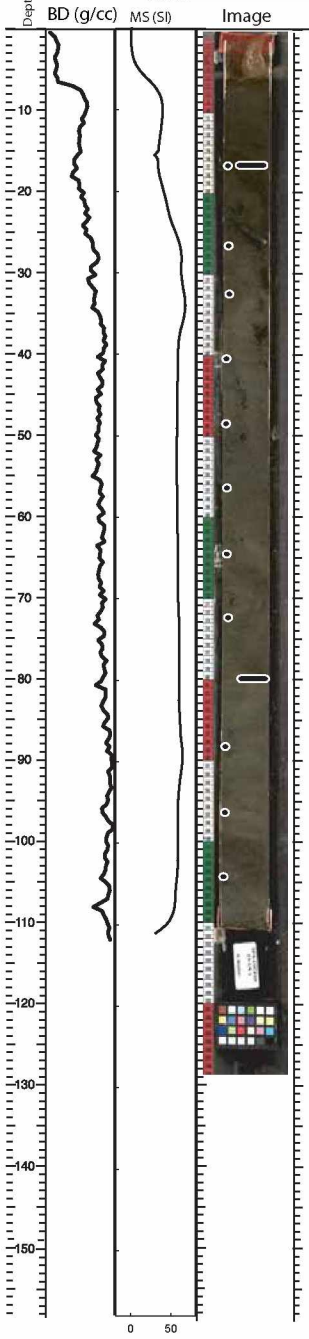

LITHOLOGIC DESCRIPTION

0-6cm zorbitrol
6-110 Medium brown (2.5Y 3/1) fine silty mud increasing in firmness towards the base.

0-22cm unconsolidated material.

22-23cm large (1x5cm) plant fragment sloping across the core.

29-32 and 36 - 38.4cm organic inclusions situated on the right side of the core (as in image).42-48cm, 1cm wide organic inclusion containing plant fragments.

Core becomes increasingly darker towards the base
(possibly due to decrease in moisture content)

Smear slides:
Unconsolidated material (11cm), organic inclusion (44.5cm), base (`109cm)

INITIAL CORE DESCRIPTION

LAKE Jaeger
CORE ID SPA-JAE09-2A-1N-1
SECTION LENGTH (cm) 74.8 mblf top ###.#
SED. LENGTH (cm) 74.6 mblf bot ###.#
Describer
Date

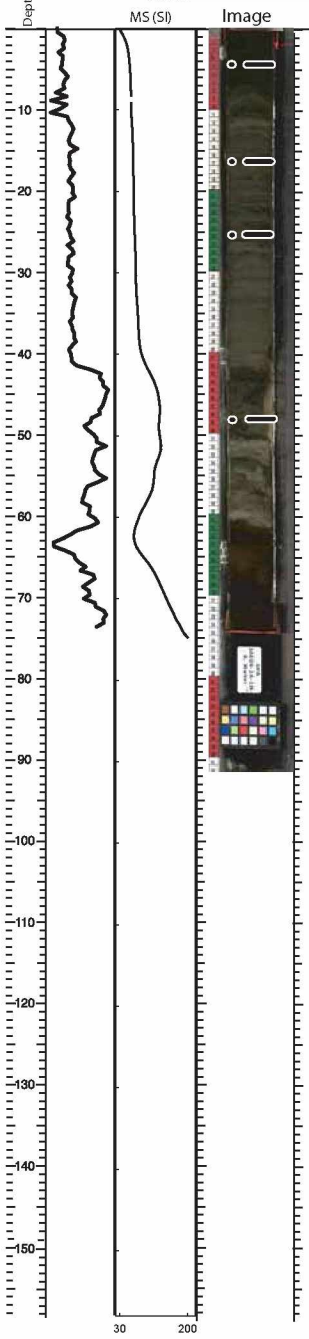

LITHOLOGIC DESCRIPTION

0-8 Medium brown (5Y 3/1)) fine silty mud. Some darker inclusions but not clearly banded.

8 - 41.5 Medium brown (5Y 3/2) fine silty mud.

45.0-51.0 dark, tephra-rich material with one ~2 mm clast at 49.0 cm

51.0-61.0 paler silty mud, soft, with non-horizontal bands and swirls of darker material
61 - 68.5 Darker gritty silty mud.
68.5 - 74.7 - Dark tehpra dominated mud.

Smear slides:
Typical light brown (5.2), fine ash or silt dominated? (60), base (74.2)

Dating?: no obvious dating materials

INITIAL CORE DESCRIPTION

LAKE Jaeger
CORE ID SPA-JAE09-2A-1N-2
SECTION LENGTH (cm) 65.6 mblf top ###.#
SED. LENGTH (cm) 65.4 mblf bot ###.#
Describer ME & LF
Date

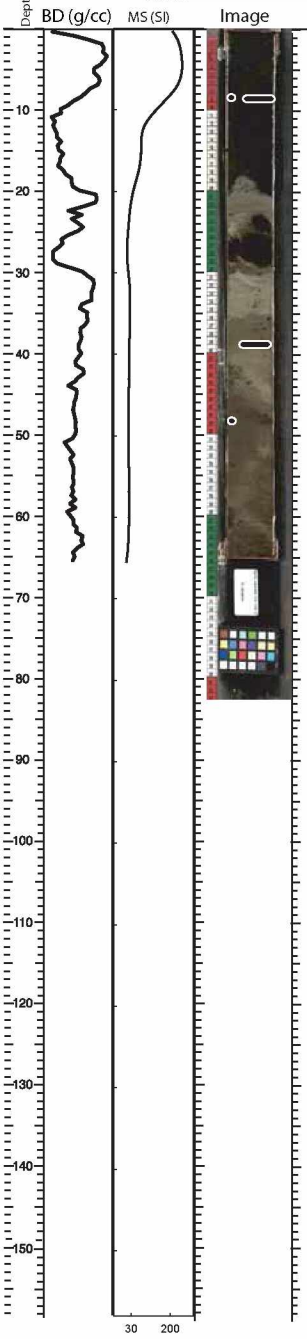

LITHOLOGIC DESCRIPTION

0 - 9 Gritty tephra. Contact sharply sloping up wards from 9 - 4.
9 - 20 Diffuse boundary to finer tephra dominated silt. Spheroidal inclusion of highly organic dark brown to very dark brown from 7 - 19. Diffuse transition between fine tephra and organic spheroid.

20 - 35.5 Diffuse stongly wavey boundary to pale silty mud. Interrupted by organic rich detrital material 2- 6cm deep (peat balls).

35.5 Indistinct boundary to slightly darker silty mud. gradually becoming darker towards base of core. Very little sign of tephra. Voids visible in silt, especially 3between 0-50.

Smear slides
organic material from large inclusion (15cm)
pale silt (22cm)
darker mid brown silty mud 50(cm)
base 65.2(cm)

Dating

INITIAL CORE DESCRIPTION

LAKE Jaeger
CORE ID SPA-JAE09-5A-1N-1
SECTION LENGTH (cm) 61.5 mblf top ###.#
SED. LENGTH (cm) 61.3 mblf bot ###.#
Describer ME & LF
Date 05/02/09

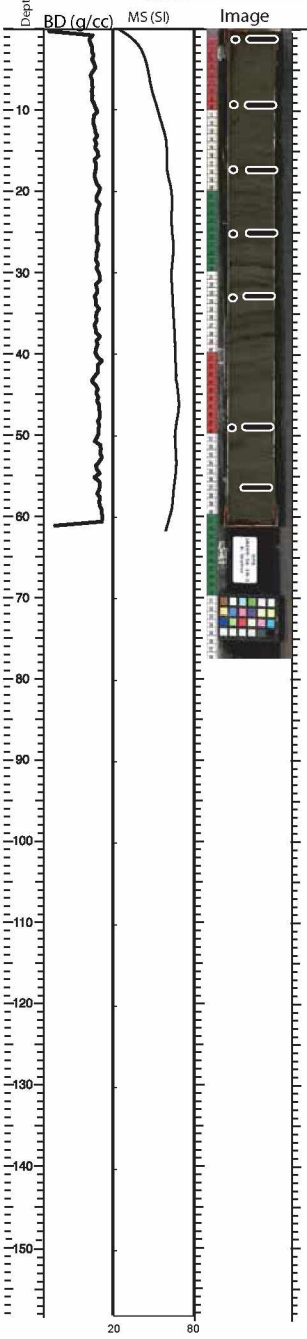

LITHOLOGIC DESCRIPTION

Entire core 0-61 cm medium brown, soft, fine slity mud
5Y 3/2

Faint darker bands, some gritty, 1mm-4mm throughout core, most prominent between 19-5 and 31 and 41.5 and 43 and 50.5 and 53.5. Banding very faint 0-19.5cm

Contacts diffuse to indistinct

banding sub-horizontal

Dating -no obvious materials

Smear slides 4.7cm brown silt; 29.5 in dark band; 60.5 (base)

INITIAL CORE DESCRIPTION

LAKE Rhonda SECTION LENGTH (cm) 82.2 mblf top ###.# Describer LF

CORE ID SPA-RHO09-2C-1L-1 SED. LENGTH (cm) 79.4 mblf bot ###.# Date 05/13/09

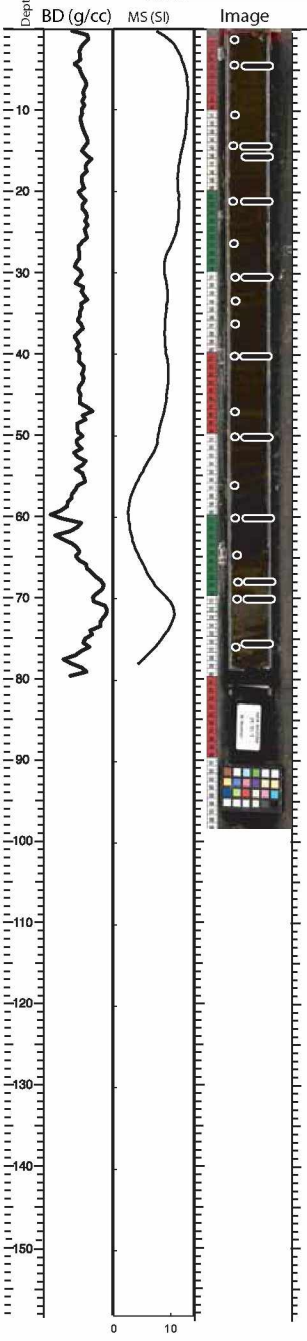

LITHOLOGIC DESCRIPTION

Number of units: 2 (0-66cm & 66-79.4cm)

0-66cm Dark brown 2.5Y 3/1 fine silty mud. Dark horizontal bands with diffuse boundaries throughout unit. Width ranging from 1mm - 1.5 cm. Bands most prominent between 14cm and 56cm.
57.5-65.5cm Darker brown organic rich inclusions with diffuse boundaries.
Some small plant fragments visible.

66.5-79.4cm Tan 5Y 3/2 colored fine silty mud. Darker organic rich inclusions at 69.5 to 70cm. Organic matter between 77 and 79cm, poorly decomposed.

Dating: If in situ plant fragment at 40cm.
Smear slides: 39.5cm darker band, 41cm fine silty mud, 60cm organic inclusion, 72cm tan fine silty mud, 78.2cm base

INITIAL CORE DESCRIPTION

LAKE Rhonda SECTION LENGTH (cm) 57 mblf top ###.# Describer LF

CORE ID SPA-RHO09-2C-2L-1 SED. LENGTH (cm) 53.8 mblf bot ###.# Date 05/14/09

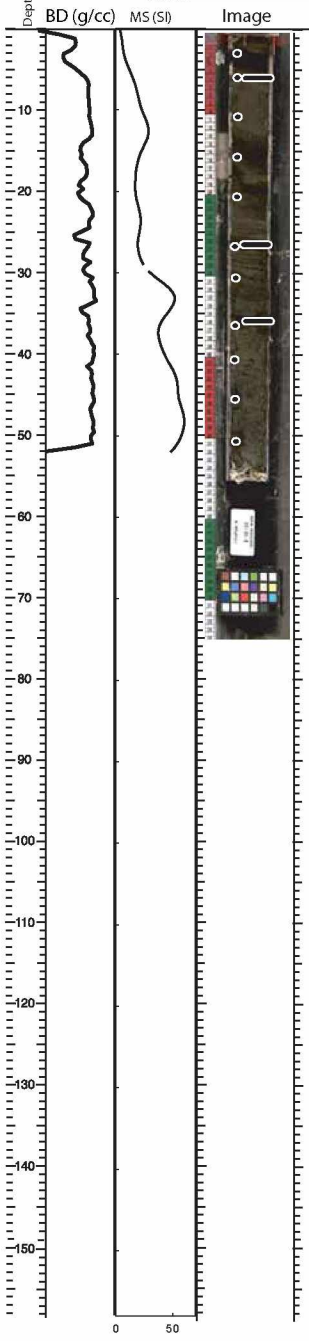

LITHOLOGIC DESCRIPTION

Number of units: 2
0-36 cm medium brown 5Y 3/1 fine silty mud
2-3.5cm horizontal band of darker organic rich material with sharp boundaries.
11-15cm gently sloping band with darker material.
13.2cm woody fragment
18.5-19.5cm horizontal darker band of organic rich material.
21cm small woody plant fragment (0.3cm x 0.3cm)
25.2-29cm Horizontal bands of organic rich material ranging from 2mm to 1cm in width
30.5-32.5cm Horizontal band of sandy material with pieces of tephra
34.5-35.2cm Horizontal band of organic rich material

36-53.8cm Medium brown 2.5Y 3/1 fine silty mud with unsorted tephra pieces ranging in size between 1-4mm.
44-45.2cm Darker inclusion (organic rich?)
47-50cm Sandy inclusion

Dating: If in situ, plant fragments at 13.2cm and 21cm.
Smear slides: 7cm medium brown fine silty mud, 13cm darker band, 53cm base

INITIAL CORE DESCRIPTION

LAKE Rhonda SECTION LENGTH (cm) 41 mblf top ###.# Describer LF

CORE ID SPA-RHO09-2C-3L-1 SED. LENGTH (cm) 36 mblf bot ###.# Date 05/13/09

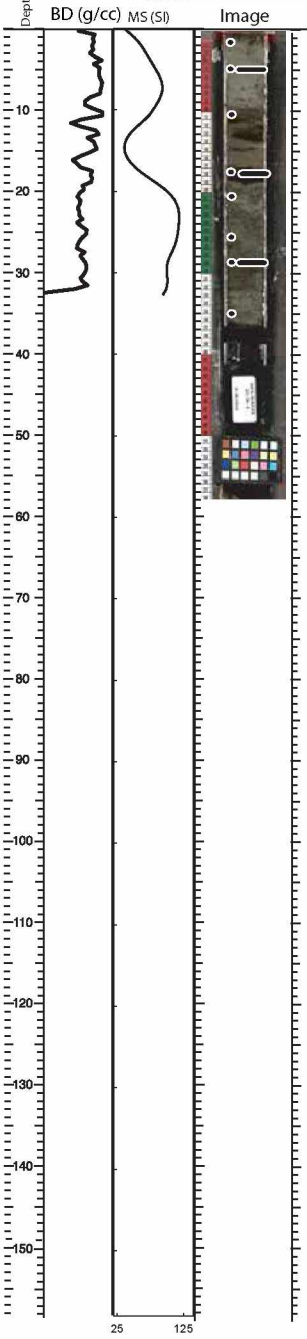

LITHOLOGIC DESCRIPTION

Number of units: 1

0-36cm Tan 2.5Y 4/2 fine silty mud. Firm and organic poor.
0-11cm Voids common.
Darker bands 9.5-11cm, 12-13cm, 14-14.5cm, diffuse boundaries
Dark horizontal organic rich band 17-18cm, diffuse boundaries.
18.5 to 36cm Darker gritty tephra inclusions.
At 19.5cm tephra piece (0.5cm x 0.5cm).

Dating: Nothing observed
Smear slides: organic poor 5cm, dark band 10.6cm, base 35.5cm

INITIAL CORE DESCRIPTION

LAKE Lake Rhonda SECTION LENGTH (cm) 29.8 mblf top ###.# Describer LF

CORE ID SPA-RHO09-2C-4L-1 SED. LENGTH (cm) 27.6 mblf bot ###.# Date 05/14/09

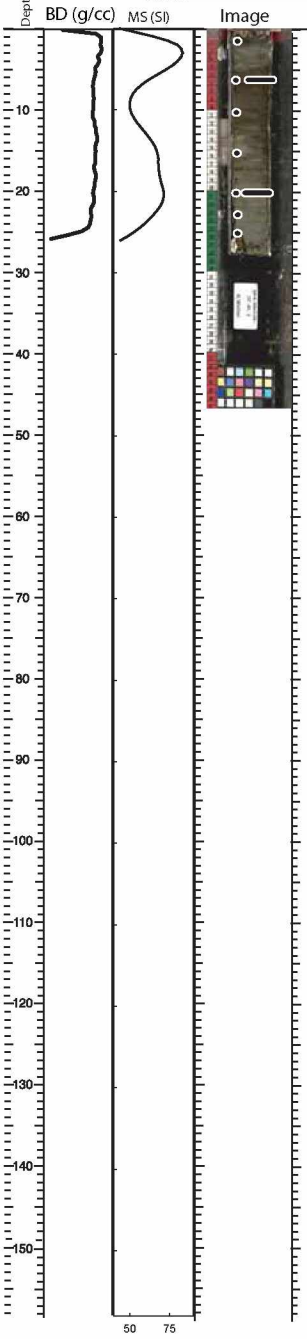

LITHOLOGIC DESCRIPTION

Number of units: 1

0-27.6 Tan 5Y 4/1, firm, fine silty mud. Small (1x1mm) voids visible throughout.
0.5 - 1.5cm Horizontal band of sandy tephra.
4.5 - 18cm horizontal medium brown bands covering only the right side of core (a sin image) between 13 - 16cm. Very diffuse boundaries separate bands which appear as almost one continuous band.

Dating: Nothing observed
Smear slides: Darker band 6cm, base 27cm

INITIAL CORE DESCRIPTION

LAKE Lake Rhonda SECTION LENGTH (cm) 30 mblf top ###.# Describer LF

CORE ID SPA-RHO09-2C-5L-1 SED. LENGTH (cm) 27.2 mblf bot ###.# Date 05/14/09

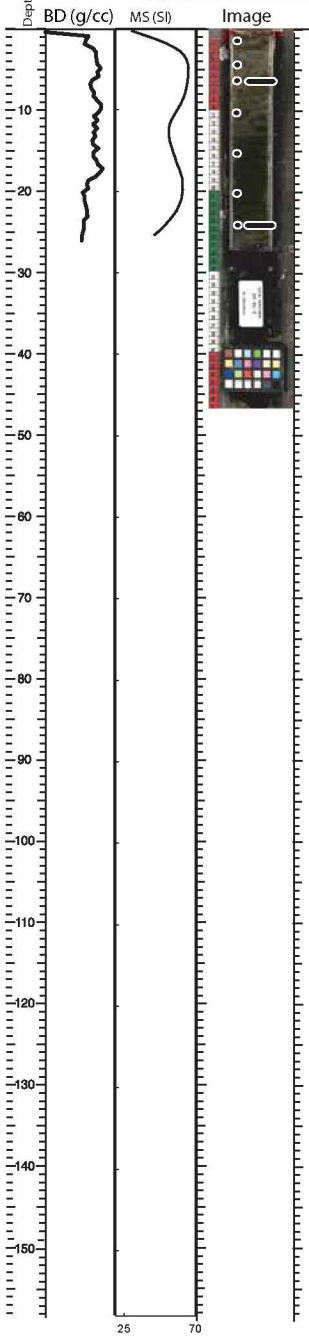

LITHOLOGIC DESCRIPTION

Number of units: 1

0-27.2cm Tan 5Y 4/1fine silty mud.
0-9 medium brown fine silty mud with small (1x1mm) tephra pieces.
12 - 25cm horizontal band of black material with indistinct boundaries. And strongest between 15 - 19cm.
25 - 27cm band (or possibly new unit?) or light brown 5Y 4/2 fine silty mud with faint darker incomplete bands.

Dating? Nothing Observed

Smear slides: tan fine silty mud 6cm, black band 15cm base/light brown 27cm